Capacitive Eye Tracker made of Carbon-Nanotube Paper Composite for Human-Machine Interface and Neuroscience Applications

Vigneshwar Sakthivelpathi

A dissertation

submitted in partial fulfillment of the

requirements for the degree of

Doctor of Philosophy

University of Washington

2023

Reading Committee:

Jaehyun Chung, Chair

Xu Chen

Robijanto Soetedjo

Program Authorized to Offer Degree:

Mechanical Engineering

University of Washington

Abstract

Capacitive Eye Tracker made of Carbon-Nanotube Paper Composite for Human-Machine Interface and Neuroscience Applications

Vigneshwar Sakthivelpathi

Chair of the Supervisory Committee:

Jaehyun Chung

Mechanical Engineering

The uniqueness of eyes, facial geometry, and gaze direction make eye tracking a very challenging technological pursuit. The gold standard for an eye-tracking device has been the scleral search coil system. Despite dominant camera-based eye-tracking systems, their bulky equipment's obtrusiveness and high-power consumption are considered challenging for wearable applications. Piezoelectric sensors, electrooculography (EOG), and capacitive sensors have been attempted for eye tracking but failed due to low sensitivity. The capacitive sensors are unique in that eye movement can be monitored in a noncontact manner, but the sensitivity dampens as the number of sensors increases due to enlarged parasitic capacitance.

In this dissertation, the capacitive sensors are reviewed with respect to their history, working principles, sensing mechanism, fabrication methods, recent nanoscale and microscale regimes, and current applications. An analytical and numerical study is presented to understand in-plane and fringing capacitances. Single- and differential sensing configurations are analyzed in terms of sensitivity and linearity by analytical equations and numerical simulations. Micro and nanostructured materials to construct capacitive sensors will be assessed in the contexts of target parameters, including pressure, strain, force, liquid level, humidity, temperature, displacement, and acceleration. The applications of capacitive sensors are presented in the emerging fields of wearable sensors, human-machine interface (HMI), biomedical implementation, human health monitoring, robotics, and industrial monitoring.

Based on the knowledge, the capacitive interaction between a novel sensor and eye movement for wearable eye-tracking is studied. The capacitive sensors are made of a pair of asymmetric electrodes; one comprising carbon nanotube-paper composite fibers (CPC) and the other being a rectangular metal electrode. The interaction between the asymmetric sensor and a spherical object mimicking an eyeball is analyzed numerically. Using a face simulator, both single- and differential capacitive measurements are characterized with respect to proximity, geometry, and human body charge. Using a prototype eye tracker, multiple sensor locations are studied to determine the optimal configurations. The capacitive responses to vertical and horizontal gaze directions are analyzed in comparison to those of a commercial eye-tracking system. The performance is demonstrated for sensitive eye-movement tracking, closed-eye monitoring, and human-machine interface.

Eye tracker performance is validated in comparison to the scleral search coil, the current gold standard in eye tracking. The capacitive interaction between the CPC electrode and a spherical eyeball is analyzed by a numerical study to understand how the shape and scale of the eyeball affect capacitive interaction. A non-human primate (NHP), implanted with a scleral search coil, is utilized to conduct an eyeball interaction study. The CPC eye tracker's response to smooth pursuit and saccadic movements is investigated and validated against the scleral search coil.

This research has important implications for the development of capacitive, wearable eye trackers, which can facilitate fields of human-machine interface, cognitive monitoring, neuroscience research, and rehabilitation.

TABLE OF CONTENTS

LIST OF FIGURES

LIST OF TABLES

ACKNOWLEDGEMENTS

I wish to express my gratitude to Associate Professor Jae-Hyun Chung, my Ph.D. adviser. His encouragement, valued advice, support, and trust in my abilities has propelled me through my graduate education. To the members of The Nanomanufacturing Laboratory, Seong Kahng, Zhongjie Qian, Tinayi Li, Zachary Taylor, Scott Soelberg, and Changwoo Lee, I thank them for their ongoing support through my doctoral research.

I want to thank my thesis committee members, Associate Professor Xu Chen, Research Associate Professor Robijanto Soetedjo, Assistant Professor Mohammad Malakooti and Professor M.P. Anantram, for their insightful comments and encouragement throughout my research.

I acknowledge the support from the National Eye Institute of NIH (R21 EY031768), Advanced Manufacturing Program of National Science Foundation (No. 1927623), IP group, and Somalytics fund.

DEDICATION

I dedicate this dissertation to my father, Dr. Sakthivelpathi Sarangapani, and mother, Karpagam Sakthivelpathi. My successes are built on their sacrifice, determination, and love.

To my uncle, Sachi Sambandan, and aunty Parveen Rasheed, for their continued support throughout my doctoral research.

To my wife, Nandha, for her dedication to our family, ever-nurturing spirit, and unconditional love.

Chapter 1. ADVANCEMENTS AND APPLICATIONS OF MICRO AND NANOSTRUCTURED CAPACITIVE SENSORS: A REVIEW

1.1 INTRODUCTION

A capacitor is one of the most important electrical components in all modern-day electrical systems. A capacitor is an element capable of storing electrical charges depending on the applied voltage. It commonly consists of two conducting plates separated by a uniform insulating/dielectric media. The media can store electrical energy at field stress levels approaching the ultimate voltage withstand value of the material. Its origin dates back to the mid-18th century, when Georg Matthias Bose, Ewald Georg von Kleist, and Pieter van Musschenbroek independently contributed to the invention of the first known capacitor, the 'Leyden Jar' [1, 2]. The inside and outside of the Leyden glass jar is covered with metal and sealed with an insulating lid. A metal rod with chain is passed through the lid and connected to the inner metal covering, creating a rudimentary high-voltage capacitor [3, 4]. Although, Bose, von Kleist and Musschenbroek gave birth to the first capacitor, the science was discovered in the late 1700s by Alessandro Volta.

Volta's law of capacitance formed the principle that the electric quantity of a conductor is proportional to the capacitance and potential ($Q = CV$) [5]. The quantity of charge Q stored on the positively charged metallic plate of the capacitor when divided by the total voltage difference (V) across the plates gives the capacitance in (farads) of the capacitor. This can be geometrically described as $C = \varepsilon A/d$, where the area of the plates is A, the distance between plates is d, and the permittivity ε. The dielectric media between a set of capacitor plates can vary from gas, air and organic/inorganic films [6]. The specific performance properties of the insulating medium/media will dominate all performance parameters of the capacitor.

Contemporary capacitors are made to perform two main functions; charge or discharge electricity and inhibit the flow of direct current (DC). The charge and discharge of electricity are applied to smoothing circuits of power supplies, backup circuits of microcomputers, and timer circuits. The feature of inhibiting DC flow is applied to filtering applications that extract or eliminate particular frequencies. The emergence of electrolytic capacitors led to full-scale commercialization of the device to satisfy the rapid growth in consumer electronics [7]. Increasing demands for electrical energy storage in applications like high-power electronic devices, implantable medical devices, and electric vehicles, which require very short high-power pulses, led to the development of electric double-layer capacitors (EDLC) or super capacitors. They are complementary to batteries as they deliver high power density and low energy density. EDLC is a type of capacitor where the electrical charge stored at a metal/electrolyte interface is exploited to construct a storage device. The interface can store electrical charge in the order of ~10^6 Farads [7-9].

The 20th century saw innovation in the development of capacitors for sensing applications. Capacitive sensors measure the influence of objects on electric fields generated by a capacitor. One of the earliest known applications of capacitive sensing is Leon Theremin's invention of The Theremin, a musical instrument controlled by the movement of a person's hands without touch [10, 11]. Capacitive sensors offer desirable properties, such as; low cost, low energy consumption, flexible form factor, and variable structure design [10, 12, 13]. The energy consumption and required processing power are small compared to other sensor technologies. Most notably, capacitive sensors have a high versatility that is achieved by modifying electrode material, geometry, excitation frequency, and voltage in accordance with the desired application. One of the most notable modern-day applications of a capacitive sensor is the touchscreen display.

Touchscreen capacitive systems can be divided into surface-capacitive and projected-capacitive methods [14-16]. Surface-capacitive touchscreens consist of one conductive layer, of which four corners are connected to four perfectly synchronized alternative current (AC) voltage signals. The projected-capacitive methods can be divided into self-capacitance and mutual capacitance architectures. It uses two patterned conductive layers that are separated and crossed to each other in the shape of a matrix. Vertical and horizontal patterns correspond to the position information of any touch occurrence. Projected-capacitive mutual capacitance is of particular importance, as it has been critical to consumer electronic touchscreen displays. The introduction of multi-touch functions in the first iPhone utilized a high durability and optically transparent indium tin oxide (ITO) capacitive matrix [17, 18].

The smartphone revolution, predictably, coincides with growth in the wearable, bio-medical, automation, and soft robotics markets. This created a need for miniaturized sensor technologies that can adapt to platforms that remained unexplored in decades past. Innovation in microelectromechanical systems (MEMS) and nano fabrication techniques have now paved the way for miniaturized, extremely flexible, and highly sensitive capacitive sensor systems. Fig. 1 shows the total number of publications over the last decade under the keywords capacitive, sensor, micro, and nano from the Web of Science Core Collection Database 2022.

Several reviews on capacitive sensors have been published in recent years. However, to the best of our knowledge, none summarize the research with respect to micro and nanostructured capacitive sensors, alongside their applications. Qin et al. curtailed their review to microstructured flexible capacitive sensors [19]. Likewise, Rivadeneyra et al. tailored their review toward a distinctive fabrication technique [20]. Other works focus on either a singular fabrication method or are specific to niche applications of capacitive sensor technology [12, 17, 21-23]. In this paper,

we review the fabrication techniques, sensing mechanics, and applications of micro and nanostructured capacitive sensors. MEMS techniques, specifically utilizing micro and nanostructured materials to construct capacitive sensors will be assessed, by categories of; pressure [24-30], strain [31-36], force [37-40], liquid level measurement and humidity [41-55], temperature [56-59], displacement [60-62] and acceleration [63-69]. And, the application of such capacitive sensors in wearable, human-machine interface (HMI), biomedical, human health monitoring, robotics, and industrial monitoring.

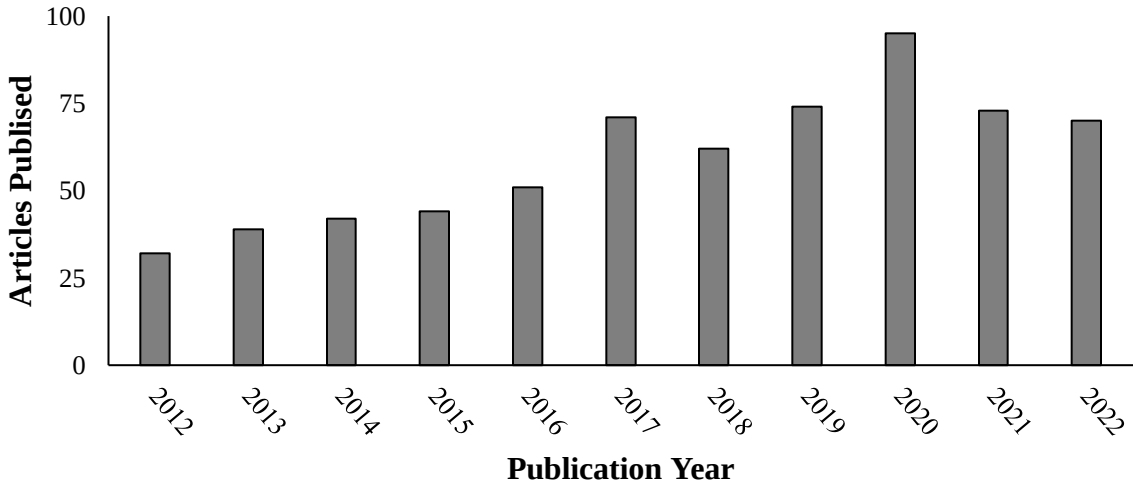

Fig. 1 Total number of publications over the last decade under keywords capacitive, sensor, micro and nano from Web of Science Core Collection Database 2022.

1.2 WORKING PRINCIPLE OF CAPACITIVE SENSORS

1.2.1 *Parallel and fringing capacitance*

When two charged plates are facing, a uniform field capacitance forms (Fig. 2a). When the ratio of the plate size to the gap (d/l) is smaller than 0.01, the capacitance of a uniform electric field dominates the total capacitance as illustrated in the green part in Fig. 2b. The uniform field capacitance (C_u) is;

$$C_u = \frac{\varepsilon_0 \varepsilon_r A}{d} = \frac{\varepsilon_0 \varepsilon_r l^2}{d} \tag{1.1}$$

Where A is the plate area, ε_0 is the vacuum permittivity, and ε_r is the dielectric constant of the medium.

As d increases, the fringing capacitance (C_f) can be approximated as;

$$C_f \approx \frac{k_1 d C_p}{\pi R} \ln\left(\frac{k_2 \pi R}{d}\right); R = \sqrt{\frac{l^2}{\pi}} \tag{1.2}$$

,where the coefficients k_1 and k_2 are determined in prior works [70-73] over certain d/l ranges or could be determined by finite element analysis. C_f derived from research which combines C_f formulas from publications between 1932 to 1986. Commonalities were found between each of the formulas and simplified into a product with k_1 and k_2 coefficients. Curve fitting to FEM and experimental data provided k_1 and k_2 values with 95% confidence [70-73].

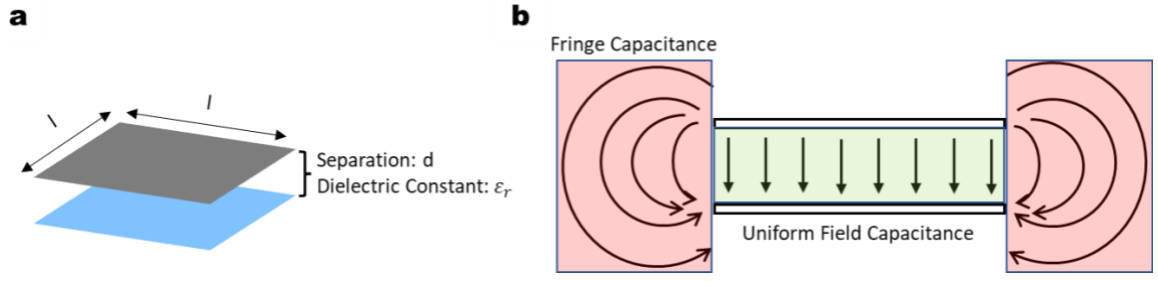

Fig. 2 a) Parallel plate capacitor b) Electric field distribution of a parallel plate capacitor at the cross-section. Parallel and fringing capacitances are expressed with green and red colors.

Using our numerical analysis, the uniform field capacitance was calculated from the surface integration of the electric flux (Φ) on the. The total capacitance (C_t) was computed from all surfaces including fringing (C_f) and uniform field capacitance. According to the simulation results, as d/l increased, C_f became dominant. When d/l was 10, the ratio of (C_f/C_t) was 62.9 %.

In our numerical analysis, C_u was calculated from an integration of surface charge density on the facing sensor plate. As we could see, when d/l was small, Cu was approximately inversely proportional to d/l, which was predicted by Equation 1.1. Despite the significant change of C_u by the equation, C_u by the numerical analysis did not change much when d/l was greater than 1. This discrepancy originated from C_u due to the fringe capacitance C_f. C_f can often be observed on microelectrode capacitance and the traces on the print circuit boards (PCB) and is utilized for coplanar capacitive sensors.

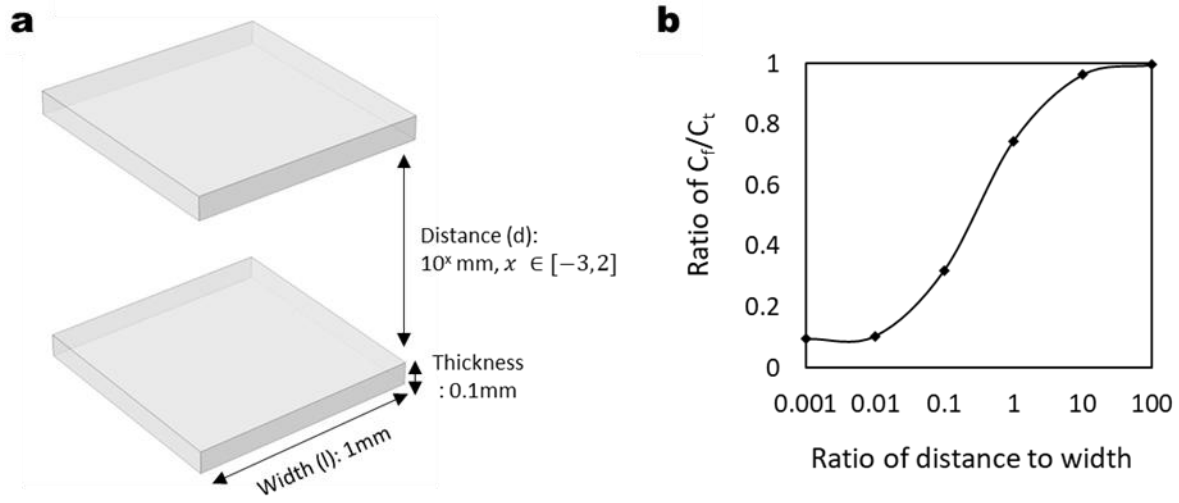

Fig. 3 a) Parallel capacitance and parameters. b) Ratio of fringing capacitance (C_f) to total capacitance (C_t) in comparison to the ratio change of the distance to the width of the parallel capacitor.

To maximize C_f, the coplanar sensors should have larger separation and width. There are very few analytical equations for all separation-to-width ratios but some approximations are made

[74]. Compared with the parallel plate capacitor, the coplanar sensors have a higher fringed electric field, which make it better for detecting far objects. Nevertheless, the complex nature of C_f requires more post-processing on coplanar capacitive sensor results due to the higher nonlinearity. Fig. 3b shows the ratio of fringing capacitance (C_f) to total capacitance (C_t), where C_f is mathematically as one minus uniform field capacitance and C_t is derived via the numerical simulation.

Table 1. Numerical computation results showing C_p and C_t.

Distance (mm)	**d/l**	**C_u by equation (pF)**	**C_u by numerical analysis (pF)**	**C_f by numerical analysis (pF)**	**C_t by numerical analysis (pF)**	**C_f/C_t by numerical analysis**
0.001	0.001	8.85	8.85	0.925	9.77	0.0946
0.01	0.01	0.885	0.887	0.0995	0.987	0.101
0.1	0.1	0.0885	0.0889	0.0411	0.130	0.316
1	1	0.00885	0.0129	0.0219	0.0348	0.629
10	10	0.000885	0.00771	0.0167	0.0244	0.684
100	100	0.0000885	0.00722	0.0159	0.0231	0.688

1.2.2 *Self-capacitance and mutual capacitance*

The capacitive sensors using a fringing electric field are categorized into self- and mutual capacitance. A self-capacitance sensor has only one driven electrode. The detection targets, either human, metal, or other grounded objects, serve as a ground electrode. Since external objects lead to extra capacitive coupling to the sensor, the total capacitance increases. The measured capacitance is approximately inversely proportional to the distance from the sensor. The proximity sensor can also be implemented by placing the ground electrode on a moving surface or a diaphragm, whose separation can be changed by pressure, acceleration, thermal expansion, and others. The examples of dielectric properties based capacitive sensing include water-level sensors and moisture sensors, where the dielectric constant of a medium increases at higher water-levels or relative humidity.

In a mutual-capacitance setting, the capacitance is measured between two charged electrodes. As a result, at least two electrodes are required to form mutual capacitance. When an external object presents, the capacitive coupling between electrodes is disrupted, which changes the capacitance. The capacitance change is not monotonously increased as a target approaches the sensor. When the distance to a sensor decreases, the capacitance decreases and increases due to the charge addition at close distance and the charge subtraction in far distance. Due to the parabolic change of capacitance, the mutual capacitance is used for contact-type pattern recognition on a smart screen.

1.2.3 *Single-ended and differential configuration*

Single-ended configuration works with a pair of electrodes. Differential configuration for a parallel capacitance is to use three electrodes (Fig. 4a). Negative, zero, and positive potentials are applied to the left, middle, and right electrodes for capacitive measurement, respectively. The left and right electrodes are stators while the middle electrode is moving horizontally. The displacement of the middle electrode is x.

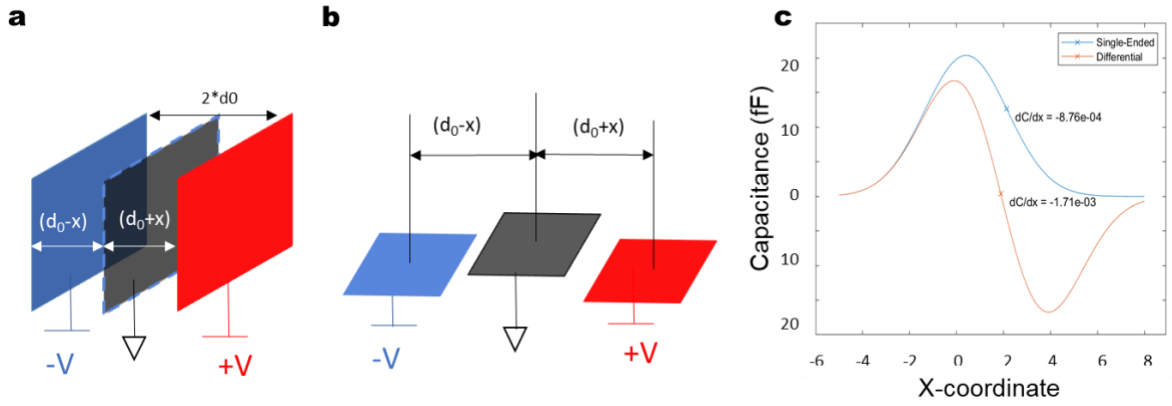

Fig. 4 a) Differential configuration for parallel capacitive sensors. b) Differential configuration for co-planar capacitive sensors using a fringing electric field. c) Red line shows the numerical results of a differential coplanar pair consisting of two sensors at x = 0 and x = 4. Blue line shows the capacitance change from one sensor. Their maximum capacitive sensitivity is described in the graph.

When the middle electrode moves by the displacement of x, the capacitance of the right pair capacitance becomes;

$$C\_r = \frac{\varepsilon A}{x+d_0} \tag{1.3}$$

When the grounded middle plate is at the center ($x = 0$), the Taylor expansion of the capacitance equation can be approximated as;

$$C\_r \approx \frac{A\,\varepsilon}{d_0} - \frac{A\,\varepsilon\,x}{{d_0}^2} + \frac{A\,\varepsilon\,x^2}{{d_0}^3} = C_0\left(1 - \frac{x}{d_0} + \frac{x^2}{d_0^2}\right) \tag{1.4}$$

In the equation, the third and higher order terms were neglected. In the same way, the left capacitance change due to x is;

$$C\_l \approx \frac{A\,\varepsilon}{d_0} + \frac{A\,\varepsilon\,x}{{d_0}^2} + \frac{A\,\varepsilon\,x^2}{{d_0}^3} = C_0\left(1 + \frac{x}{d_0} + \frac{x^2}{d_0^2}\right) \tag{1.5}$$

The total capacitance change is obtained by subtracting C_l from C_r;

$$C(x) = C\_r - C\_l = \frac{-2A\varepsilon x}{d_0^2} \tag{1.6}$$

For parallel capacitors, the differential configuration offers better linearity by eliminating the non-linear terms and higher sensitivity due to the factor of 2 in the equation. The above equation does not apply to coplanar capacitive sensors. In our numerical model, the target moved horizontally between two sensors at a fixed distance to the sensor plane. The capacitance change (ΔC) was computed for one pair of electrodes. The ΔC due to the differential sensors was computed by the superimposition of the positive and negative capacitance changes as conducted in the parallel capacitors. It was found that the differential configuration increases the sensitivity approximately two times in comparison to the single electrode configuration (Fig. 4b). If the separation of the differential pairs increases, the sensitivity will decrease because the distance

between the target and electrodes is larger. At the extreme case, when the separation is so large that the sensing ranges of both sensors are not overlapped, each sensor acts as a single-ended sensor without further gaining sensitivity. Also, if the middle electrode moves and passes the right electrode, the capacitance change decreases (as shown in Fig. 4c).

1.3 MICRO AND NANOSTRUCTURED PHYSICAL CAPACITIVE SENSORS

1.3.1 *Force*

Multi-directional and flexible force sensors play an important role in wearable devices, medical sensing, and HMI applications. According to the sensing mechanism, force sensors can be classified into piezoresistive, piezoelectric, inductive, and strain gauges [37, 38]. Capacitive sensors gain more interests [37, 39, 40]. Capacitive sensors have high sensitivity, temperature stability with less drift, and low power consumption. Furthermore, they offer high spatial resolution and a good dynamic response within a simple structure [37, 75-77].

Zhu et al. presents a carbon black-polymer based flexible capacitive sensor for multi-directional force sensing [37], shown in Fig. 5a. The sensor was assembled with a carbon black polydimethylsiloxane (PDMS) composite dielectric that is sandwiched between top and bottom CNT and PDMS composite electrodes. When the sensor was subject to a normal force, the capacitance change was caused by the distance change between the two plates. Upon a tangential force, the capacitance change was caused by the change of the overlapping area. The filling of carbon black particles into PDMS increased the effective dielectric constant under pressure, resulting in improved sensitivity. The minimum detectable forces were 0.1 and 0.2 N in the normal and tangential directions, respectively [37].

In another work, flexible polyimide-based microstructure sensors were used for force sensing [38]. The capacitive sensor was capable of kN force measurements. It was fabricated utilizing lithographic resist-reflow and dry etching techniques. The sensor had high strength and durability with a sensitivity of 0.5~1 fF/N. The sensor can continually withstand a load higher than 3 kN without damage.

1.3.2 *Pressure*

Capacitive pressure sensors have been paid attention to in recent years due to their high sensitivity, fast response time, small form factor, and low power consumption [26, 29]. Micro and nanomaterial fabrication methods enabled the formation of highly sensitive, flexible piezocapacitive sensors suited to human motion detection, biomedical diagnostics, robotic technologies, and wearable healthcare monitors [24-26, 29].

Electronic textile (e-textile)-based piezocapacitive sensors have been noted to show high sensitivity in a flexible form factor [78-80]. Lee et al. realized a textile piezocapacitive sensor using highly conductive fibers coated with dielectric rubber materials. The e-textile was fabricated by coating polystyrene-block-butadien-styrene (SBS) polymer on the surface of poly p-phenylene terephthalamide fiber and converting silver (Ag) ions into Ag nanoparticles directly in the SBS polymer [24]. A piezocapacitive sensor was fabricated by additional coating PDMS as dielectric layers on the fiber surface and stacking the two PDMS coated fibers perpendicularly. The applied pressure changed the capacitance at the crossing point of the conductive fibers. The conductive fibers exhibited a high sensitivity of 0.21 kPa^{-1} for a textile-based sensor.

Albrecht et al. reported screen-printed capacitive pressure sensors with high sensitivity and accuracy on flexible substrates, for security and robotics applications. Silver was screen printed in a circular pattern onto a PET substrate to create top and bottom electrodes. The dielectric between electrodes was made of screen-printed microstructured PDMS hills [30, 81]. Under pressure, the electrode distance was reduced and the effective relative permittivity increased, while the area remained constant. This resulted in a capacitive change with respect to applied pressure. The piezocapacitive sensor showed logarithmic sensitivity above 20% dB^{-1} at the peak pressure of 750 kPa. As well as 80% kPa^{-1} at the lowest test pressure value of 0.5 kPa [30]. Hysteresis was

combated by increasing PDMS hill radii, producing a highly sensitive and robust sensor large-area integration [30].

Piezocapacitive sensors have proven effective in high-density integration of precision sensors within a small size [29]. Chen et al. introduced a multi-sized planar capacitive pressure sensor with ultra-high sensitivity. Small 1 μm platinum squares were deposited using a liquid metal ion source, onto a polished SiO_2 substrate. Then, an air gap with a width of 200 nm was formed using ion beam cutting. High sensitivity was attributed to the lack of an integrated elastic dielectric layer, which enabled emerging charge exchange channels between neighboring electrodes induced by external touching stimuli. Pressure of 0.02 Pa resulted in a 750% increase in the relative capacitance or an equivalent sensitivity of 3.75 × 105 kPa^{-1} between 0~0.05 Pa. Providing a promising platform for high-density integration of precision sensors within small-size [29].

Hollow PDMS foam with a 3D interconnected network was used to produce highly sensitive capacitive pressure sensors [28]. Copper foam with 95% porosity was immersed in a PDMS immersion mixture (Fig. 5b). A wet etching method was then used to remove the sacrificial copper foam, resulting in a PDMS foam with a hollow network structure. The porosity of the PDMS dielectric layer in the fabricated pressure sensors was controlled by changing the weight percentage of PDMS in the immersion solution [28]. The pressure sensor was assembled by sandwiching the PDMS foam between top and bottom electrodes, comprised of polyethylene terephthalate (PET) film and double-sided bonding copper conductive tape. The piezocapacitive sensor exhibited low hysteresis, a wide pressure range, and durability at 120 kPa for 2,000 cycles.

1.3.3 *Strain*

Traditional strain gauges have been limited to rigid substrates and strain levels below 5% [31]. They were ill suited toward high-strain, low-stiffness applications. With a growing need for

flexibility, real-time measurements with electrical output signals led to the development of capacitive strain sensors [32]. The main applications were motion detection, soft robotics, structural health monitoring, and biomedical platforms [33-36]. Cohen et al. reported a flexible elastic strain gauge based on capacitive sensing of parallel, carbon nanotube-based electrodes with a dielectric elastomer. The strain sensor coupled planar strain to capacitance change due to Poisson's contraction. Uniaxial, planar strain resulted in the contraction of the orthogonal axes that brought two electrodes closer showing a linear capacitance increase [31]. Carbon nanotubes were suited for use in percolation networks as they exhibited high conductivity with a high aspect ratio. The capacitive output of the sensor remained stable within 3%, while showcasing linear performance through an 100% strain cycle and a gauge factor (GF) of 0.99 [31]. This sensor was found to be a low-cost alternative to an angle encoder within robotic linkage systems [31].

Kim et al. debuted a wearable and transparent capacitive strain sensor with high sensitivity based on patterned Ag nanowire networks, for human skin applications [82]. The strain sensor was fabricated using capillary force lithography (CFL) with silver nanowires. The interdigitated pattern embedded onto a flexible PDMS substrate showed better strain (ε) sensitivity, linearity, and low hysteresis in comparison to other capacitive strain sensors. If the two electrodes and the PDMS dielectric layer were placed in the same plane, the capacitance value was less affected by any applied pressure. The gauge factor at 30% strain was -2.0, much higher than the sensitivity of typical parallel-plate capacitive sensors. The sensor displayed no hysteresis up to 0.15-strain and showed stable sensing performance during the cyclic testing [82]. The strain sensor was proven very effective in detecting human finger and wrist muscle motions, lending itself applicable towards large- and small strain sensing functions.

Nur et al. reported a highly sensitive capacitive-type strain sensor using wrinkled ultrathin gold films, for wearable applications [33]. An extremely high gauge factor (3.05) was reported through the addition of out-of-plane deformation via a pre-stretched dielectric. A 50 nm-thick gold (Au) film was thermally evaporated onto a parylene substrate, to create the top and bottom electrodes (Fig. 5c). These were then transferred onto a pre-stretched 3M VHB adhesive elastomer. Upon release, a compressive wrinkled film sensor was created. The accordion-like structure aided in suppressing width contraction during uniaxial strain application. Micron-sized thick electrodes provided resistance in suppressing the Poisson's effect by maintaining a constant width [33]. The change in dielectric thickness during uniaxial elongation correlated to a capacitance change. The strain sensor demonstrated a GF above 3 and high linearity with minimal hysteresis over 1.4-stratin. The wearable nature was demonstrated by mounting the sensor to a finger joint and correlating the angular change to a capacitance change [33].

Compressive strain was often used to attain the stress-strain relationship of structural elements under static loading. Although capacitive strain sensors have been proven to show low hysteresis and high linearity, their traditionally rigid form factor has limited their adoption into structural environments with robust requirements. As such, a strain sensor with a high and constant GF, coupled to a flexible substrate was needed to address these shortfalls. Qiu et al. introduced a highly sensitive and flexible elastomeric sensors for compressive strain measurements for structural health monitoring [34]. This was the first study on direct measurements of compressive strains, under static loading via flexible capacitive strain sensors. A nanocomposite dielectric, consisting of carbon black nanoparticles was mechanically mixed with ethylene-propylene-diene monomer, to create an elastomer matrix. The elastomer matrix was then sandwiched between two fabric electrodes to create a flexible strain sensor. The nanoparticles dispersed in the elastomer

matrix gradually formed electrical networks under static load in response to compressive straining [34]. With a GF over 3.5, the sensor was suitable for detecting compressive strains up to 30% under static load. The sensor showed high linearity over 99.4%, cyclic stability, and low cyclic hysteresis. The sensor proved viable for accurate compressive strain measurements for health monitoring of civil structures and also showed potential for normal force or stress sensing applications.

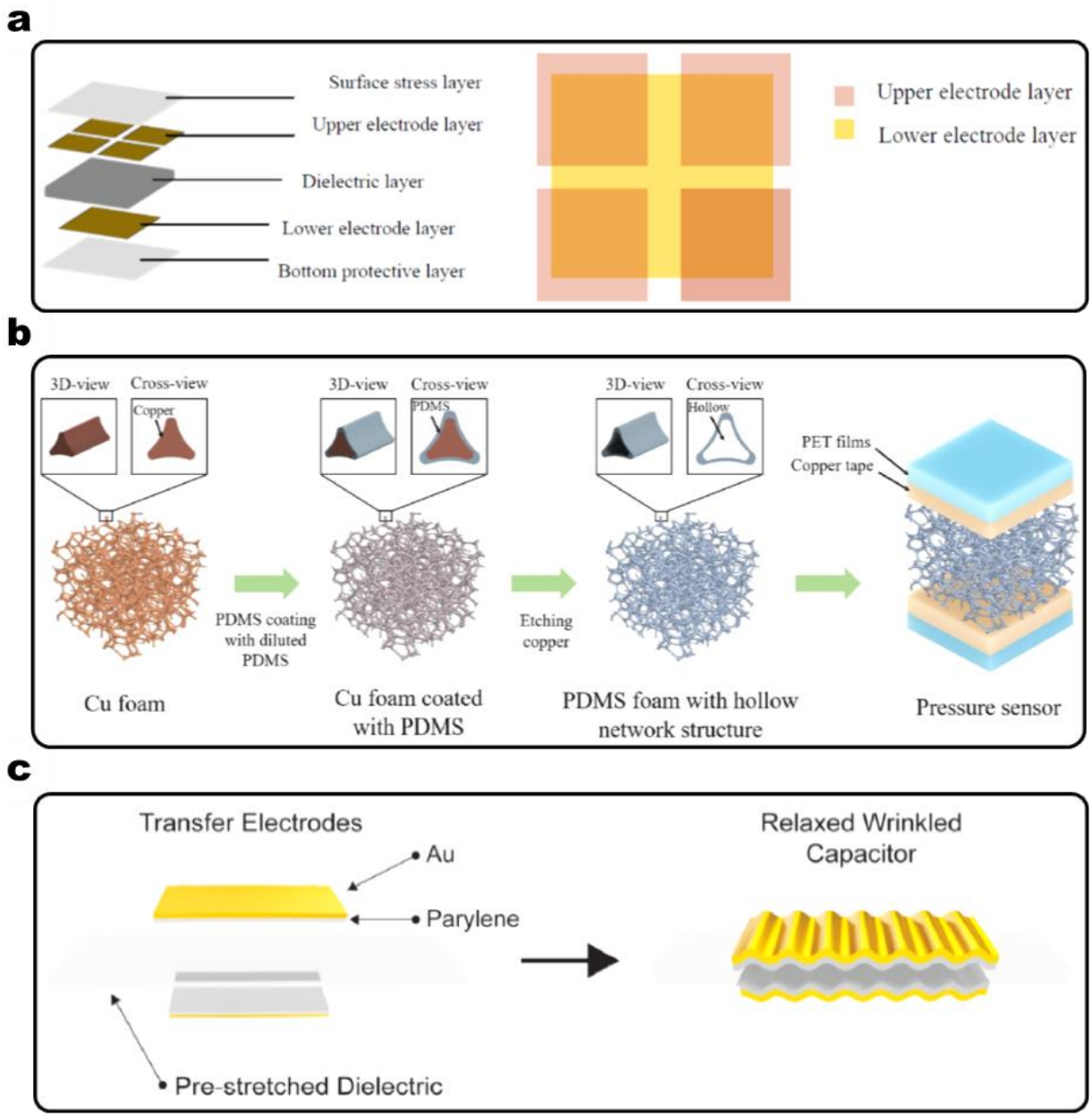

Fig. 5 a) Carbon black / PDMS tactile force sensor structure [37]. b) Schematic illustration of the fabrication process of the porous structured capacitive pressure sensor using copper foam as a template [28]. c) Ultrathin wrinkled Au film strain sensor. Schematic of the assembly and structure of the Au film strain sensor [33]

1.3.4 *Acceleration and displacement*

Accelerometers have been reported based on piezoelectric, piezoresistive, optical, thermal, and inductive technologies [64, 83]. Historically, however, the fabrication methods used to produce accelerometers with these sensing mechanisms have resulted in one-dimensional elements. In other words, detecting acceleration in three axes required the use of three sensors [64]. Capacitive accelerometers using microfabrication techniques allowed for the development of triaxial accelerometers with simple structure, low noise, low power consumption, cost-effectiveness, and reliability [39, 65, 68].

Burbaum et al. introduced one of the first microfabricated accelerometers using a LIGA (German acronym for githogralie galvanoformung, abformung) process [65]. Built on this work, Qu et al. introduced the fabrication of a 3D differential capacitive accelerometer by UV-LIGA [64]. The UV-LIGA fabrication process consisted of photolithography, electroplating, electrochemical growth, and chemical etching. By combining UV-lithography and electrodeposition technique, UV-LIGA was noted to enlarge the possibilities of surface micromachining in a low-cost manner [64] (see Fig. 6a). The sensor had a comb structure, where the seismic proof-mass was suspended by two folded tethers. The tethers were anchored to support islands that were fixed to the substrate. The seismic mass was then free to move in a plane perpendicular to the tethers. A series of finger-like structures projected from the central mass, with each finger acting as a grounded middle plate of a side-wall air-gap variable capacitor. When the seismic proof-mass was accelerated, the gap width between one electrode and the proof-mass increased, while the gap width of the other pairs decreased. Acceleration can then be determined by the capacitance change [64]. The final dimensions of a sensor was only 2650 x 2650 x 30 μm^3.

Rao et al. designed a similar comb accelerometer using microfabrication techniques, to fabricate a silicon-based accelerometer. The microstructured mass was sandwiched between upper and lower glass plates (see Fig. 6b) [68]. Through-silicon-wafer deep reactive ion etching (DRIE) was used to increase the weight of proof mass for lower thermal noise. The micro-g accelerometer demonstrated a scale factor of 510 mV/g, a noise floor of 2 $\mu g/Hz^{1/2}$ at 100 Hz, and a bias instability of 4 µg at an averaging time of 1 s [68].

Capacitive proximity sensors are of particular importance as they can detect the presence of conductive and non-conductive objects. Although optical and ultrasonic sensors present similar use cases, their power consumption, hardware intricacy, and environmental sensitivities make them a complicated option for integration into robust mechanical systems [60]. Capacitive proximity sensors have become synonymous with displacement detection. Micro- and nanostructured capacitive proximity sensors are enabling highly sensitive displacement detection in an ultra-small form factor with low-power hardware.

Wei et al. introduced a dispenser-printed proximity sensor on fabric [60]. Dispenser printing is a bespoke printing method developed at the University of Southampton [60, 84, 85]. Dispenser printing was a drop-on-demand technology, where ink was only deposited in the designed areas. It enabled the additive deposition of a uniform thickness film of various materials. The dispenser printer involved a syringe containing the ink, mounted on XYZ translation stages, with pneumatic or mechanical forces applied to the top of the syringe to deposit the ink [84]. Conductive ink was dispenser-printed, with an average thickness of 35 µm, onto a 360 µm thick polyester woven fabric. The conductive ink was made silver flakes blended with a polymer binder and printing enhancement additives. Post printing and processing the fabric were noted to have a conductivity of 1.2 x 10^6 S/m. A single electrode detection mechanism was used, as the fabric

pattern varied (see Fig. 6c). A maximum detection range of 400 mm was attained through a 400 mm-wide sensor. Blaz et al. also employed similar additive manufacturing techniques, comprised of inkjet technology and 3D printing [62]. A circular sensor casing was 3D-printed with a cover, top and bottom electrode couplings, with a spacer to create an air gap. The top electrode was fabricated by printing silver ink onto a flexible 125 μm thick polyimide membrane. Flexing of the top electrode varied the gap to the bottom electrode, enabling a capacitance change with respect to displacement. The sensor was noted to distinguish 100 μm-displacement.

A contact-type linear encoder-like capacitive displacement sensor (CLECDiS) was proposed for use in nano-positioning systems [61]. This sensor consisted of two parallel plates, each composed of a substrate layer covered with an electrode grating and a thin dielectric film coating. An electric source was supplied to one plate and the output signal was detected from the other plate. The electrode grating for detecting the signal in the receiver was enclosed by a grounded shield. The electrode grating on each plate consisted of a set of regularly spaced parallel rectangular patterns of a uniform size, which were connected in series. This electrode design offered a linear variation in the overlapped area when one plate was moved horizontally. The grounded electrode in the receiver was used to block the influence of stray capacitance and electric field out of the electrode grating of the receiver. Due to the accurate micromachining techniques, the fabricated sensor showed a resolution of 0.9 nm, sensitivity of 3.14 pF/μm, the measurable range of 15 mm, and a linearity error of 0.0026% [61].

Li et al. showcased an ultrasensitive nanostructured capacitive sensors composed of cellulose fibers embedded with carbon nanotubes [86]. The asymmetrically designed 10 mm single fibrous electrode had a 300 mm detectable range for the human hand. Furthermore, water mass could also be detected by the 10 mm single fibrous electrode, in both glass and metal containers.

1.3.5 *Temperature*

Thermal sensors form one of the largest classes of microsensors, with temperature being one of the most important parameters [87]. Compared to resistive, inductive, and LC counterparts, capacitive sensors have many advantages such as high sensitivity, excellent stability, fast response, high resolution, good frequency response, less loading effect because of high input impedance, no self-heating, and less power requirement [58].

Ma et al. introduced a micro-machined capacitive temperature sensor using a silicon wafer. The micro-composite cantilever consisted of four layers. Low-pressure chemical vapor disposition (LPCVD), chemical etching, and reactive ion etching (RIE) were utilized to fabricate the temperature sensor. The top- and bottom layers were aluminum and silicon, respectively, which were also used as the electrodes of the sensing capacitor. The center dielectric layers were made of silicon nitride and silicon oxide. When the multilayer structure was subjected to a temperature change, thermal stress was introduced due to mismatch of the thermal expansion coefficient between adjacent thin films. A resultant moment was then generated from the stresses. The cantilever was bent upward or downward as the temperature decreased or increased, causing a capacitance change [59]. shows a schematic of the cantilever temperature sensor. The sensor (Fig. 6d) showed a sensitivity of 7 fF $\circ C^{-1}$ in the $-70 \sim 100$ ^{o}C range [59].

Salmaz et al. fabricated a reliable and inexpensive, parallel plate capacitor with a PDMS dielectric that was sensitive to temperature. The sensor worked on the principle that the density of sensing layer decreased with an increase in temperature following the Clausius–Mosotti equation, subsequently causing a decrease in permittivity [58]. The fabrication of the temperature sensor began with a PCB substrate that was screen-printed and etched to transfer an electrode mask. Degassed PDMS solution was coated onto the PCB strip with a dip coater. A copper plate was

then fixed to a semi-cured 56 μm thick PDMS film. The sensor (Fig. 6e) showed a mean sensitivity of 156 fF/^{o}C in the range of 20 ˜ 200 ^{o}C [58].

A set of bilayer cantilever beams made of thin polycrystalline silicon and gold films used a mismatch in the thermal expansion of the two materials to create out-of-plane displacement as the ambient temperature changed [57]. The capacitance of the device was consequently changed due to the change in gap size between electrodes. Sensors presented in this work were fabricated using polysilicon multi-user MEMS Processes or PolyMUMPs [88]. For a ~10 °C temperature range, the sensor exhibited high sensitivity of 20 fF/°C and relative sensitivity of 3.33 %/°C.

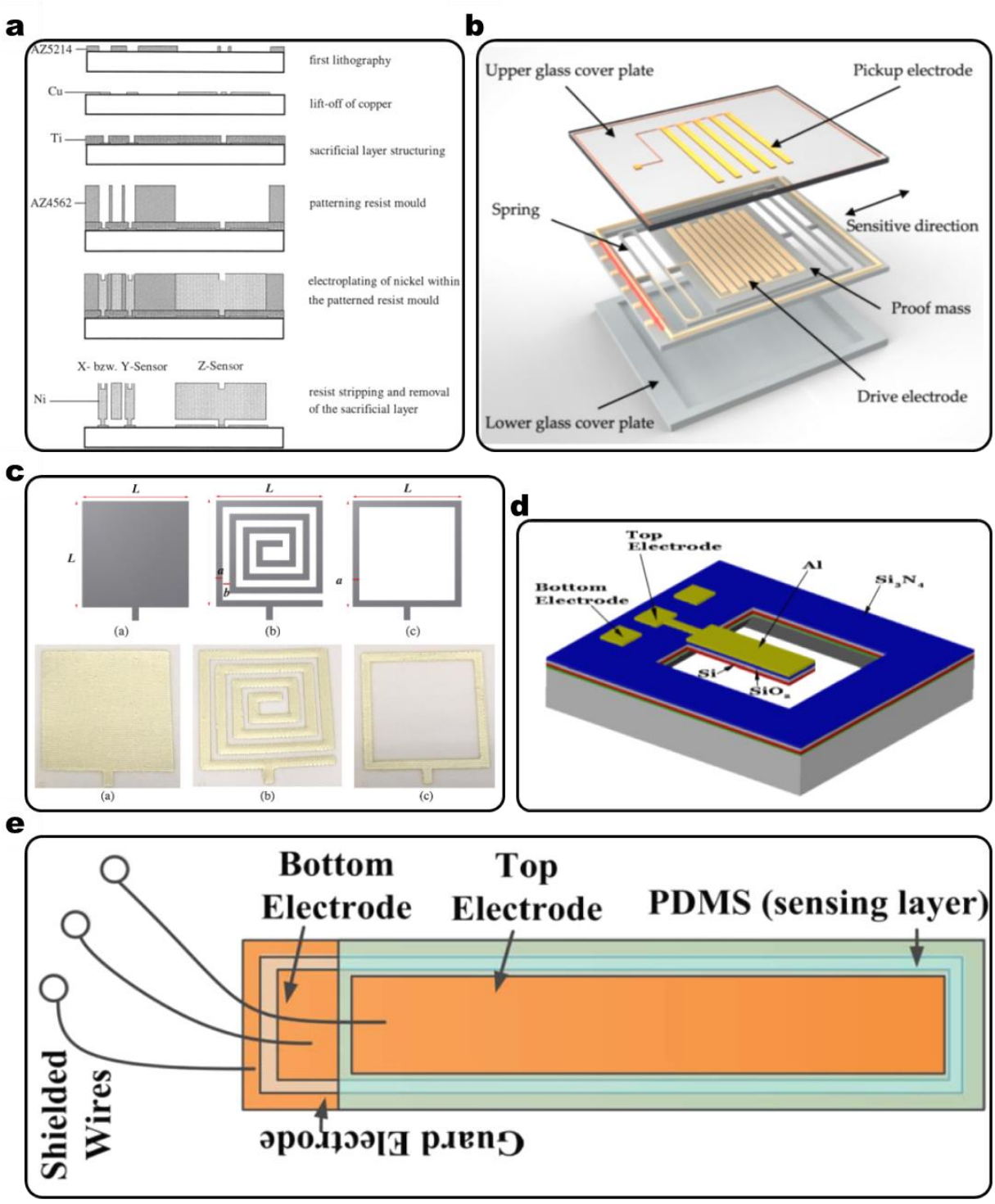

Fig. 6 a) Fabrication process for UV-LIGA accelerometer [64]. b) Silicon-based acceleration sensitive spring-mass structure accelerometer [68]. c) Dispenser printed capacitive proximity sensor on fabric [60]. d) Structure of capacitive temperature sensor based on a multilayered cantilever [59]. e) Capacitive temperature sensor using PDMS dielectric [58].

1.3.6 *Liquid level and humidity*

The capacitive sensors have been used in measuring the relative humidity due to their low power consumption, high sensitivity, and small form factor. Most capacitive sensors have two formats. The first one consisted of two electrodes configuring as parallel plates and a humidity sensitive dielectric layer between the two layers while the other type was a pair of interdigitated electrodes.

For the parallel plate capacitor, the decisive factor was the dielectric medium between the two electrodes for high sensitivity. Extensive study was conducted to modify its porosity, surface area, water absorption ability, and stability. Using polyimide composite as the dielectric medium has been studied [41, 42] due to its good absorption ability and linearity. The excellent linearity was achieved in the RH range of 20~80%. Both sensors were fabricated through a microfabrication process. The polyimide layer was spin-coated on the electrode with the thickness of 3μm and 800nm.

The substrate of silver inkjet-printed interdigitated electrode (IDE) capacitive sensors was modified to obtain the short response time in humidity sensing. A Nafion/TiO_2 composite film[43] was inkjet-printed to provide accurate relative humidity in 35%-95%. The amorphous nanostructured TiO_2 was coated on the IDE sensor through physical vapor deposition [44] which showed a 1 μF-capacitance change for relative humidity of 2~92 %. The porous structure composed by MWCNTs and SiO_2 was proposed as the sensing substrate using capillary condensation and percolation of CNT networks [45]. Commercial paper was also used as the sensing layer without additional coating, which showed good reproducibility and linearity in the humidity environment in 40~100% [46].

Liquid detection has drawn a lot of attention because of industrial demands, medical applications, environmental monitoring, and appliances in daily life. There were a few aspects of liquid detection, for example, liquid level, liquid content, and flow rate in the pipe or containers. With respect to all the demanding perspectives, sensors including pressure, optical, resistive, and capacitive have been developed to measure the real-time signal from applications that involve liquid. With the advantages like low-cost, non-contact measurement, and high sensitivity, the capacitive sensor has been recognized as a prospective candidate for handling all the aspects of liquid detection. Detecting liquid contents in the biodiesel [47] and microfluid [48] and liquid level measurement [49, 50] were good examples.

To improve the sensitivity, the comb shape interdigitated electrode sensor was one of the leading directions. The fringing field generated between the two close distance coplanar electrodes enhanced the capacitance signal near the sensor surface [51]. The sensor was very sensitive to the dielectric constant change of the object that was close to the sensor which was applied to liquid content detection. However, the limited sensing distance hindered the liquid level detection, which needed a large coverage for a large size container. To overcome the challenge, the larger size sensors corresponding to the actual container dimension were developed [50, 52, 53].

The flow rate in a tube [54, 55] could be measured and attained from capacitive sensors but required the orifice configuration because the velocity profile changed after passing the orifice, which resulted in a change of the dielectric constant.

1.4 APPLICATIONS

1.4.1 *Wearable and human machine interface*

Capacitive sensors have a novel interaction relationship with the human body. Human body communication (HBC) is a term describing the use of the human body as a conductive channel to enable communications between, on, or around the individual [89]. A standing human body insulated from ground is in principle an insulated conductor and as such, has a capacitance. The capacitive charge carrying ability of the human body is estimated at 100 pF [19]. In a recent study, the currents flowing through the human body and ground are estimated at the nanoampere range and correlated to the individual's motion [20]. As such, the human body exudes variations in charge, with respect to motion, which subsequently lends itself to highly sensitive interactions between the human body and capacitive sensors.

Micro / nanostructured capacitive sensors with flexibility and high sensitivity lend themselves naturally to wearable and human-machine interface (HMI) applications. Electronic skins (E-skin) capacitive sensors have been reported by numerous studies [36, 90-92]. They are highly stretchable, robust, and sensitive, with a wearable form factor. Zeng et al. reported a highly stretchable, compressible all-hydrogel soft supercapacitor, with high capacitive retention for wearable applications [90]. Fig. 7a shows the highly elastic and deformable nature of the hydrogel capacitor. Lei et al. investigated mineral hydrogel as a self-healable, mechanically adaptable ionic skin for pressure sensing [91]. The capacitive sensor was proven self-healable and sensitive to subtle pressure changes, such as a gentle finger touch, and human motion. Dhakar et al. created an intelligent skin-based self-powered finger motion sensor integrated with triboelectric nanogenerator [92]. It demonstrated a low-cost, wearable, self-powered motion detection of the human finger for static and dynamic motions. PeriSense, a ridged gesture interaction system

utilizing capacitive proximity sensing, was able to recognize multi-finger gestures in form of a wearable ring (see Fig. 7b) [93].

A study of the oculomotor system correlated eye movements with neuronal activity in areas of the brain. To accurately understand this relationship, an eye-tracking sensor needed to capture both spatial and temporal characteristics of eye movement with high fidelity [94]. Eslucent, an eyelid interface for detecting eye blinking (see Fig. 7c) by Luo et al. showcased novel eyelid stickers that could detect blinks with variations in pressure from the eyelid skin creasing [95].

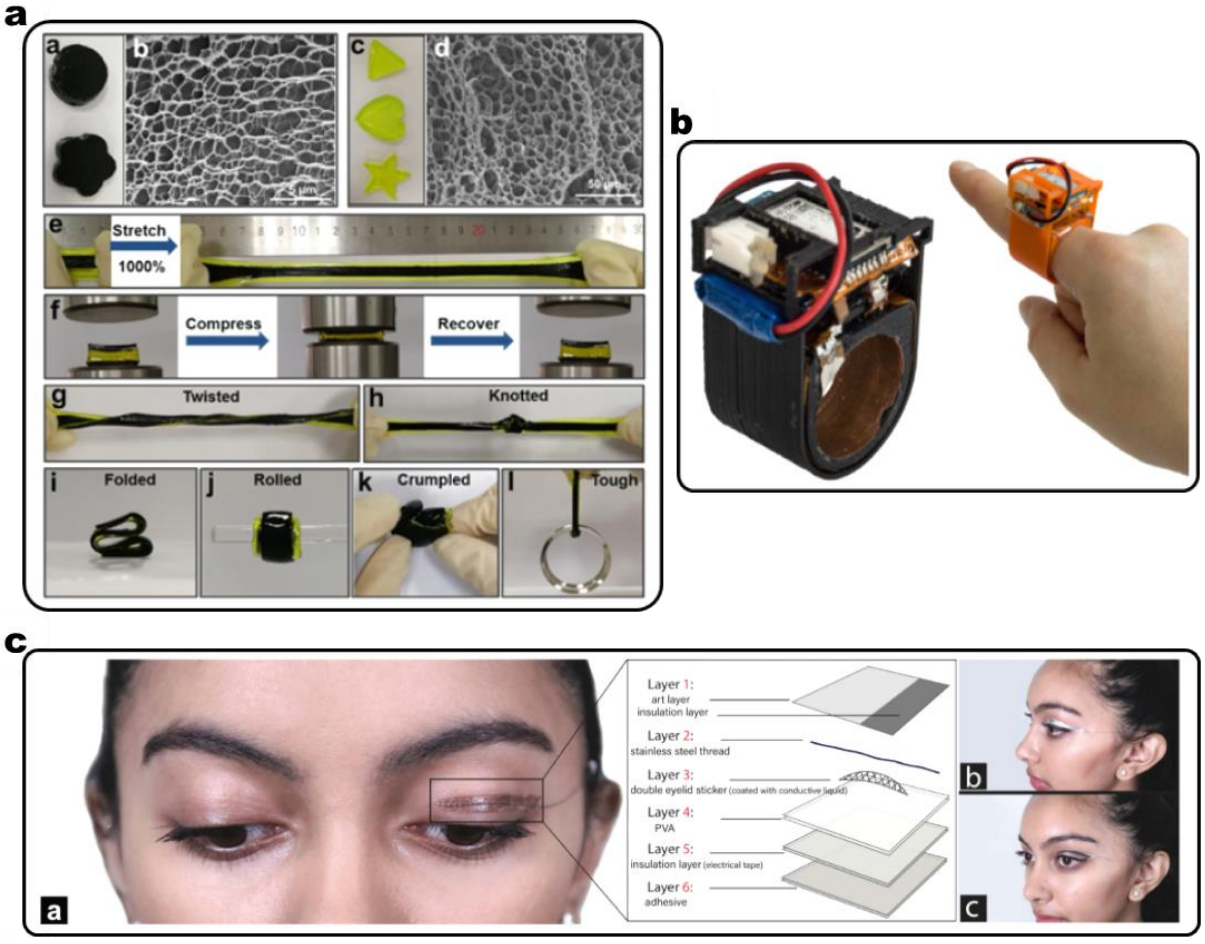

Fig. 7 a) Electrode hydrogel with different geometries and deformations [90]. b) PeriSense finger ring prototype enabling multi-finger gesture recognition [93]. c) Eslucent, an eyelid on-skin interface for tracking eye-blinking [95].

1.4.2 *Biomedical and human health monitoring*

With current healthcare systems facing ever increasing expenses, governments struggled to seek solutions that rendered adequate medical care without increasing healthcare costs [96]. Preventive and personalized treatment approaches, that changed with health status, could be utilized for early disease detection and diagnosis [97]. Health monitoring systems and their interface to the human body could measure various signals with high specificity and sensitivity [98]. As aforementioned in Section 4.1, micro and nanostructured capacitive sensors could aid in providing a means to real-time human health monitoring and biomedical analytics.

Sekar et al. discovered a new approach to simultaneously evaluate coagulation function, platelet count / function, and hematocrit using a carbon nanotube-paper composite (CPC) capacitance sensor [99]. The high sensitivity of the CPC sensor showed sensitivity towards multiple clotting elements. Lei et al.'s mineral hydrogel, self-healable, capacitive pressure sensors (Fig. 8a) were responsive in detecting a subject's blood pressure that was raised or lowered by an aerometer [91]. A dental model for bite force mapping utilizing capacitive pressure sensors (see Fig. 8b) was shown by Iwasaki et al. [100]. Continuous human gait analysis was explored by Park et al [101]. In Fig. 8c a porous PDMS dielectric structure with composite electrodes formed a capacitive pressure sensor, which could be placed in an insole for real-time gait-signal monitoring.

Capacitive sensors have also been widely used as a wearable solution to real-time respiratory monitoring [102-105]. Kundu et al. showed a conductive textile-based wearable capacitive sensor for respiratory rate sensing. The sensor consisted of two conductive textile electrodes that can be easily integrated into garments [102]. Fig. 8d shows Hoffmann et al.'s respiratory monitoring system based on capacitive textile force sensors. Different respiration

patterns were reliably detected and could be subdivided even during intensive motion of the person [103].

He et al. investigated a wearable microstructured capacitive pressure sensor (see Fig. 8e), which could detect speech and air blowing, when fastened to a subject's throat or cheek [36].

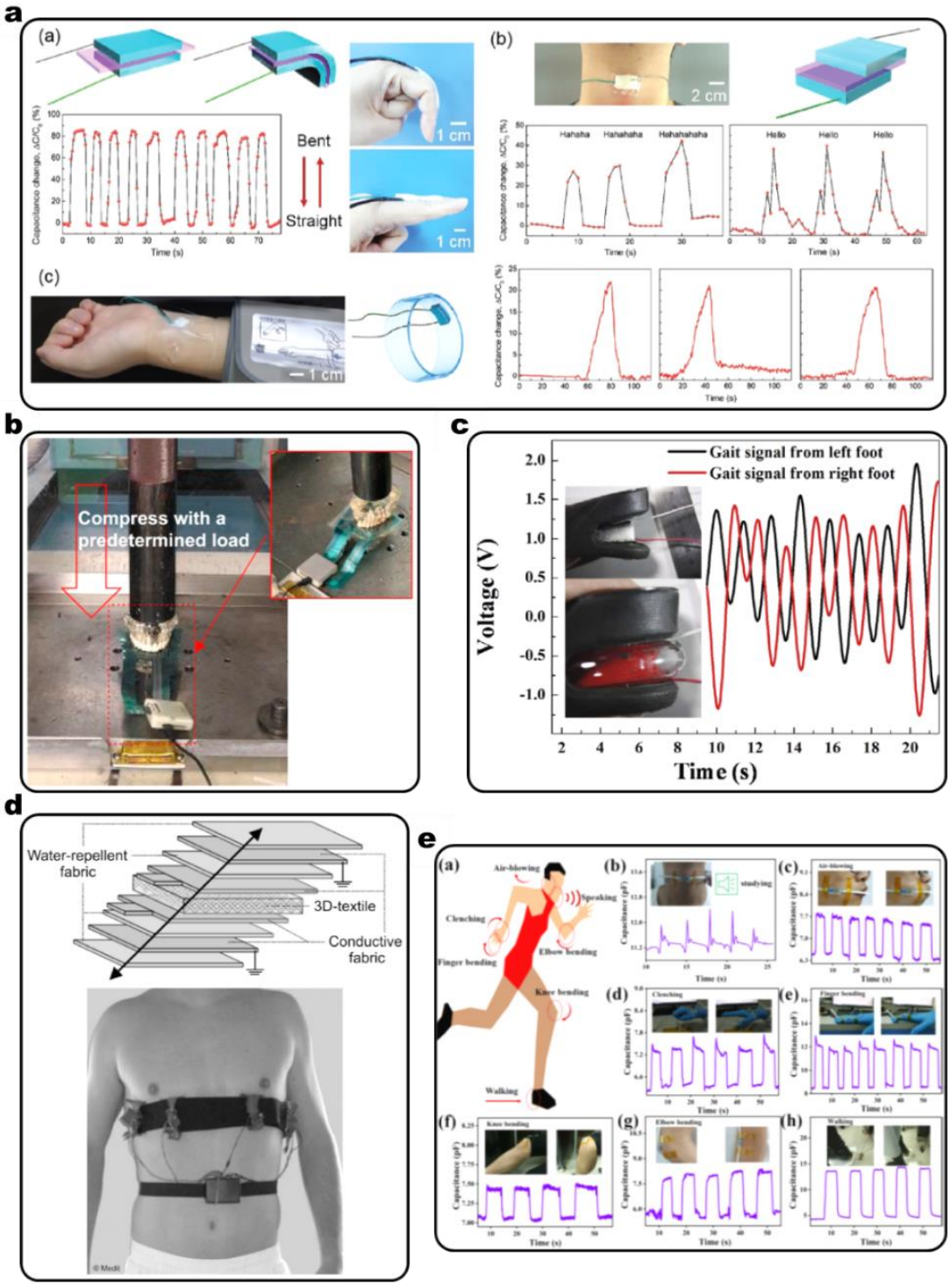

Fig. 8 a) Schematic design and real-time capacitance signals of finger motion, throat motion and blood pressure [91]. b) Capacitive pressure mapping sensor installed on a dental model to deduce bite-force [100]. c) Record of left and right foot gait signal using smart insole system [101]. d) Force based respiration measurement system [103]. e) Capacitive pressure sensor responses of vocal cord vibration, repeated air blowing, clenching, releasing of finger/knee/elbow bending, and walking [36].

1.4.3 *Robotics and industrial monitoring*

Robots have been developed with the hope of aiding human activities with manipulating objects in unstructured environments. Although, versatile manipulation has been achieved, robots cannot dexterously manipulate objects of different weights unlike humans [106]. A broad range of sensors are currently implemented into robotic systems to enable safe and efficient operation. Capacitive sensor systems have been used to equip robots with perception capabilities, using the electrical properties of conductive objects to measure physical quantities [107]. Moreover, micro and nanostructured capacitive sensors offer unprecedented sensitivity and flexibility that allows for unobtrusive integration into next generation multiple degree-of-freedom (DOF) systems. Fu et al. developed a capacitive tactile sensor for robotic hands [106]. The sensor had a carbon nanotube / PDMS dielectric, which aided in improving sensitivity. When integrated into a robotic gripper, the system could successfully differentiate object shapes and manipulate light and heavy objects with closed-loop pressure feedback. In other work, a capacitive strain gauge based on nanotube networks was demonstrated as an angle transducer for a robotic four bar linkage (see Fig. 9a) [31].

Structural health monitoring is a key aspect in ensuring long life span of large-scale infrastructure. Traditional non-destructive testing methods, such as ultrasonic waves, acoustic emission, thermography, and vibrothermography, cannot be applied in real-time [108] and required cumbersome electronic hardware. Ni et al. explores a transparent capacitive sensor for structural health monitoring applications [108]. The capacitive sensor was fabricated using a dielectric elastomer with ionic (polyacrylamide hydrogel with hygroscopic salt and lithium chloride) stretchable transparent electrodes. The sensor proved its ability to detect small cracks on an over-reinforced concrete beam. Qiu et al. investigated flexible capacitive elastomeric sensors for compressive strain measurements [34]. Fig. 9b shows the elastomeric compressive strain sensor

configured to perform structural health monitoring of concrete structure under compressive loading. Conductive carbon black nanoparticles were dispersed and controlled in the dielectric layer to increase sensitivity.

The majority of microfabricated flow sensors were designed using the principles of asymmetric thermal conduction or piezoresistive sensors [109]. However, these traditional systems posed several drawbacks, as heated elements near combustible liquids/gases were dangerous. Piezoresistive sensors were highly susceptible to ambient temperature changes. Nguyen et al. developed a silicon-on-insulator (SOI), comb-drive capacitive sensor for gas flow velocity detection (see Fig. 9c) [109]. In another work, vertically-aligned carbon nanotube electrodes were utilized within a capacitive deionization (CDI) system to filter brackish water [110].

High volume commercial devices like condenser microphones relied on advancements in microstructured capacitive sensors to capture a large frequency range and had a good transient response. The bending membrane fluctuating with a sound input contributed greatly to the microphone's performance. Torkkeli et al. demonstrated a low-stress polysilicon membrane and high-stress polysilicon backplate capacitive microphone [111]. The study showed a microphone with a membrane area of 1 mm^2 could be fabricated (Fig. 9d).

Table 2 provides an applications summary of reviewed capacitive sensors, with respect to material, structure, detection metric and electrical field.

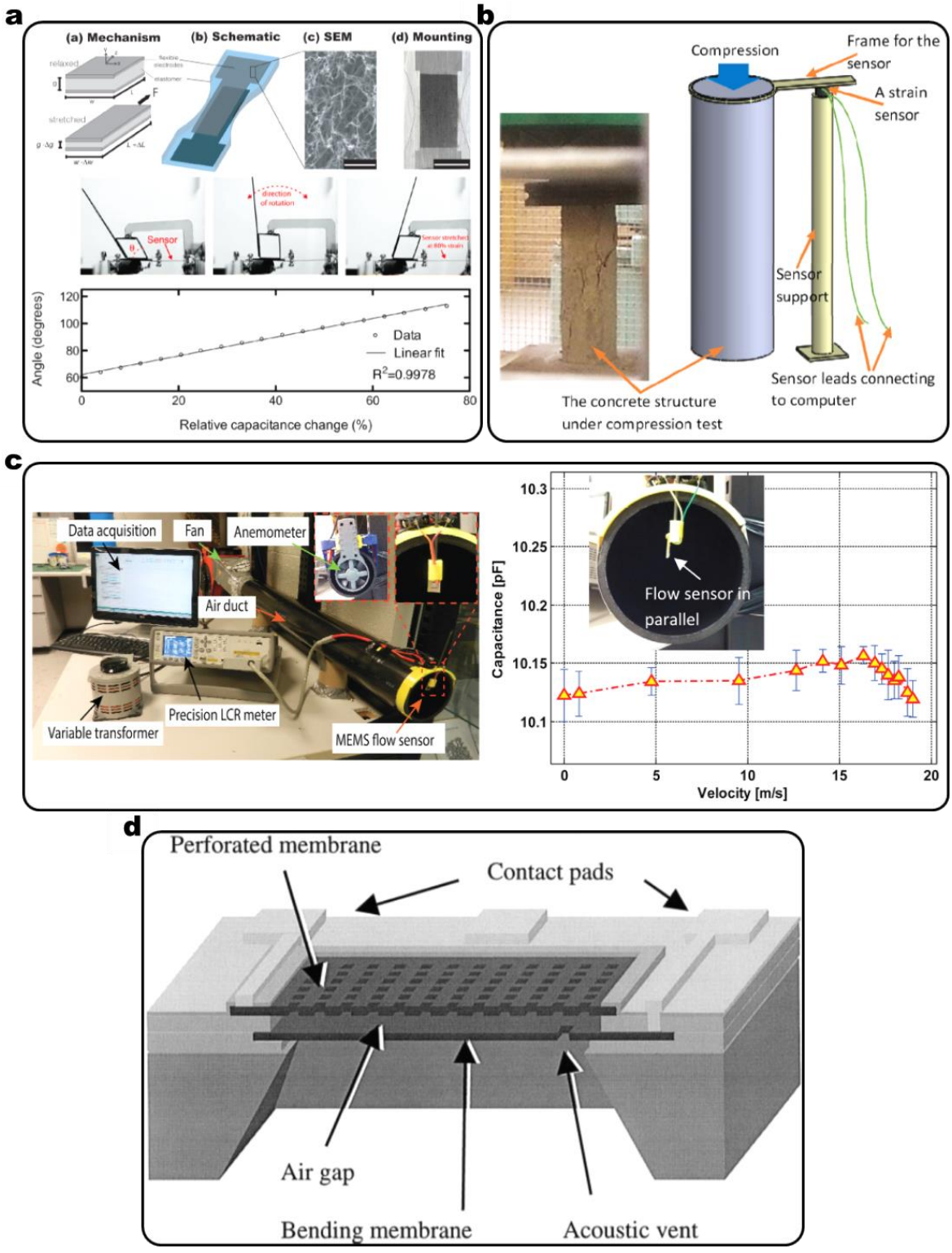

Fig. 9 a) Demonstration of sensor as an angle transducer for a robotic four bar linkage [31]. b) Diagram of how a nanocomposite strain sensor is configured to perform structural health monitoring in civil engineering [34]. c) Response of a capacitive flow sensor when it is placed parallel to the air flow [109]. d) Low-stress polysilicon membrane capacitive microphone [111]

Table 2. Applications of micro and nano structured capacitive sensors.

Application	Materials Used	Structure	Capacitive Detection Metric	Electric Field	Reference
Wearable and HMI	Cu thin film	Single electrode array	Proximity	Fringing	[93]
	Ag nanoparticles and conductive fibers	Crossbar structure	Pressure	Uniform	[24]
	Carbon nanotubes	Parallel plate	Strain	Uniform	[90]
	Carbon nanotubes	Co-planar	Proximity	Fringing	[94]
	PEDOT: PSS liquid conductor	Parallel plate	Pressure / Proximity	Uniform	[95]
Biomedical and Human Health Monitoring	SOI	Interdigitated electrode	Acceleration	Uniform	[67]
	Ti/Cu coated glass	Parallel plate	Pressure	Uniform	[25]
	Platinum microparticles	Co-planar	Pressure	Uniform	[29]
	Gold film and polysilicon	Parallel plate	Temperature	Uniform	[57]
	PDMS	Parallel plate	Temperature	Uniform	[58]
	ACC/PAA/alginate hydrogel	Parallel plate	Pressure	Uniform	[91]
	Polymer type carbon paste	Interdigitated parallel plate	Pressure	Uniform	[100]
	MWCNT/PEDOT:PSS composite and Porous PDMS	Parallel plate	Pressure	Uniform	[101]
	Conductive Ag fabric and 3D textile	Parallel plate	Force	Uniform	[103]
	Conductive textile network	Parallel plate array	Proximity / Contact	Uniform/Fringing	[112]
Robotics, Industrial Monitoring	Screen printing	Parallel plate	Pressure	Uniform	[30]
	Au nanoparticles	Parallel plate	Displacement	Uniform	[61]
	Al and polysilicon	Parallel plate	Displacement	Uniform	[113]
	SOI	Interdigitated electrode	Displacement	Uniform	[109]
	Carbon black nanoparticles	Parallel plate	Strain	Uniform	[34]

1.5 CONCLUSION

In this paper, we reviewed the fabrication techniques, sensing mechanics, and applications of micro and nanostructured capacitive sensors. Different capacitive sensors targeting applications like wearable sensors, HMI systems, biomedical devices, human health monitoring systems, robotics, and industrial monitoring systems were discussed in this review. The fabrication methods used were focused on expanding and optimizing microfabrication techniques. Different material groups like carbon nanomaterials, elastomeric composites, metallic nanomaterials, and polymer compounds were noted as key components in the development of next-generation capacitive sensors. The controlled dispersion of nanomaterials into dielectric layers and electrodes was a highlight, as they proved to increase sensitivity while maintaining flexibility and a small form factor. The selection of materials and sensor format varied based on desired functionality. As the range of applications for micro and nanostructured capacitive sensors continue to grow, new novel materials and fabrication methods will need to be continually discovered to fulfill the demand.

Chapter 2. INTRODUCTION TO EYE TRACKING TECHNOLOGIES

The primary goal of this research is to design a nanostructured capacitive eye tracker and investigate its capabilities for human gaze monitoring. Carbon nanotube paper composite (CPC) capacitive sensors will be fabricated to enable a highly sensitive, non-invasive and wearable eye tracking device. This chapter will explore the advances and uses of wearable sensor technologies. Then, delve into recent developments in eye tracking alongside the benefits of eye tracking with respect to human-machine interface (HMI) applications.

2.1 WEARABLE SENSORS

A wearable sensor can be defined as a self-contained integrated device that can provide quantitative or qualitative information using a biological recognition element [114]. It comprises of three main elements: a physiological receptor (sample), transducer (sensing element), and signal processor (data analyzer). With the rapid development of microprocessor chips and micro / nanoscale fabrication methods, traditional wearable sensors have evolved into thin, flexible, highly sensitive substrates. Advancements in manufacturing and packaging technologies have enabled the integration of microelectronic and micromechanical sensors into minuscule rigid or flexible substrates with high sensitivity and low-cost [115]. These advancements coupled with interchanging desktop processors with mobile technologies (i.e., smartphones, tablets etc.) has allowed wearable sensors to challenge the arena of affordable healthcare, enabling point-of-care monitoring, and non-invasive analysis of an individual's vital physiological elements [116]. Eye trackers, heart rate monitors, sleep monitors, fitness trackers and smart glasses are examples of a multitude of sensory devices that can be classified as a form of wearable sensor devices. A key indicator of growth in wearable sensors is the expansion of the global market for wearable medical

devices, with BBC Research suggesting a $8.9 billion market share in 2018 rising to $29.9 billion by 2023.

Though chipset and microprocessor advancements have aided in the development of the wearable sensor, the quintessential element in reducing scale and increasing accuracy has been the advent of nanostructured manufacturing. A nanostructure is an object with at least one dimension equal to or smaller than 100 nanometers (nm) [117]. There are various nanostructures such as; nanoparticles, nanopores, nanorods, nanowires, nanoribbons, nanotubes. Carbon-based nanostructures display unique properties and morphological flexibility, which is characteristically multifunctional and compatible with detecting variations in organic and inorganic systems [118]. Specifically, carbon nanotubes (CNT) have aspect ratios in the order of thousands, which renders high specificity and sensitivity. The molecular dimension is ideal for low-power operation for a wide range of wearable sensors [118, 119].

2.2 EYE TRACKING

The study of eye movements is a source of valuable information to both clinicians and scientists. Abnormalities of ocular motility are frequently a sign to the localization of a disease process. The study of the control of eye movements can present an opportunity to understand the mechanisms of the brain. Visual and perceptual consequences of eye movements are important to both clinicians and scientists, with the information from the study of eye movements contributing to the knowledge of motor control [120, 121].

The three main functional classes of human eye movements critical to neurological studies are smooth pursuit, visual fixation, and saccades. Smooth pursuit holds the image of a small moving target on the fovea and aids gaze stabilization during continued head movement. The pursuit system, however, generates smooth tracking movements of the eyes that closely match the

pace of the target. To overcome the delays inherent in the visual system (the latency of responses, which ranges between 70-120ms), predictive mechanisms can adjust the eye movements when the motion of the target can be anticipated. The brain relies on numerous sensory inputs and its own motor efforts to determine the motion of an object during smooth pursuit. Thus, diminished smooth pursuit may be construed as a sign of neurologic dysfunction [120].

Visual fixation of a stationary object represents a special case of smooth pursuit, where there is suppression of ocular motion. This mechanism reflects the ability of the visual system to detect retinal image motion caused by unwanted drift of the eyes and initiate corrective movements. Another aspect of steady fixation is the ability to suppress saccadic eye movements that turn the fovea away from the object of interest. Thus, certain neurons in the frontal eye fields and superior colliculus seem important for suppressing saccades when steady fixation of a target is necessary. The concept of a fixation system becomes important in certain disease states [120].

Saccades, convey images of objects of interest onto the fovea. Saccades can be triggered by objects seen, heard, from memory, or as part of an involuntary motion to scan a visual scene. There is usually a delay of about 200 msec from the stimulus for a saccade and its presentation, with this time presumably including neural processing in the retinal, cerebral cortex, superior colliculus, and cerebellum. Furthermore, neural instruction for voluntary saccades can also arise from brain stem neurons in the paramedian reticular formation that generate the quick phases of nystagmus (involuntary up/down, side to side, or circular motion of the eyes) [120, 121].

Eye movement has been investigated for neurological disorders since the beginning of the 19th century [116, 122]. Real-time monitoring of eye movement is crucial to correlate neural activity accurately. With current oculomotor research turning to optogenetics [123, 124], light is used to manipulate the activity of specific neurons with high temporal resolution. The real-time

characteristics of an eye-tracking device are essential to describe the effects of an optical excitation on eye movement [125].

The gold standard eye-tracking device for oculomotor research has been the scleral search coil system [126, 127]. Other than an invasive method, eye trackers have been developed with a camera-based imaging system, piezoelectric sensors, electrooculography (EOG), and capacitive sensors. With significant progress of semiconductor chips and image processing technology, the eye trackers using a camera are most popular with high accuracy. Current camera-based eye tracking systems include eyeglass-mounted monitors and stationary monitors, both of which are inconvenient for usability. For example, existing measures of eye movement require wearing specific monitoring hardware and frequent manual calibration. Camera-based tracking systems are sensitive to the subject's movement. Bulky equipment significantly complicates inspection, limiting the application to wearable applications. The high cost of current eye-tracking systems is an additional burden to render eye monitoring accessible to patients. It has also been questioned if the assessment in laboratory settings represents the behavior in real life.

EOG is frequently used to monitor eye movement, which requires cumbersome electrical contact on skin and trained personnel for measurement. A capacitive sensor array was developed to determine eye gaze detection [128]. The movement of the eyeballs, muscles, and eyelids induced a change in the capacitance of a capacitor placed at a fixed point near the eye [129]. However, the sensitivity was insufficient for precise measurement for eye movement. A truly versatile, non-invasive, low cost, eye tracker has yet to be realized.

2.3 CURRENT EYE TRACKING TECHNOLOGIES

2.3.1 *Camera based eye trackers*

To date, most commercial eye trackers are based on video cameras and image processing algorithms. The system is both bulky and expensive, and usually requires trained personnel to operate them. Because of these challenges, very few eye movement studies have been conducted outside the controlled lab environment. Eye tracking technology has been used in several different fields including human-computer interface for assisting a disabled person in interacting with a computer. For instance, an eye gaze tracker may be used as a mouse emulator for a personal computer, helping a disabled person move a cursor on a display Screen to control their environment and communicate messages with their eyes. Gaze tracking has also been used for industrial control, aviation, and emergency room situations where both hands are needed for tasks other than operation of a computer. Eye gaze tracking systems have used cameras positioned on a wearable headgear frame to measure eye movement/position. Non-intrusive eye tracking most commonly uses a technique called pupil corneal reflection (PCR) [121, 130]. A light source is used to illuminate the eye causing highly visible reflections, which are captured by a camera to track the movements of the eye. Dark pupil tracking, where a light source is placed away from the optical axis causing the pupil to appear darker than the iris, is the preferred PCR approach (refer to Fig. 10) [131]. Unlike bright pupil tracking, where the illumination source must be co-axial to the camera causing the pupil to be ‘lit up’, dark pupil tracking doesn’t pose such restrictions on the camera and illumination source. Dark pupil PCR has become an industry-standard technique, currently being used by Applied Science Laboratory, LC Technology, and Tobii Systems [121].

PCR systems are inherently plagued by low sampling rates (up to 220 Hz), low accuracy in bright environments, range of view, and lack of torsional data. Furthermore, the use of a camera

to monitor eye movement and position can be problematic due to the cost of camera equipment, high power requirements, and the bulk or obtrusiveness of a camera mounted on the headgear [128, 132].

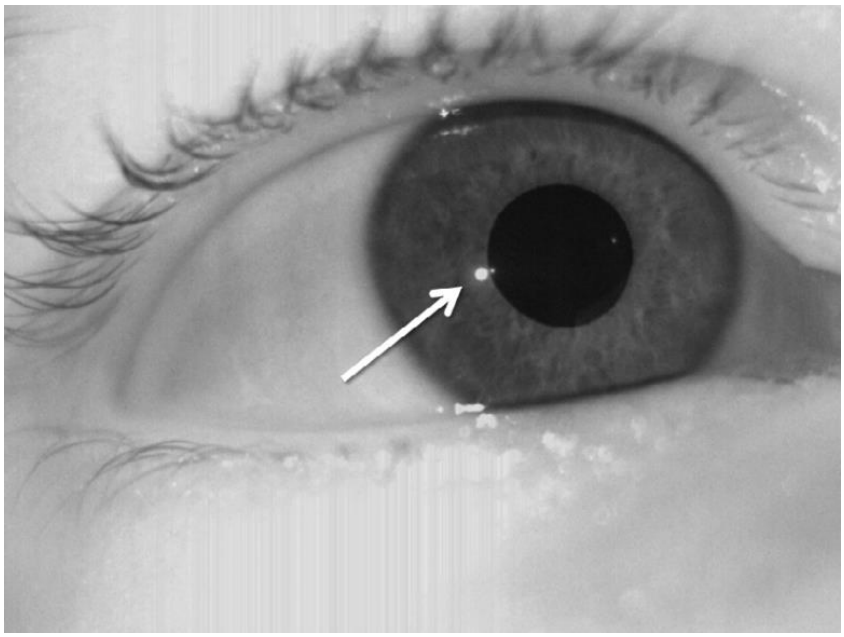

Fig. 10 High-definition infra-red eye image. The bright white spot marked with a white arrow left of the pupil is the corneal reflection (PCR) [130].

2.3.2 *Electrooculogram*

Investigation of brain activity specific to eye movement control is commonly measured via electroencephalographic (EEG) signals and eye movements simultaneously. Saccadic eye movements can also be measure through electrooculography (EOG). EOG is based on the mechanism that the eyes are the origin of a steady potential field that can be modeled as a dipole with its positive pole at the cornea and negative pole at the retina. With electrodes placed in the periocular region (around the eyeball) to measure changes in electrical potential. As the eyes move from a center position to a peripheral point, the cornea nears one electrode while the retina approaches another. The change in the orientation of the dipole results in a change in the measured EOG signal. EOG signals vary between 250 and 1000 mV, with a frequency range of 0 to 30 Hz.

Acuna et al. (2014) investigated the eye-tracking capabilities of low-cost EOG system. The study tested eye gaze angles of ± 30^{o} horizontal and ± 50^{o} vertical. Vertical gaze estimation was noted to perform poorly with correct estimation only within 5^{o} [133]. Horizontal signals presented linearity within ± 30^{o}. Jia et al. (2019) investigated the measurement of saccadic eye movements by EOG for simultaneous EEG recording [134]. The study showed saccadic eye movements and blinks could be identified at a bandwidth of 500 Hz. However, simultaneous recording of EOG and scalp EEG were required to achieve results as accurately as typical optical eye-tracking devices.

2.3.3 *Magnetic scleral search coil*

The scleral search coil is worn by a subject in the form of a contact lens. The lens contains a hollow center to maintain unobstructed vision with a primary and torsion coil (Fig. 11). The primary coil lies in a plane perpendicular to the line of sight, with the torsion coil lying parallel to the line of sight. This enables a measure of directional (vertical and horizontal eye movement) and torsional eye movement. A typical magnetic scleral search coil system has two pairs of orthogonal field coils oscillating at non-harmonic frequencies, in a 1 m^{2}, producing a magnetic field intensity of 0.088 gauss. Overall bandwidth is at least 1000 Hz, signal-to-noise ratio is 65 dB, with less than 0.1^{o} crosstalk between channels and resolution of better than 0.05^{o}. However, two sets of fields coils are not sufficient for measuring eye orientation in three dimensions. Thus, a third pair of fields coils is added for accurate ocular tracking. The maximum voltage is induced in the coil when it is parallel to a given set of field coils, with the minimum voltage induced when it is orthogonal to the same field coils. The coil area visible to the field determines how much signal is picked up from that field. The human subjects must head be restrained to ensure a baseline coordinate system for the search coil during use. The resolution, linearity, range, stability and simultaneous measure

of horizontal, vertical and torsional movement have made the scleral coil the gold standard in eye tracking [121, 135]. However, due to its invasive nature, surgical implantation requirements and bulky processing hardware, the sclera search coil is seldom used outside of scientific research settings.

Whitmire et al. (2016), introduced a study investigating a wearable scleral search coil tracking system, which eliminated the need for a head restraint and large field coils [136]. The EyeContact scleral coil system mounts five rigid field coils within a virtual reality headset, creating a mobile magnetic field around a subject's head. The system was tested on a x-y-z mechanical test rig, capable of adjusting the orientation and position of a scleral coil within the headset. Gaze tracking was estimated using two methods; physical model and neural network model. The physical and neural network model produced a mean gaze error of 0.18° and 0.094°, respectively. Accuracy of the neural network model was sacrificed for higher data sampling rates.

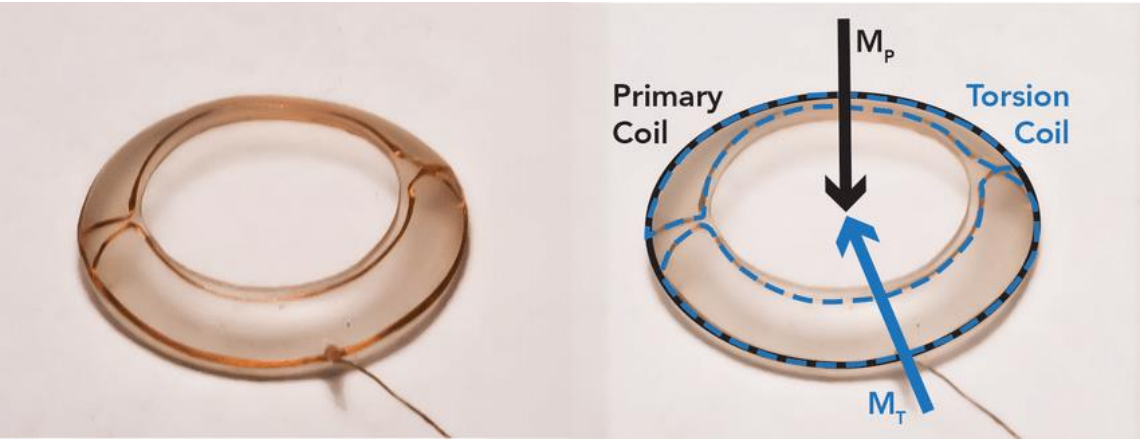

Fig. 11 Scleral search by Chronos Vision, with a primary and torsion coil embedded within a contact lens [136].

2.4 CHALLENGES

Eye tracking sensors have proven essential to wearable technologies in virtual and augmented reality (VR and AR), disease diagnosis, and HMI settings. However, current eye systems are hindered by bulky electronics, high power consumption, low sampling rates, and highly sensitive devices restricted to high-cost laboratory environments.

A capacitive sensing eye tracker could be the solution to alleviate the disadvantages seen with current eye tracking technologies. Capacitive sensors have been widely applied to various types of proximity sensing on monitoring a human's activities [10, 137]. Gesture recognition has been realized by capacitive proximity sensor array [112]. A car seat with a capacitive proximity sensor system has also been developed to monitor a driver to recognize their inattentiveness.

Eye gaze tracking using capacitive sensors is based on the specific shape of the eye. Specifically, the cornea of an eye bulges or extends from the eye socket and otherwise spherical shape of the eye. The direction of a user's gaze may be determined based on the proximity of the bulge in the cornea to the capacitive sensor positioned in front of the eye. Such an eye tracking system using capacitive sensors may therefore be configured to each individual user based at least on universal aspects of all potential users or individual aspects of the shapes of a user's eyes. Microsoft patent US2016/0353988 A1, describes a plurality of capacitive sensors (array) to detect the proximity of the eyeball during eye movement. It consisted of a eyeglasses frame, designed to support an array of capacitive sensors positioned in front of the eye. Control circuitry designed to receive signals from the sensor array, with an electrode grounded to the subject's body. Using an array of capacitive sensors, however, increases the parasitic capacitance and results in low sensitivity.

The current challenges plaguing capacitive eye tracking technology are: (1) Lack of an interaction model between capacitance and eye movement, (2) High fabrication cost and complexity of an array with numerous sensors in a miniature form. (3) Bulky sensor design with low sensitivity and resolution. (4) Imprecise sensor location without optimization based on the anatomical structure of the eye and its movement.

Therefore, an unobtrusive capacitive sensor array with high sensitivity, wearability, and small form factor is critical to facilitate future eye tracking applications.

2.5 OBJECTIVES

It is hypothesized that a limited number of CPC capacitive sensors can be used to effectively monitor human eye movements with high sensitivity, non-invasive form factor, with low power consumption and at low cost, for human-machine interface applications. To test the hypothesis, the specific objectives in this dissertation are:

1. To investigate the interaction between eyeball movement and capacitive sensors using single and differential signal inputs, and develop an interaction model of facial geometry, eye movement, and human body charges on capacitive sensitivity.
2. To characterize capacitance signals for up-down and left-right eye movements and compare a prototype wearable eye tracker to a commercial camera-based system.
3. A primate study in conjunction with Washington National Primate Research Center (WaNPRC). To validate the performance of the capacitive eye tracker against the scleral search coil, the *gold standard* in eye tracking.

Chapter 3. CAPACITIVE EYE TRACKER MADE OF FRACTURED CARBON NANOTUBE-PAPER COMPOSITES FOR WEARABLE APPLICATIONS

3.1 INTRODUCTION

Since naked-eye observation in 1879, eye movement has been investigated for diagnosing neurological disorders [116, 122], sleeping disorders [138, 139], and learning disabilities [140, 141]. For example, deficits in making saccades to a memorized location and suppressing a planned-saccade are potentially associated with intellectual disability, epilepsy, cerebellar ataxia [142], and other disorders related to metabolic diseases [143, 144]. Abnormal saccades are also associated with several neurological disorders, including Creutzfeldt-Jakob disease [145], autism [146], Parkinson's disease [147], and Huntington's disease [148].

A study of the oculomotor system correlates eye movements with neuronal activity in different areas of the brain [149-151]. To accurately describe this relationship, an eye-tracking sensor needs to capture both spatial and temporal characteristics of eye movement with high fidelity [152]. With current oculomotor research turning to optogenetics [123, 124], light is used to manipulate the activity of specific neurons with high temporal resolution. The real-time characteristics of an eye-tracking device are essential to describe the effects of an optical excitation on eye movement [125].

The gold standard for oculomotor research has been the scleral search coil system [126, 127, 153]. The scleral search coil system has the advantage of real-time, low-latency electronics, low noise, and high accuracy (< 0.1°) [154]. Currently, camera-based eye-tracking systems are the major workhorse for commercial applications. Due to the high demands for power and

computational resources, current wearable eye trackers are tethered to a battery and a high-performance processor.

To address the challenges, other methods have been attempted. When eyes move, the polarization of the retina can be measured with electrooculography (EOG) [133, 155]. Graphene electrodes have been used to improve the electrical interface to the skin [156]. Another eye-tracking technique measures the voltage generated by a piezoelectric nanogenerator attached to the eyelid [157, 158]. In contrast to the contact methods, a capacitive sensor has the potential to determine eye gaze direction [128]. The movement of eyeballs, muscles, and eyelids induces a capacitive change with respect to a fixed point near the eyeball [129]. However, traditional capacitive sensors have not been able to produce an accurate eye tracking.

This chapter presents a wearable capacitive sensor made of a pair of asymmetric electrodes; one is carbon nanotube paper composite (CPC) fibers, and the other is a rectangular metal electrode. CPC is chosen as the electrode material because the high aspect ratio of the CPC fibrous structure increases the surface area and capacitance, acting as micro-sized antennas and improving sensitivity. These fibrous antennas sticking out of the CPC are fabricated by a wet-fracture method, which allows for flexibility and miniaturization suitable for wearable eye tracking devices. The capacitive interaction between asymmetric electrodes and a spherical eyeball is analyzed by numerical study. Using a face simulator, both single- and differential capacitive measurements are characterized to correlate eyeball movement and capacitive changes in terms of proximity, geometry, and human body charge.

3.2 CAPACITIVE EYE TRACKER

The wearable eye tracker envisioned is an eyeglass frame with integrated capacitive sensors (Fig. 12a). The miniaturized sensors allow for integration into existing headgears, such as

virtual reality (VR) headsets. To fit individual face shapes, malleable mounts are used to adjust the sensor location and distance (Fig. 12b). Fig. 12c shows the geometry of the designed sensor that has 1 x 5 mm^2 area with 0.1 mm thickness. For capacitive measurement, the asymmetry in the geometrical shape of the eyeball near the scleral-corneal junction causes the distance change of the eyeball surface to the sensor under rotation. The distance change affects the fringing electric field, which in turn changes the capacitance.

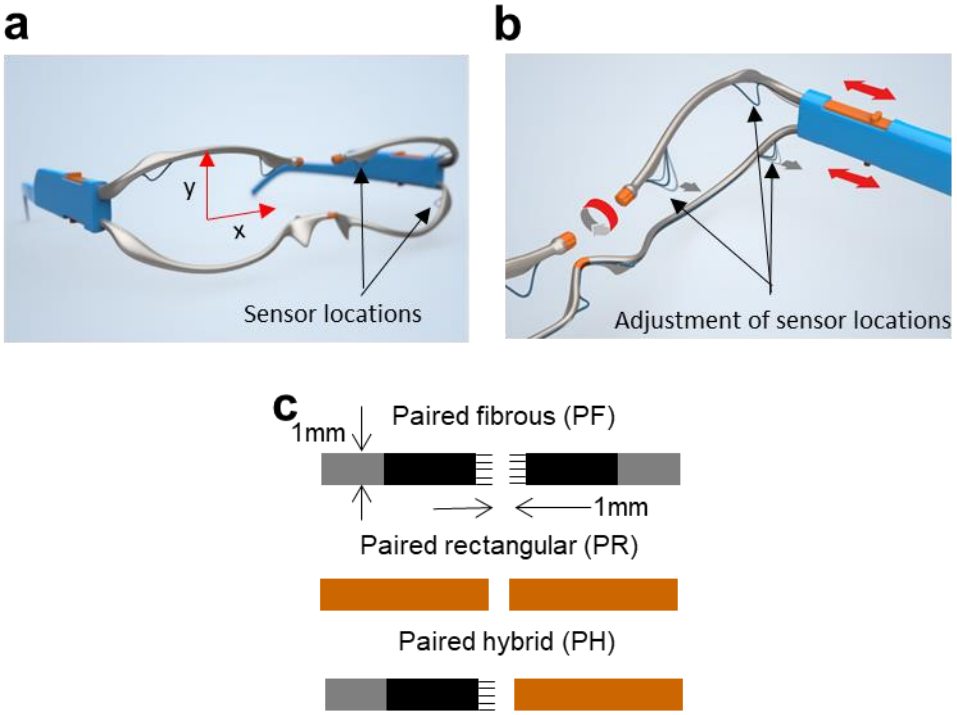

Fig. 12 (a) Prototype design of an eye tracker. (b) Adjustment of sensor distance to the human eyeball. (c) The tested capacitive sensors consist of paired fibrous (PF), paired rectangular (PR), and paired hybrid (PH) electrodes.

Three different electrode combinations were tested for sensitivity evaluation by numerical computation. One was paired fibrous (PF) electrodes, another was paired rectangular (PR) electrodes, and the last one was paired hybrid (PH) electrodes consisting of fibrous and rectangular electrodes. The capacitive sensitivity was defined as the ratio of capacitance change to distance change ($\Delta C/\Delta d$), where C was the capacitance and d was the distance between a sensor and an

eyeball. A numerical model was built for the three sensor configurations with an eyeball. The rectangular metal electrode was 40 x 10 μm^2 in cross-section and 1 mm in length. The fibrous electrode was composed of four fibers having 10 x10 μm^2 in cross-section and 1 mm in length.

A COMSOL numerical model was built to study the proximity sensitivity of a capacitive sensor. Fig. 13a shows the geometry of a spherical object mimicking an eyeball and paired electrodes for capacitive detection. Capacitive sensors were placed at the bottom of a square domain with air permittivity. One side was 25 mm. The potential of 5V was applied between two electrodes. The capacitive sensors were made of paired rectangular (PR), paired fibrous (PF), and paired hybrid (PH) electrodes (Fig. 13b, c, and d). Three different types of geometries were compared to study a capacitive sensitivity to proximity detection of a charged object. For all the electrodes, the total volume was designed to be the same. The rectangular electrode was represented by a monolithic rectangular slab with has a cross-section of 40x10 μm^2 with 1 mm in length. The geometry of the fibrous electrode was created by placing four parallel rectangular fibers at 20 μm apart. Each electrode had 10x10 μm^2 in cross-section and 1 mm in length. For hybrid electrodes, 5V was applied to the fibrous electrode while the rectangular electrode was grounded. A 25 kHz frequency was applied for an electrostatic model. The sphere had a dielectric constant of 80. For all configurations, the gap size was 1 mm. The 5 mm diameter target represented a capacitive sensing target floating in the center. The observed capacitance was calculated from the imaginary part of the admittance, which is:

$$C = \frac{imag(Y_{11})}{\omega} \tag{3.7}$$

Where the symbol Y is the observed admittance at an electrode, and the ω is the excitation radian frequency, which is 50,000 πrad/s.

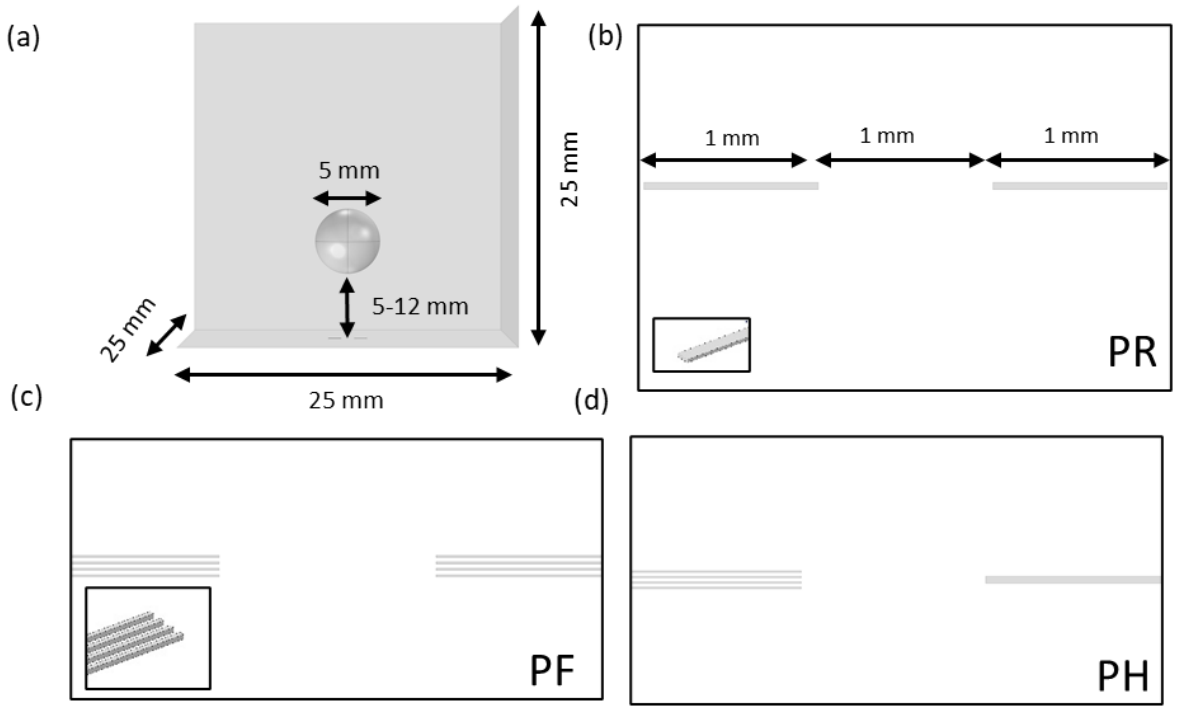

Fig. 13 (a) Geometry and boundary conditions of the numerical analysis. (b) Paired rectangular (PR) electrode configuration. (c) Paired fibrous (PF) electrode configuration. The inter-electrode gap is 20 μm wide. (d) Paired hybrid (PH) electrode configuration.

The gap size was 1 mm. A 5 mm-diameter sphere, representing an eyeball, floats in the center (Fig. 14a). A 5V AC potential with 25 kHz frequency is applied between the two electrodes. For hybrid electrodes, 5V is applied to the fiber electrode while the rectangular metal electrode is grounded. The relative permittivity of a spherical object is 80.

The ΔC due to the fringing electric field could be computed by either single (Fig. 14b) or differential methods (Fig. 14c). The single method was convenient but suffered from the nonlinear relationship between capacitance and rotation angle. The differential method applied AC voltage 180° out of phase to the second sensor. The differential method doubled the sensitivity, canceled the nonlinearity, and, therefore, produced better linearity between capacitance and rotation angle.

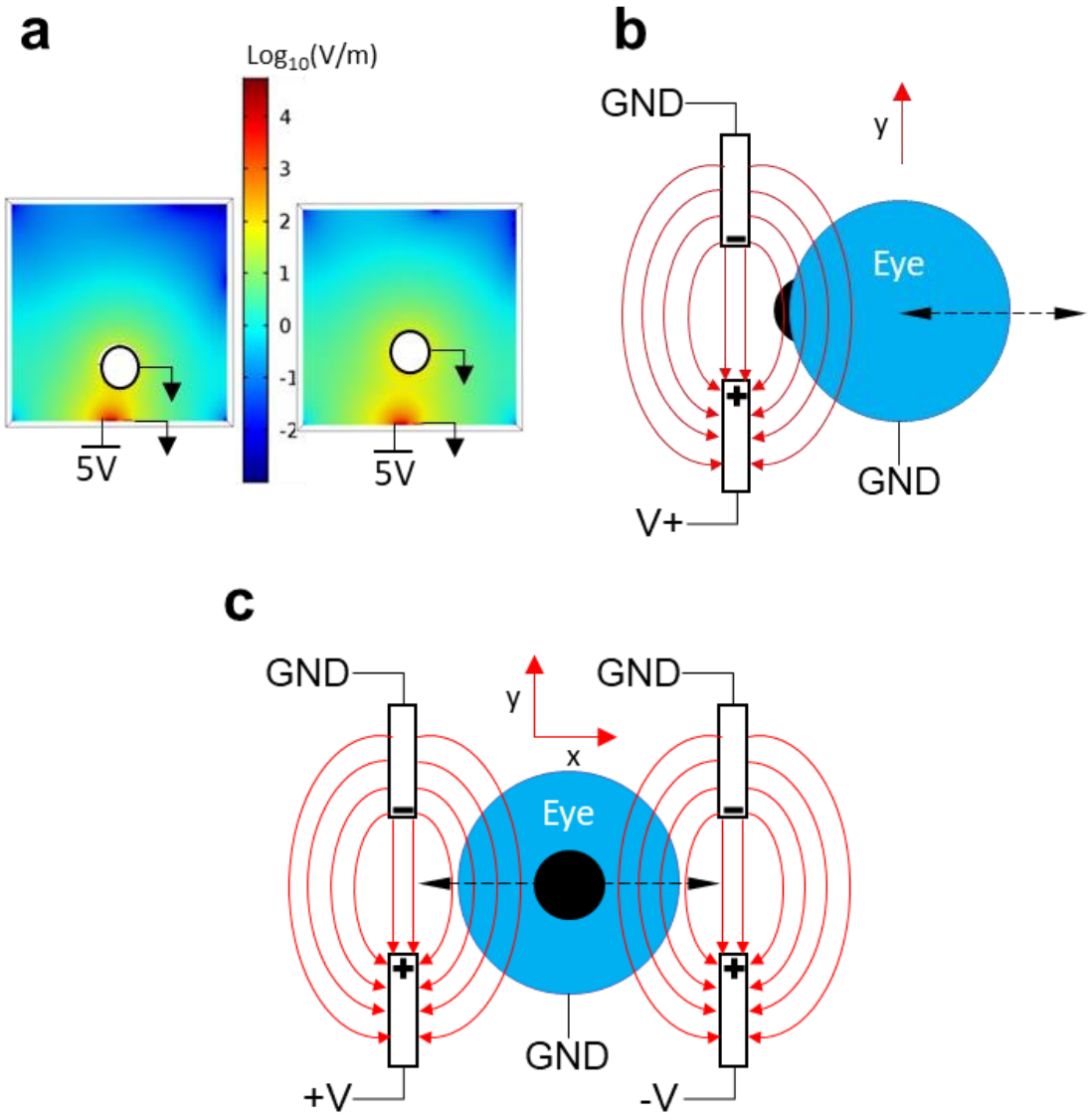

Fig. 14 (a) Electric field distribution with a spherical object at 4 and 6 mm distances from a PH sensor. (b) Single capacitance measurement. (c) Differential capacitance measurement.

The numerical study indicates that as the distance between the sphere and the sensor decreased from 6 to 4 mm, the charge interaction increased significantly between the eyeball and the positive electrode (Fig. 14a). Without the eyeball, the initial capacitance (C_0) of PR, PH, and PF sensors increased sequentially due to the increased surface area of the electrodes (Fig. 15).

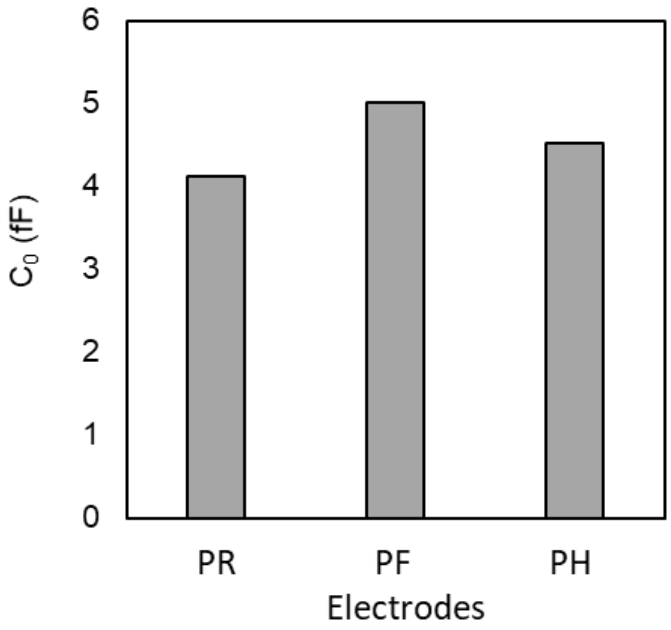

Fig. 15 Initial capacitance values (C_0) without a spherical object are computed for PR, PF, and PH electrodes.

When the eyeball was moved from 4 to 6 mm with 0.5 mm intervals, the ΔC increased gradually. Among the three sensor configurations, PH electrodes showed the highest ΔC followed by those of PF and PR electrodes in our numerical results (Fig. 16a). When the differential measurement was applied on ΔC, the sensitivity was further increased with better linearity (Fig. 16b). The advantage of differential measurement is best expressed by the mathematical description given by the Taylor's series expansion. Single capacitance configuration is widely used for capacitive detection. In comparison to single capacitance, differential capacitance measurement is conducted by applying the positive and negative voltage signals as illustrated in Fig. 14c.

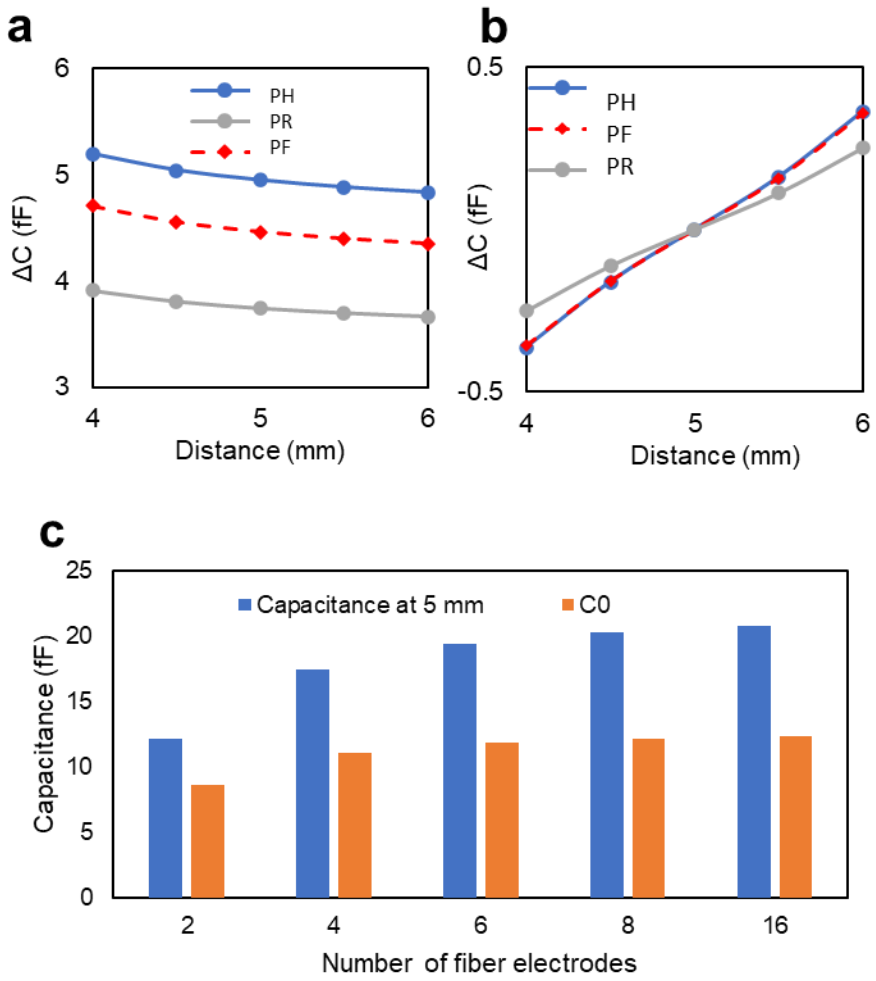

Fig. 16 (a) Numerical model of ΔC of PF, PR, and RH capacitances for the distance between 4 and 6 mm to a target sphere. (b) Numerical model of ΔC of differential measurement using PF, PR, and PH sensors. 5 mm is set as 0 fF for differential sensing. (c) Numerical model of initial (C_0) and working (C_1) capacitances of a PH sensor depending on the number of fibers. C_1 refers to the capacitance with the spherical target at 5 mm and C_0 is the capacitance without target.

In order to clarify the advantage of differential measurement, the Taylor series expansion of the parallel capacitance plate was performed.

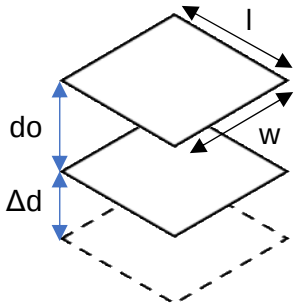

Fig. 17 Typical parallel plate capacitor schematic.

Fig. 17 shows the parallel plate capacitance, which is described as;

$$C = \frac{\varepsilon A}{d} = \frac{\varepsilon A}{d+\Delta d} \tag{3.8}$$

Where ε is permittivity, A (l x w) is area, and d is the distance between electrodes. The Taylor series expansion for single capacitance is;

$$f(d+\Delta d) = f(d_o) + \Delta d \frac{\partial f(d_o)}{\partial d} + \frac{\Delta d^2}{2} \frac{\partial^2 f(d_o)}{\partial d^2} \ldots \tag{3.9}$$

Substituting in function (*f*) into the parallel plate equation while neglecting the remaining order terms;

$$C = \frac{\varepsilon_o A}{d}\left(1 - \frac{\Delta d}{d} + \frac{\Delta d^2}{d^2}\right) \tag{3.10}$$

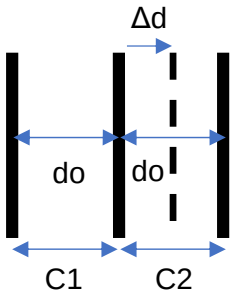

Fig. 18 Differential capacitor schematic.

For differential capacitance, Fig. 18 describes the change in capacitance between two sensors. Change in capacitance is therefore;

$$\Delta C = C_2 - C_1 \approx \frac{\varepsilon_o A}{d-\Delta d} - \frac{\varepsilon_o A}{d+\Delta d} \tag{3.11}$$

By substituting Eqn. 3.9 into Eqn. 3.10, differential capacitance can be defined as;

$$\Delta C \approx \frac{\varepsilon_o A}{d}\left(1 + \frac{\Delta d}{d} + \frac{\Delta d^2}{d^2}\right) - \frac{\varepsilon_o A}{d}\left(1 - \frac{\Delta d}{d} + \frac{\Delta d^2}{d^2}\right) \tag{3.12}$$

The change in capacitance is then simplified as;

$$\Delta C \approx \frac{\varepsilon_o A}{d}\left(\frac{2\Delta d}{d}\right) \tag{3.13}$$

According to the Eqn 3.13, the non-linear terms $\left(\frac{\Delta d^2}{d^2}\right)$ are cancelled and the linear term $\left(\frac{2\Delta d}{d}\right)$ is doubled, which increases the sensitivity. The equation of differential sensors becomes linear in comparison to the single sensor in 3.10. Since the equation is corresponding to the capacitance between two parallel plates, additional simulation was conducted to validate the linearity and the sensitivity in Fig. 16b.

PH electrodes showed the highest ΔC due to the reduced C_0 without an eyeball and the larger C_1 (capacitance with the spherical target at 5 mm) with an eyeball. The larger ΔC resulted in the enhanced sensitivity. The PH sensor was composed of a fibrous CPC electrode mated to a rectangular metal electrode. The fractured CPC generated conductive, high aspect ratio fibers at the end of electrode, which led to larger electric field strength and surface area in comparison to traditional plate electrodes. Due to the larger surface area, C_0 without an object increased in the following order: PR, PH, and PF electrodes. When a charged object like an eyeball was present, the fibrous electrodes of PH and PF showed a higher capacitance (C_1). As a result, the sensitivity (ΔC/Δd) of the PH sensor, which combined PR and PF electrodes, outperformed the PR and PF sensors. The C_0, C_1, and ΔC saturated as the number of fibers increased for a hybrid capacitance

(Fig. 16c). ΔC saturated when the number was greater than 8. Despite the random fiber shapes, the aspect ratio (length/width) greater 100 and the fiber number greater than 8 could offer uniform ΔC values due to the saturation.

3.3 FABRICATION OF FIBROUS ELECTRODES

A capacitive sensor was made of carbon nanotube-paper composites (CPC) using the previously reported methods [159, 160]. The fabricated CPC had a mean thickness of 88.4 ± 3.1 μm. For sensor fabrication, the initial material was cut into 1x10 mm^2 (Fig. 19a). After patterning silver (MG Chemicals, 8330S-21G, USA) electrodes on both ends of the material, a 0.1 mm capillary pen was used to print a water line at the center of the material. With the water line weakening CPC fibers, tensional fracture was induced to separate the material. Through the wet-stretching process, two 1x5 mm^2 fibrous electrodes were fabricated. For rectangular electrodes, silver ink (Engineered Materials Systems, Inc. Cl-1001, NY) was uniformly coated on a polyethylene terephthalate (PET) film. A silver-coated PET film was trimmed to 1x10 mm^2. By combining fibrous and rectangular electrodes in a co-planar configuration, three kinds of electrode pairs were fabricated; PF, PH, and PR electrodes (Fig. 19a). A 50 μm-thick self-adhesive polyethylene terephthalate (PET) film was used for laminating the capacitive sensors. The fabricated PF, PH, and PR sensors are shown in Fig. 19b. The gap between electrodes was set to 1 mm. For fibrous electrode, the gap size was the distance between the final ends of PF electrodes. For PH electrode the gap size was the distance from the end of the fibers and square edge of the rectangular electrode. For the PR electrode the gap size was the distance between the square edges.

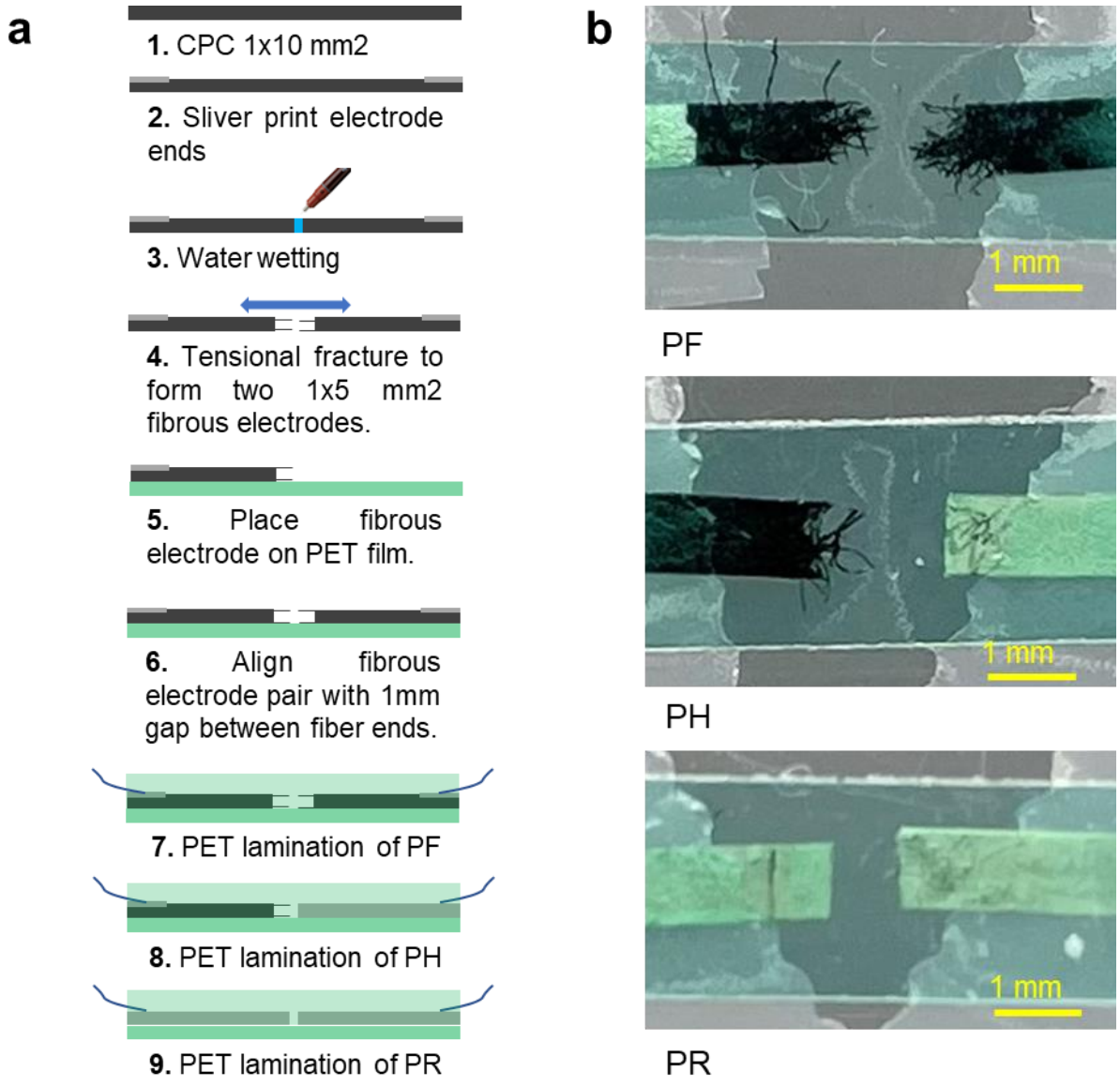

Fig. 19 (a) Sensor fabrication process and fabricated sensors. (b) Fibrous, hybrid, and rectangular sensors.

When C_0 values were compared for PR, PF, and PH electrodes, the average values were 321.0 ± 2.6 fF, 373.0 ± 13.2 fF, and 360.7 ± 7.7 fF, respectively (N=3, Fig. 20). The ratio of the standard deviation to the average was 0.8, 3.5, and 2.1 % for PR, PF, and PH electrodes, respectively. Although the morphology was not exactly the same, the variation in the measured capacitance of PF electrodes remained within 3.5%, which resulted in consistent sensitivity across

the fabricated sensors. The sequential increase of C_0 values for PR, PH, and PF electrodes agreed with the sequence of the numerical modeling results (Fig. 15).

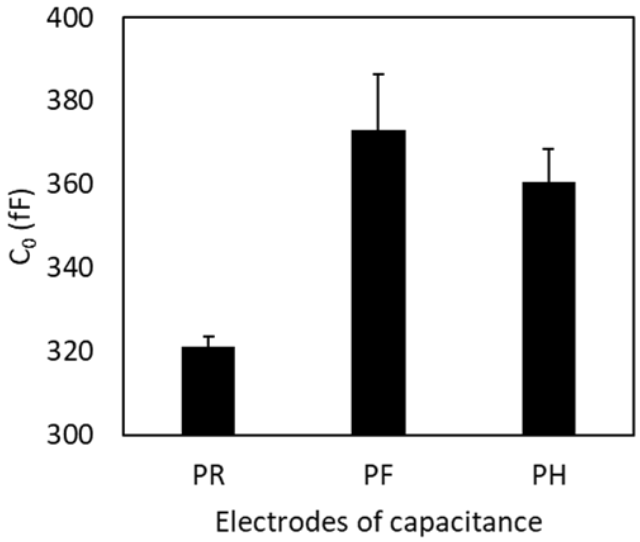

Fig. 20 Initial capacitance values for PR, PF, and PH electrodes (N=3).

According to scanning electron microscope (SEM) study, the average thickness of fibers was 5.9 ± 1.6 µm (Fig. 21). The aspect ratio determining the electric field strength ranged from 200 to 490. The linear density of fibers was 14.5 ± 3.6 mm^{-1}. X-ray diffraction (XRD) profiles (Fig. 22), collected showed that CNTs were uniformly dispersed in the CPC matrix, which is crucial for predictable capacitance of the cantilevered fibers [161-163].

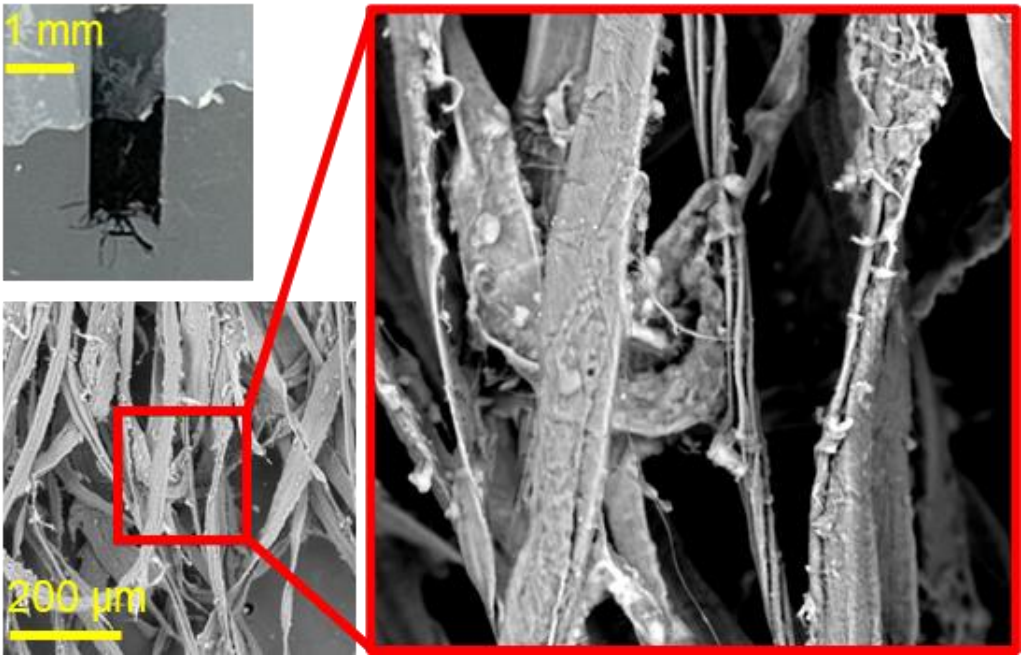

Fig. 21 Optical and SEM images of a representative fibrous electrode.

XRD profiles of as-prepared CPC were collected using a Bruker D8 Discover X-ray diffraction system equipped with a high-efficiency Cu (1.54 Å) anode, a microfocus X-ray source, and a PILATUS 100 K large-area 2D-detector. The X-ray diffraction patterns of pristine cellulose paper and CNT-containing paper (Fig. 22) both exhibit peaks centered at 15.8° and 22.5° from the (101) and (002) plane reflections, respectively, which are characteristics of the transverse arrangement of crystallites in a cellulose I structure [161]. No obvious shift or broadening of these representative cellulose features are observed when CNTs are present in the paper composition, revealing the good dispersion of CNTs in the fibrous network with minimal disruption of crystalline cellulose regions [162, 163].

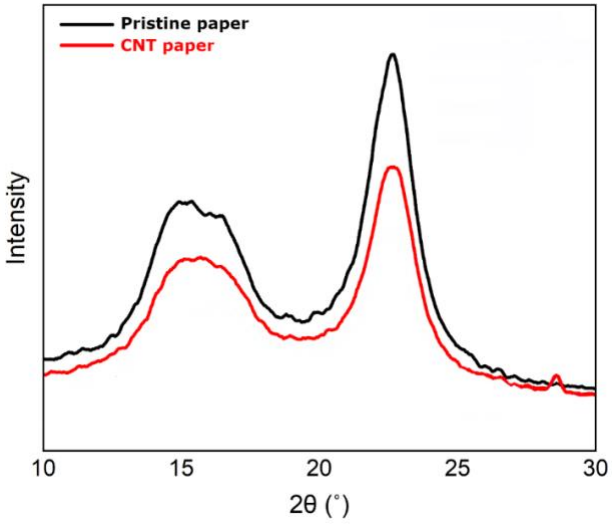

Fig. 22 X-ray diffraction patterns of pristine cellulose paper (in black) and CNT-containing paper (in red).

3.4 MEASUREMENT CIRCUIT

The asymmetry in the geometrical shape of the eye near the scleral-corneal junction caused a variance in distance from sensors as the eye rotates. The change affected the fringing field, which subsequently changed the capacitance. This change in capacitance could be measured by either singled or differential sensor configurations. The capacitive eye tracker was fabricated in three parts; Arduino nano microprocessor, capacitance-to-digital converter (CDC) and PH sensors. Two kinds of capacitance-to-digital converters (CDC) were used to measure capacitance, AD7747 (Analog Devices) and FDC1004 (Texas Instruments).

An AD7747 chipset was used for single- or differential measurement of capacitance. AD7747 is a two-channel high-resolution, Σ-Δ CDC. It features a resolution down to 20 aF, active shielding, ±8 pF capacitance range, 16 kHz excitation frequency and 45 Hz sampling rate. The AD7747 capacitance input range is balanced by a programmable on-chip digital-to-capacitance converter. The AD7747 is designed for single and differential functional modes. The CDC chipsets communicated to the Arduino microprocessor via an I^2C communication protocol. I^2C bus is a bi-

directional interface that uses a controller, known as the master, to communicate with slave devices. For this prototype the Arduino nano acts as the master and FDC1004 as the slave. A slave may not transmit data unless it has been addressed by the master. Each device on the I^2C bus has a specific device address to differentiate between other devices that are on the same I^2C bus. Slave devices are configured when the master accesses the slave's internal register maps, which have unique register addresses. A device can have one or multiple registers where data is stored, written, or read. The physical I^2C interface consists of the SCL and SDA lines. Both SDA and SCL lines must be connected to power through a pull-up resistor. It was powered by a 3.3 V input, enabling a 16 kHz excitation output and 45 Hz sampling rate. Although an AD7747 offered a high accuracy capacitance measurement (0.1 aF), the chip could measure only two capacitance channels.

An FDC1004 chip was used to construct the eye tracker circuit for benchmarking against the Tobii Pro Nano. The FDC1004 is a high-resolution 4 channel capacitance to digital converter. It has a measurement resolution of 0.5 fF, full scale range of ±15 pF per channel and 25 kHz excitation frequency. It was powered by a 3.3 V input. The excitation frequency was 25 kHz with a measurement resolution of 0.5 fF. FDC1004 was capable of four single or two pairs of differential sensors, with a sampling rate of 100 Hz/sensor. This allowed for monitoring horizontal and vertical eye movement over 60 Hz, which was the standard for camera-based eye trackers. The electrical schematic shown in depicts a typical layout used to connect CPC sensors to the FDC1004 and Arduino microprocessor.

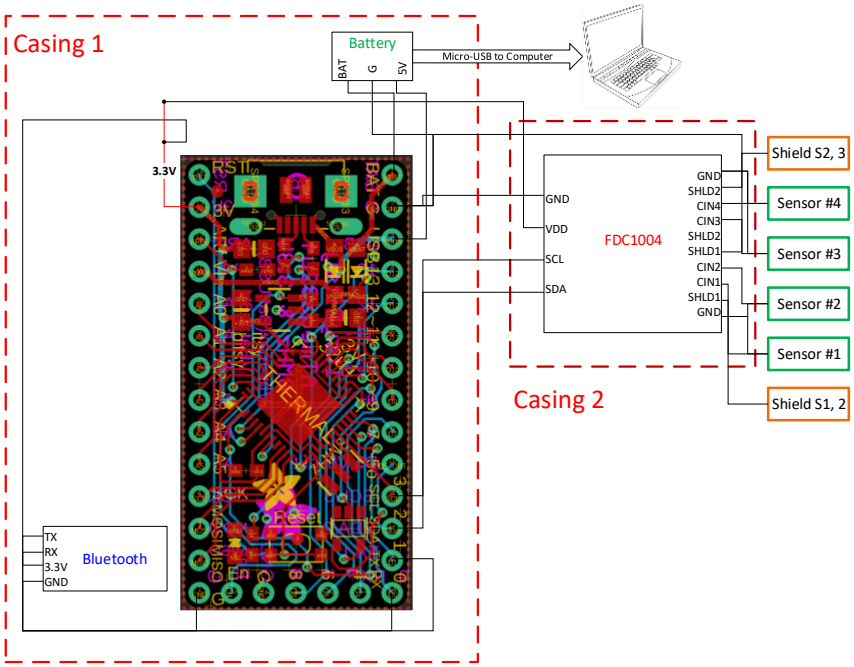

Fig. 23 Typical electrical schematic showing CPC sensors connected to FDC1004 and Arduino nano microprocessor.

The coding sequencing was derived from the respective CDC user manuals, which dictated the programming structure required to interface the CDC to the Arduino microprocessor. The code can be separated into three main sections; setup, read / write measurements, and data conversion. The setup utilizes the CDC's configuration and data registers to point to the channels required, setting capacitance offsets for each channel, and configuring the sensors to operate in a single or differential format. The CAPDAC is used to compensate for large base capacitance. Each register is written in 16 bits, starting with the most significant bits (MSB) and least significant bits (LSB). Each of the 16 bits aid in configuring the CDC's operation. To trigger a measurement event, information is written to the CDC configuration register. Channels required are enabled with the sampling rate defined. The CDC provides capacitance in 24-bits, which is read via two 16-bit registers (MSB and LSB portion of each channel). Data is retrieved and stored as three separate bytes, each consisting of 16 bits. The stored data is converted and quantified in term of farads, prior to displaying the data on a serial monitor.

3.5 SENSOR CHARACTERIZATION USING FACE SIMULATOR

The response of the fabricated capacitive sensors was characterized by using a face simulator to study ΔC according to the sensor configurations, geometry, and electric charge of a human face model with an eyeball. The human face model was 3D-printed using a polylactic acid (PLA) (Fig. 24a). The face and eyeball were covered with conductive aluminum foil and connected via a copper wire. The eyeball was placed on an x-y-z control stage to simulate human eye movement. The facial model and eyeball were located on an x-y plane, with stepper motor control along the z-axis. The body charge was applied to the facial model via a copper wire attached to the human hand. Capacitive sensors were placed at the bottom of a 3D printed PLA puck, which was titled at 10 degrees to match the contour of the facial model and directed towards the eyeball. Sensors were connected to a capacitance-to-digital chip and a microprocessor. The face model had the geometry of a human face with an independent actuation of the eyeball and the nearby sensor. Fig. 24b shows the electric measurement configuration.

Using the setup, three tests were conducted to characterize the sensitivity of the capacitive sensors against various facial conditions. In test 1, PR, PF, and PH sensors were displaced by 6mm from the face fixed with an eyeball to characterize the sensitivity depending on the facial shape and body charge. Test 2 was conducted to evaluate the most sensitive PH sensor only when the eyeball was displaced 0 to 6 mm from the face. This test could also provide ΔC depending on the charge induced by the eyeball. The goal of test 3 was to compare single sensor configuration to differential sensors for ±1 mm-horizontal eye movement at a 6 mm-distance. This test aimed to emulate a portion of actual eyeball movement during smooth pursuit. Tests 2 and 3 were performed with 1 mm-wide PH sensors, with and without body charge.

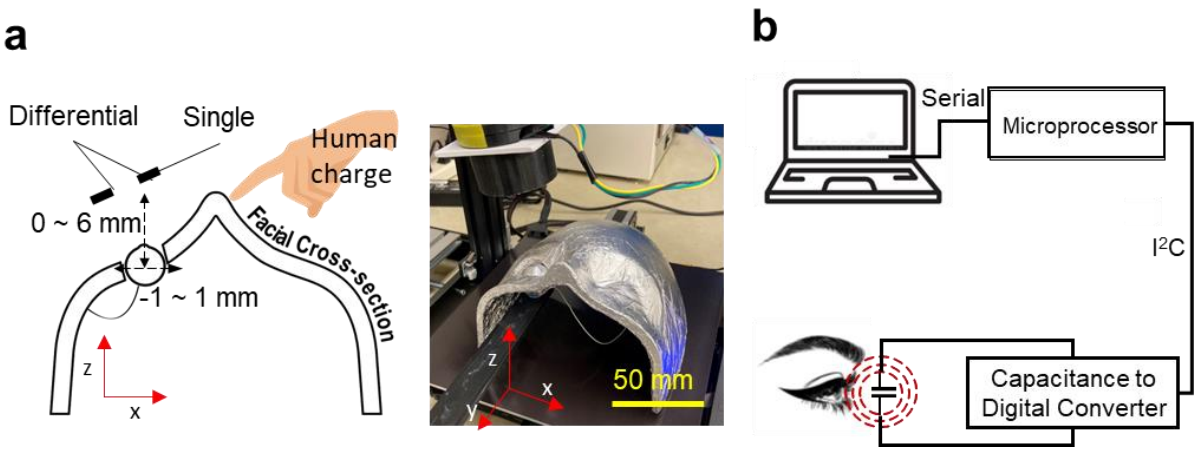

Fig. 24 (a) An eye and a face simulator covered with a conductive aluminum foil. (b) Capacitance measurement configuration using a capacitance-to-digital chip.

3.6 RESULTS

3.6.1 *Capacitive response to a face simulator*

The presence of the human facial shape and charge profoundly affected the ΔC of the capacitive sensors. Fig. 25a compares ΔC of PH, PF, and PR sensors for the 0~6 mm-displacement between the sensors and the face with an eyeball with and without human charge. The starting position of 0 mm did not include a 50 μm-thick PET film thickness that covered sensors. In the comparison, the PH sensors showed the largest ΔC of 0.224 pF and 0.200 pF with and without a human charge, respectively. A PF sensor showed ΔC of 0.175 pF and 0.160 pF with and without a human charge, respectively. The PR sensor showed the smallest ΔC. These experimental data qualitatively agreed with the results of the numerical analysis.

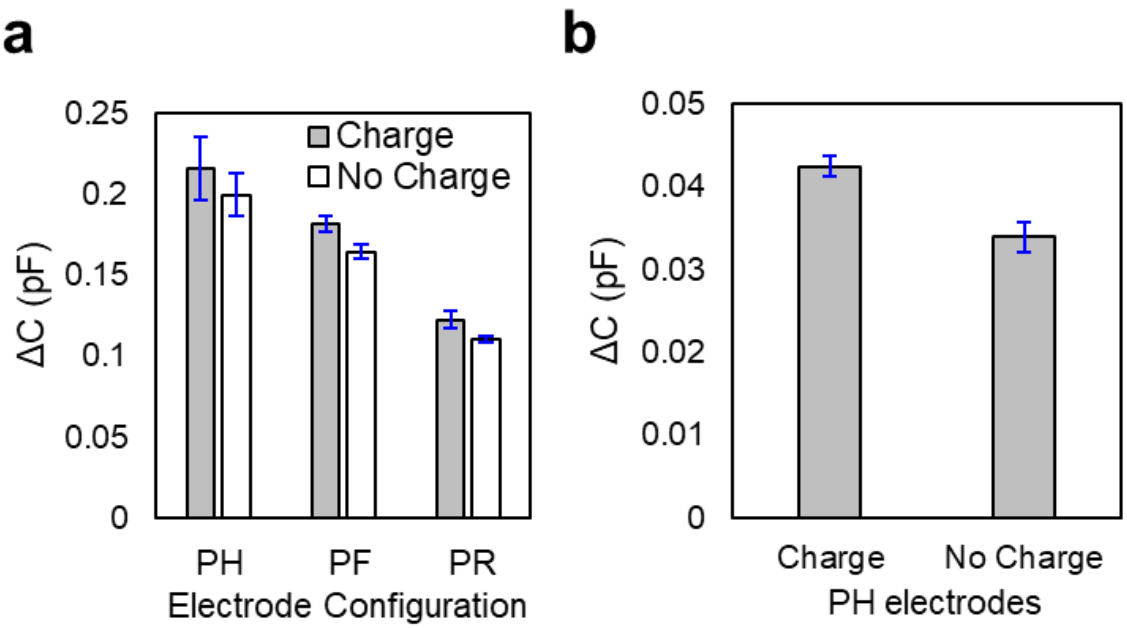

Fig. 25 (a) ΔC for hybrid, fibrous, and rectangular sensors for 0~6 mm displacement between a face plus eyeball and a sensor (N=3). ΔC is measured with and without human charge. (b) ΔC for a hybrid sensor with the displacement of an eyeball without moving a face (ΔC

Fig. 25b displays ΔC of PH sensors with and without body charge when an eyeball was moved from 0 to 6 mm from the face (N=3). A PH sensor showed only ΔC=42 fF with the human charge. In comparison to the experiment moving a PH sensor from the entire face in Fig. 25a, ΔC was only 18.7 %. Although the human charge contributed to increasing ΔC, the isolated eye movement with the background of the whole face showed only limited ΔC. Considering a 6 mm-displacement, the actual capacitance change for human eye movement could be further reduced.

Besides the out-of-plane displacement, a human eye could move horizontally from a sensor. When a single capacitive measurement was conducted for 1mm-horizontal movement at 6 mm proximity of a sensor, the ΔC was only 1.7 fF (Fig. 26). The differential capacitive measurement increased ΔC by 55 %. Therefore, differential capacitive measurement increased ΔC and, thus, sensitivity.

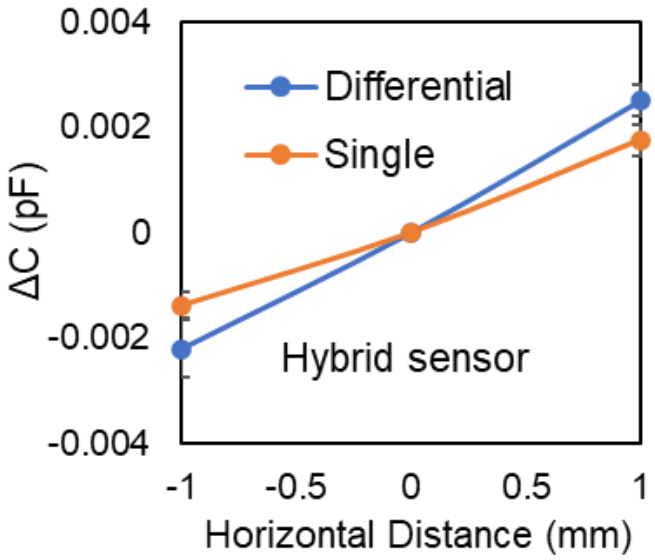

Fig. 26 Comparison of ΔC for single- and differential capacitive measurement for ±1 mm horizontal movement of an eyeball at the distance of 6 mm to a sensor.

3.7 CONCLUSION

A capacitive eye tracker was demonstrated to monitor eye movement. Based on the numerical analysis, a hybrid capacitive sensor made of fibrous and rectangular electrodes had the highest sensitivity due to the reduced initial capacitance and increased capacitance change in the presence of an eyeball. In comparison to a single sensor, a differential sensor configuration showed the better detection performance. In the study using a face model, the human charge increased capacitance change (ΔC), but the face background reduced ΔC of eye movement.

Chapter 4. CAPACITIVE EYE TRACKER HUMAN SUBJECT STUDY

4.1 INTRODUCTION

Capacitive sensors have a novel interaction relationship with the human body. Human body communication (HBC) is a term describing the use of the human body as a conductive channel to enable the communications between, on, or around the individual [89]. A standing human body insulated from ground is in principle an insulated conductor and as such, has a capacitance. The capacitive charge carrying ability of the human body is estimated at 100 pF [19], with the currents flowing through the human body and ground estimated at the nanoampere range with correlation to a subjects motion [20]. As such, the human body exudes variations in charge, with respect to motion, which subsequently lends itself to highly sensitive interactions between the human body and capacitive sensors.

Based on the interaction study presented in Chapter 3, multiple sensor locations are explored to find the optimal sensor locations for tracking the human eyeball. Vertical and horizontal eye movements are compared to those produced by a commercial eye tracker. The prototype eye tracker is demonstrated for smooth-pursuit eye-movement tracking, human-machine interface, and closed-eye movement monitoring.

4.2 EXPERIMENTAL

4.2.1 *Capacitive measurement of human eye movement for sensor location optimization*

For Chapter 3, the most sensitive PH sensor was used to track the motion of human eyes. A vertical eye movement test protocol was devised to evaluate sensor performance, whereby a human subject gazed at markers to rotate the eye vertically ±20º. To calibrate vertical eye movements, a whiteboard was placed 680 mm away from the user's eyes and marked with two

points, 248 mm above and below the neutral gaze position. Moving the gaze between these two markers was equal to a vertical angular rotation of ± 20º. Eye gazing was restricted to vertical movement, negating any diagonal or circular pathways. The eye movement process for vertical tests was as follows; three repetitions of vertical movement between the ±20º markers, three repetitions of 0 ~ 20º from neutral location, and two repetitions of 0 ~ -20º from neutral position. Movement time between markers was 1 s, with a hold time of 3 s at each marker. The eye displacement test was used to characterize the sensors, with respect to position, ΔC, and sensitivity.

For horizontal eye movement, differential capacitive measurement was conducted to study the optimal sensor locations. The same experimental setup was used but the gaze moved between two markers located ± 35º from the central position. The subject made alternating left- and right 70° horizontal eye movements between the two markers. A single human subject was used during sensor optimization trials.

4.2.2 *Comparison test to a commercial eye tracker*

The capacitive sensor signals of vertical and horizontal eye movements were compared to the eye tracking outputs of a video-based commercial eye tracker (Tobii Pro Nano). The commercial system captured gaze data at 60 Hz using a video-based pupil and corneal reflection eye tracking system with dark and bright pupil illumination modes. This eye tracker was designed for fixation-based studies after user calibration. The capacitive eye tracker's signal was compared to that of the commercial eye tracker in terms of motion accuracy and response time.

The capacitive eye tracker was assembled with one pair of differential sensors for horizontal eye tracking, together with a single sensor for vertical eye movement detection using FDC1004. The sampling rate was 45 Hz and data were recorded. The time-dependent capacitive data were horizontal and vertical movement for differential and single measurements, respectively.

The test was conducted on three different human subjects. Due to the limitations of the commercial system, vertical and horizontal angular displacements were set to ±9° and ±16°, respectively. The degree of angular displacement was determined by the monitor size (diagonal distance: 685 mm) of a commercial eye tracker and the distance from the monitor to the human subject's face (788 mm). The corresponding data for a commercial eye tracker was unity displacement for horizontal and vertical movement. All tests were conducted indoors at room temperature. All study related to the capacitive eye tracking and the comparison test to the commercial eye tracker was approved by the institutional review board (IRB) at the University of Washington (IRB ID: STUDY00010741).

4.3 CAPACITIVE RESPONSE TO VERTICAL EYE MOVEMENT

For vertical eye movement, a single capacitive measurement was conducted to study the optimal sensor location. In Fig. 27a, the locations of a sensor are presented. For vertical movement, the tested sensor locations were tested from (0, 20) to (0, -25) by varying the vertical position in -5 mm increments. The origin of the coordinate represents the center point of the cornea. The x-y coordinates correspond to the x-y plane of the glasses shown in Fig. 12a. Vertical and horizontal eye movement was conducted according to the designed protocol by watching the spots on a whiteboard (Fig. 27b). For vertical eye movement, only a single measurement was conducted because differential capacitive measurement showed undesirable patterns (Fig. 27c). While vertical movements were measured by single capacitance, horizontal differential sensors were also sensitive to the vertical movements. With the increased sensitivity of differential capacitance, the change in proximity of the cornea and eyelid to the differential sensors during vertical movement led to detection of this movement as a sinusoidal pattern. As such, a single vertical measurement

was used to reduce sensitivity to horizontal eye movements while, enabling sensitivity towards only vertical eye movements.

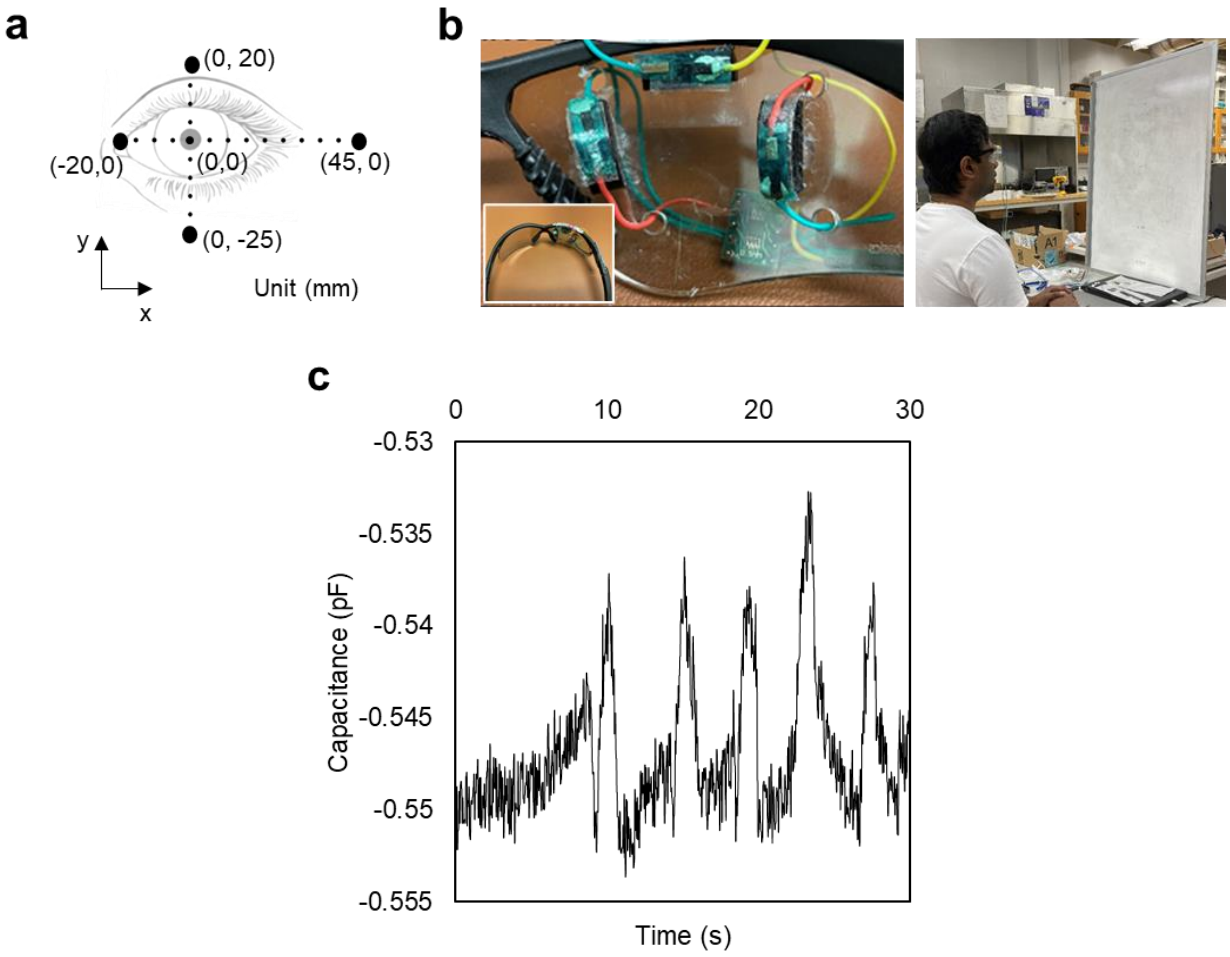

Fig. 27 (a) Locations of sensors for single and differential capacitive measurement. (b) Monocular eyeglasses installed with single vertical and differential horizontal sensors. (c) Differential vertical sensors tracking left-right movements.

The time-dependent protocol of eye movement in the top graph of Fig. 28 showed vertical displacement of ± 20º. The sensor location of (0, 20) clearly showed the reproducible measurement of eye movements and identified the straight neutral gaze at the midline (Fig. 28). At the sensor location of (0, 0), the phase of ΔC started to be inverted. As the sensor moved to (0, -10) and (0, -20), ΔC was inverted in comparison to that of (0, 20), as the sensors at these locations were

inversely influenced by the eye. Moreover, the amplitude decreased as the sensor location was below (0, 0). At location (0, -25), the sensor produced inconsistent amplitude and distortion.

It was speculated that the capacitive signal for vertical eye movement was dominated by cornea movement rather than eyelid movement. To evaluate the source of the capacitive signal, photographic angular analysis (Fig. 29a) of the eye was conducted. A frame-by-frame photo analysis was undertaken to determine the displacement of the cornea and eyelid during vertical eye movement, with respect to sensor position (Supporting information, Figure S5b). From the initial distance of 6 mm, the cornea diagonally retracted by 7.1 mm as the eye gazed between 20 to -20°. A diagonal retraction of 7.1 mm equated to ~2 mm of corneal retraction in the x plane (refer to Fig. 29a). In comparison, the eyelid was located at -1 mm at 20° and withdrawn by 3 mm at -20°. This data confirmed a complex movement relationship between the cornea and eyelid, where the photographic displacement could not individually explain the relationship between the capacitance signal and gaze position.

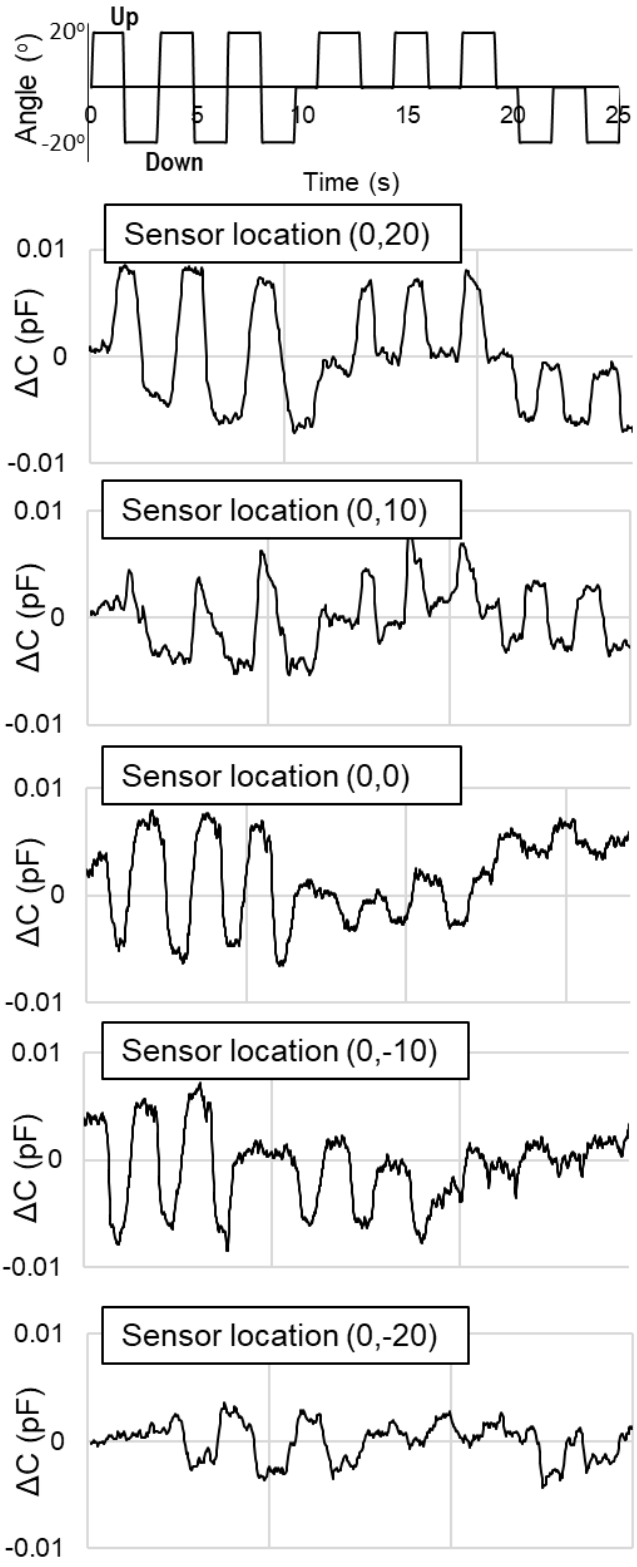

Fig. 28 ΔC depending on vertical sensor locations at (0, 20), (0, 10), (0, 0), (0, -10), and (0, -20).

As such, the capacitance effect of the eyelid encasing the cornea was also examined. As the eyelid moved from nearly closed- to fully closed state, a sharp spike rose in capacitance (Fig. 29c). The dielectric nature and electric charge of the cornea and eyelid could dominate ΔC. To mimic the capacitance interaction between a wet eyeball and dry eyelid, when a sensor moved between wet and dry skin, the capacitance change was much greater on the wet skin (Fig. 29d). On average, the wet skin exhibited ΔC of 24 fF, greater than that of the dry skin. The larger ΔC could be caused by direct electrical connection to the human body charge and the electrical double layer forming on the skin.

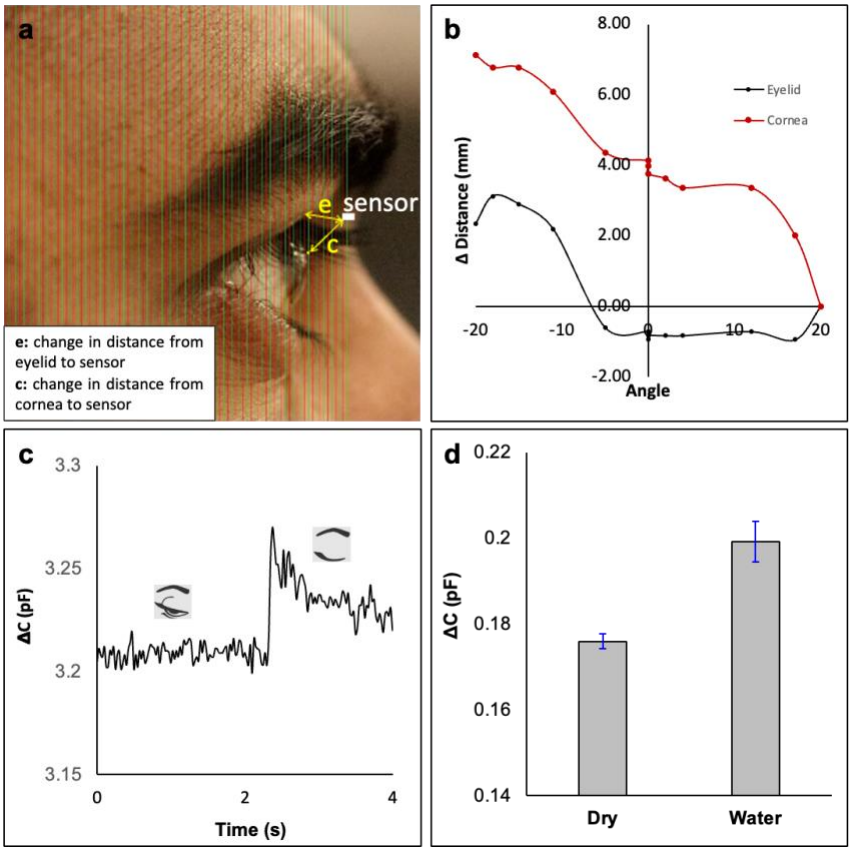

Fig. 29 (a) Image frame 1 out of 30 images during vertical smooth pursuit, displaying the distance from a sensor to the eyelid or to the cornea that are indicated by 'e' and 'c', respectively. (b) Distance change between a sensor and the eyelid, and distance change between a sensor and the cornea for the vertical rotation angles. (c) Capacitance change from nearly closed eye to fully closed eye. (d) Capacitance change between dry and wet skin.

According to the results, the cornea with the thin water layer could dominate ΔC until the eyelid was completely closed. The inversion and decreased amplitude of ΔC at the vertical sensor locations (0, 0) and below could be explained with respect to cornea and eyelid protuberance. The signal was inverted at sensor locations (0, 0) and below as the cornea was at a closer proximity to the sensor during its downward trajectory. The amplitude decreased, as less of the cornea was interacting with the sensor. Further study is required to quantify the impact of the eyelid on ΔC. In summary, the sensor location between (0, 20) and (0, 10) was optimal with a maximum range of ±10 fF. Considering the noise level of 0.56 fF_{RMS} and sensitivity of 0.5 fF/deg, the accuracy was 1.1 degrees.

4.3.1 *Capacitive response to horizontal eye movement*

For horizontal eye movement, differential capacitive measurement was chosen to study the optimal sensor locations. The same experimental protocol was used, but the gaze moved between two targets located at -35° (left) and +35° (right). The subjects repeated the 70^{o} gaze shift four times (Fig. 30). The horizontal eye movement excursion was limited by the subject's oculomotor range. Single capacitive measurement was not used due to the low sensitivity.

Both sensors in the differential configuration were placed on the left and right sides of the right eye. The design of the glass frame only allowed the left sensor to be placed at (-20, 0) near the nose bridge. The location of the right-side sensor was tested between (20, 0) and (40, 0) in 5 mm increments to find the optimal sensors' emplacement. The midline of the waveform corresponded to a straight neutral gaze.

When the right sensor was located between (20, 0) and (30, 0), the capacitive signals clearly showed rightward, leftward, and zero-crossing movements. Moreover, the signals showed

consistent movement amplitudes. At location (35, 0), the signal reduced amplitudes. At the most peripheral location (40, 0), the sensor failed to produce a predictable signal. The failure was caused by the lack of sensitivity from the right sensor because the sensor was located beyond the eye corner. Differential sensors located at [(-20, 0) & (20, 0)] and [(-20, 0) & (30, 0)] were optimal with a maximum range of ±10 fF and sensitivity of 0.28 fF/deg. With a noise level of 0.35 fF_{RMS}, the accuracy was within 0.8 degrees.

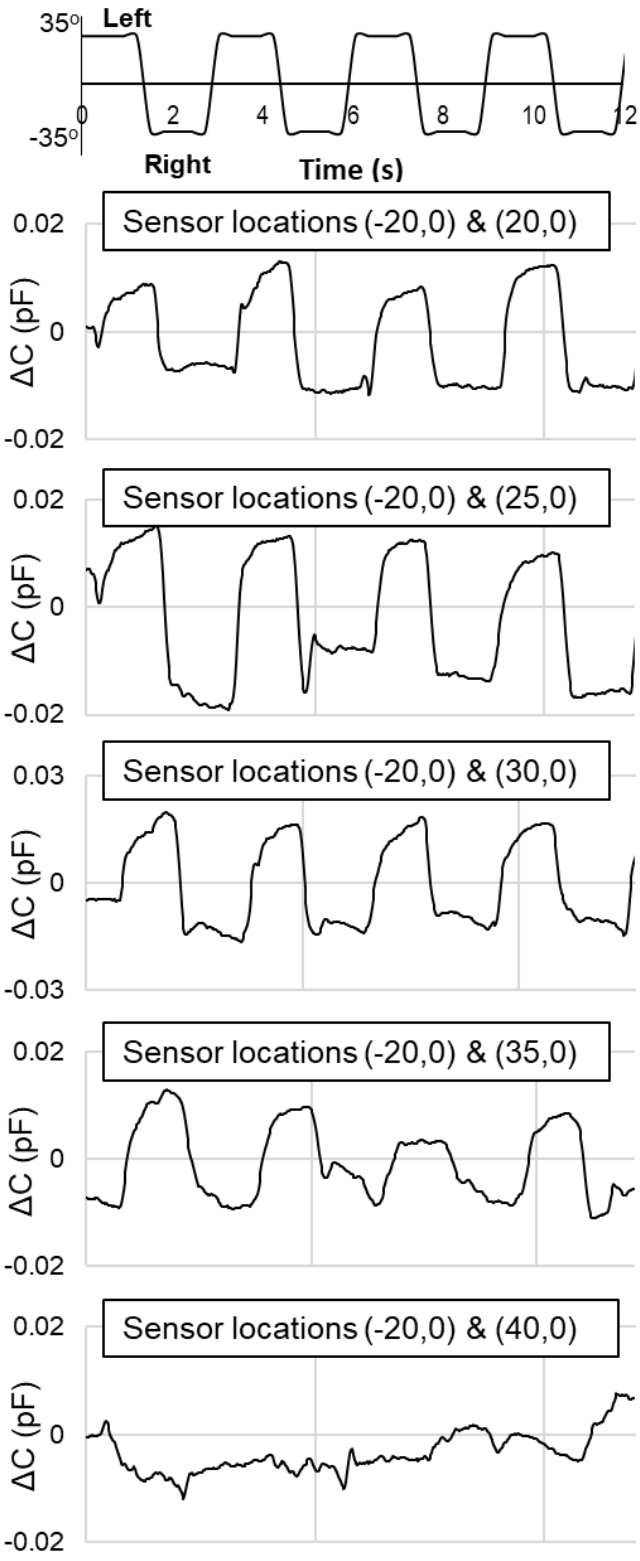

Fig. 30 ΔC depending on horizontal differential sensor locations at [(-20, 0) and (20, 0)], [(-20, 0) and (25, 0)], [(-20, 0) and (30, 0)], [(-20, 0) and (35, 0)], and [(-20, 0) and (40, 0)].

4.3.2 *Comparison test to a commercial eye tracker*

The capacitive sensor signals of vertical and horizontal eye movements were compared with those produced by a camera-based commercial eye tracker (Tobii Pro Nano). Fig. 31a shows the vertical movement of an eyeball. As the eye moved vertically, both the vertical and horizontal ΔC clearly showed the movement signals with similar amplitudes and opposite phases. The commercial eye tracker also produced eye movement signals in both the vertical and horizontal channels during a pure vertical eye movement, but the amplitude of the horizontal signal was ~3% of the vertical signal.

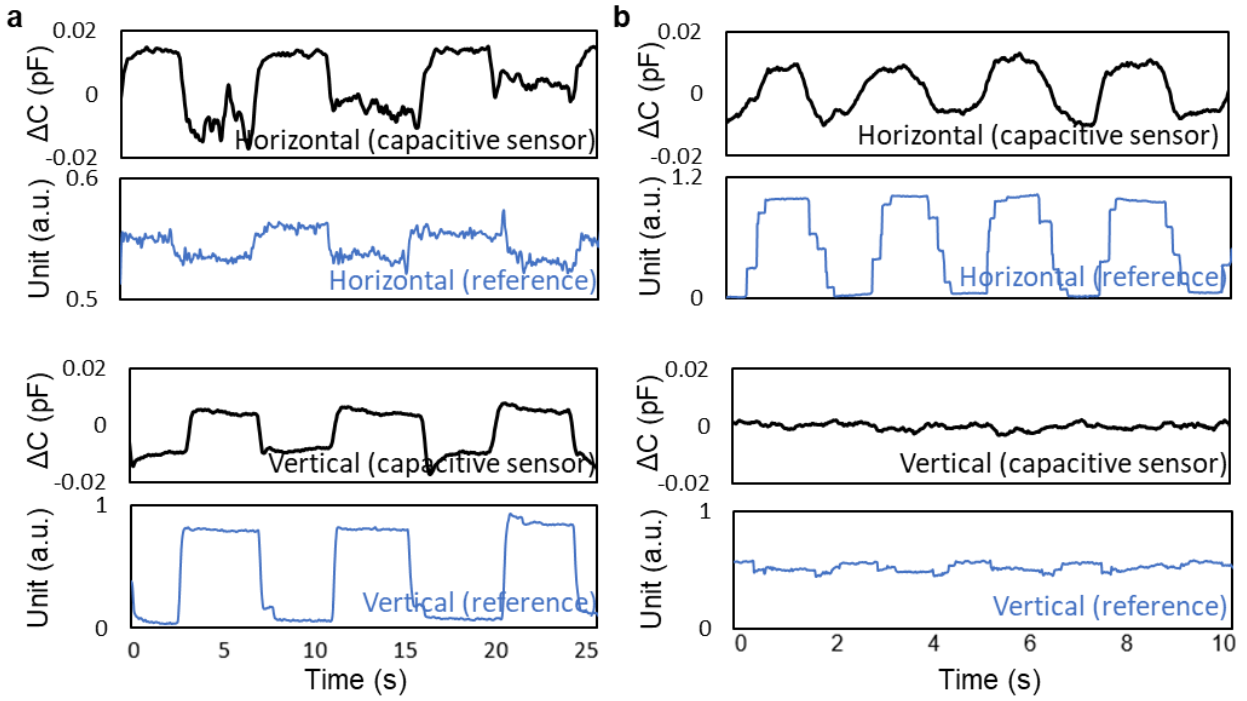

Fig. 31 (a) Comparison of a capacitive eye tracker to a commercial eye tracker for vertical eye movement. (b) Comparison of a capacitive eye tracker to a commercial eye tracker for horizontal eye movement.

Fig. 31b shows the comparisons of horizontal eye movement signals produced by the capacitive sensors and the Tobii eye tracker. In contrast to vertical eye movement, the horizontal

ΔC showed a robust horizontal movement signal, but the vertical ΔC did not show any signals related to the horizontal eye movement. Based on the results, the vertical capacitive sensor determined the movement direction of an eyeball. Based on the results shown in Figure 4a and 4b, combining both amplitude and phase information from both vertical and horizontal capacitive sensors allowed for horizontal and vertical signal separation due to the crosstalk during vertical eye movement.

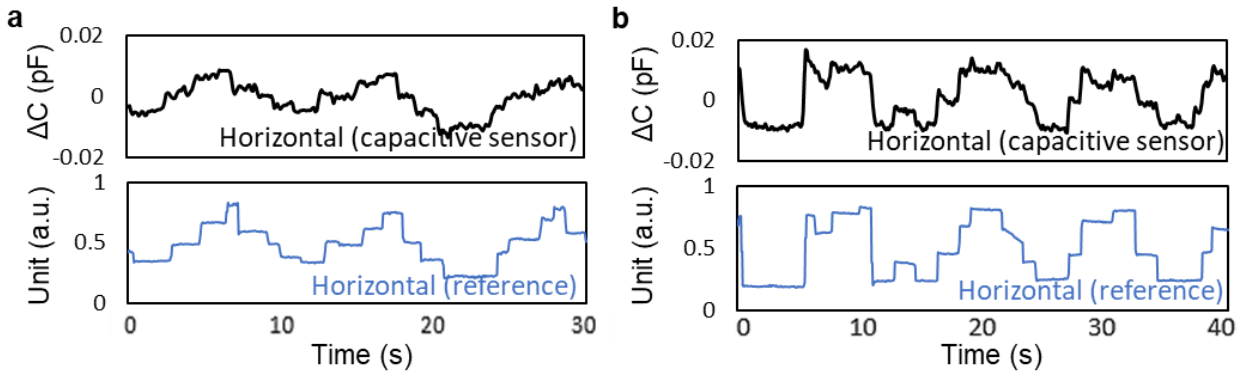

Fig. 32 (a) Comparison of a capacitive eye tracker to a commercial eye tracker for horizontal eye movement (b) Comparison of a capacitive eye tracker to a commercial eye tracker for horizontal eye movement.

Fig. 32a and Fig. 32b shows the comparison of horizontal eye movement signals between capacitive sensors and a commercial eye tracker for two other human subjects. The capacitive sensors clearly detected the saccades. In comparison to the ΔC shown in Fig. 31b, the saccadic eye movements were more distinctly shown and clearly correlated to those produced by a commercial eye tracker. Overall, ΔC ranged between 10~20 fF. Considering horizontal eye movements of ±12°, 1° accuracy could be achieved for horizontal eye movement. Fig. 33 depicts the phase diagrams for vertical and horizontal smooth pursuit movement, for qualitative deduction of the direction of eye movement. During horizontal smooth pursuit, the phase diagram produced a plot

with negligible vertical amplitude. However, during vertical smooth pursuit, the phase diagram produced a diagonal plot. A clear qualitative distinction was evident between the phase diagrams.

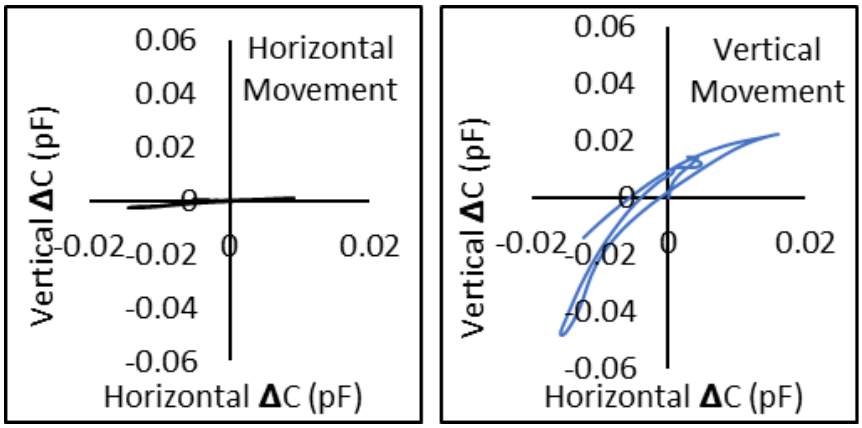

Fig. 33 Phase diagrams for horizontal and vertical smooth pursuit movements shown.

4.4 DISCUSSION

For a capacitive eye tracker, the performance of a high accuracy capacitance-to-digital chip was crucial for accurate detection of eye movement. In our tests, various chips were tested, including AD7747 (Analog Devices), FDC1004 (Texas instrument), and FDC2214 (Texas instrument). Also, LM 555 timer (Texas instrument) could be used for capacitive eye tracking. According to our characterization, 0.1 fF of accuracy was critical to obtain 1 degree-accuracy for eye movement. In this regard, AD7747 was the best in terms of accuracy. Despite the lower 1 fF accuracy of FDC 1004, the higher sampling rate up to 400 Hz could be useful for ultimate eye tracking. FDC 2214 was an electrical resonance circuit with operation frequency of 1~3 MHz. Due to the resonance, the ΔC was high with the increased noise level. The sampling rate of FDC 2214 could be increased to 1 kHz, which had a potential for eye tracking. The capacitive eye tracker was also tested to monitor horizontal eye movement with the eyelids closed and opened (Fig. 34). The capacitive sensors reliably detected eye movement in both conditions. The

amplitudes were larger when the eyelids opened. The ability of the sensors to detect eye movement with the closed eyelids would allow the sensors to be used in sleep studies.

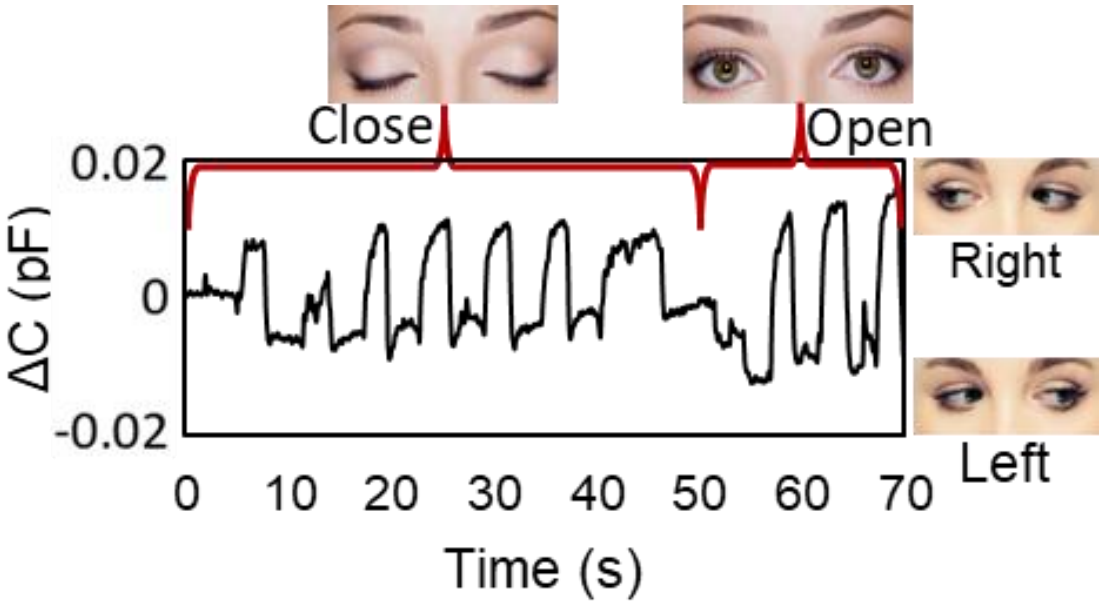

Fig. 34 ΔC of closed and open eyes for horizontal movement.

To demonstrate the real-time response for detecting eye movement, the capacitive sensing eye tracker was interfaced with a laptop computer to control a cursor on the screen (Fig. 35). Starting from a center point, the eyes moved to the left, center, and right locations according to verbal signals. The cursor showed corresponding movements to the three locations. Eye blinking (Fig. 35, red arrows) showed spikes but did not appear to affect the accuracy of the cursor placements (Real eye tracking HMI.mp4). The wearable eye tracker demonstrated the capability to control a machine using eyeball movement.

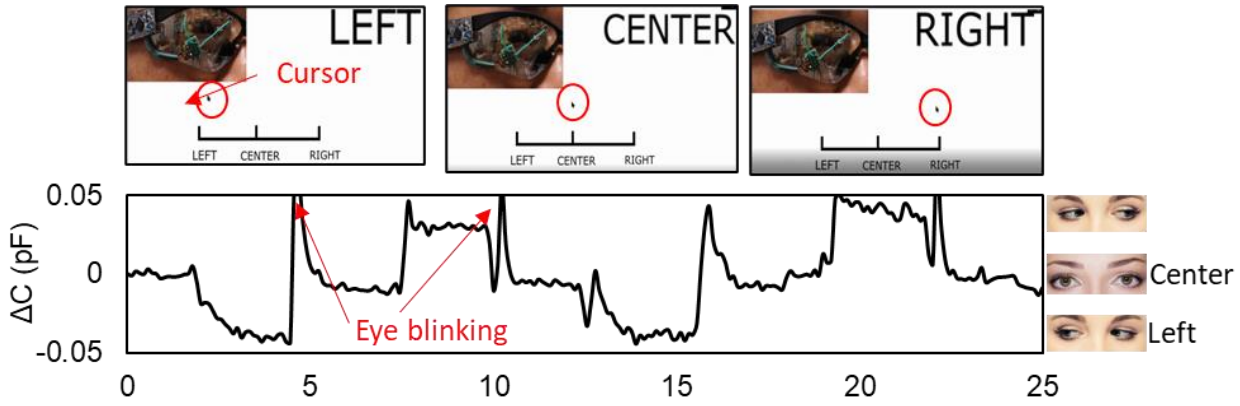

Fig. 35 Human-machine interface for horizontal eye movement. Eyes are controlled at the left, center, and right locations.

4.5 CONCLUSION

In the human subject test, the single capacitive measurement was optimal for vertical eye movement at the locations of (0, 20) ~ (0, 10) mm. For horizontal eye movement, the differential capacitive methods allowed accurate measurement at the locations between [(-20, 0) & (20, 0)] and [(-20, 0) & (30, 0)]. The accuracies for vertical and horizontal movement were 1.1 and 0.8 degrees, respectively. The comparison of a capacitive eye tracker to a commercial eye tracker showed a good correlation for horizontal- and vertical eye movements. A phase diagram between vertical and horizontal signals was used to qualitatively assess eye movement. The presented capacitive eye tracker detected horizontal eye movement with the closed and open eyelids. The relationship between cornea and eyelid position was studied to understand their consequence on the capacitance signal. The cornea was found to dominate the capacitance signal, until the eyelid was fully closed. The presented wearable capacitive eye tracker shows potential for eye tracking in various fields, including neuroscience, cognitive science, eye function diagnosis, and entertainment.

Chapter 5. VALIDATION OF A CAPACITIVE EYE TRACKER USING A PRIMATE EYE TRACKING STUDY

5.1 INTRODUCTION

The study of the oculomotor system investigates the relationship between eye movement and associated neuronal activity [149-151]. The ability to measure eye movement with high spatial and temporal resolution underlies a long series of studies of the neural basis of the oculomotor system and its motor learning [164-166]. Eye movements can provide a forecast into cognitive functions, such as decision making [167] and attention [168]. Furthermore, diseases diagnosis has been associated with abnormal saccadic functions and several neurological disorders, including Creutzfeldt-Jakob disease [145], autism [146], Parkinson's disease [147], and Huntington's disease [148]. Thus, eye movement measurement is paramount to studying an oculomotor system and neurological disorders.

An eye tracking device must capture both the spatial and temporal characteristics of the movements with high fidelity [152]. The measurement of eye position should operate in real-time so that the correlation of neural activity to eye movement is accurate. Optogenetics is a technique that allows light to manipulate the activity of specific neurons with high temporal precision and examines the effect of the neuron activities on eye movements. The real-time characteristics of an eye tracking device become critical [123, 124].

A camera-based eye tracking system has the advantage of being non-invasive, but it is generally too slow because of its long image processing time. Thus, a camera-based eye tracker may not be suitable for experiments requiring accurate real-time eye movement signals. The gold standard eye tracking device for oculomotor research has been the scleral search coil system [126, 127, 153]. In this system, a coil of a few turns of thin insulated wire is surgically placed on the

surface of the globe under the conjunctiva. The two wire ends are twisted together, passed subcutaneously, and soldered to a connector at the top of the skull. A voltage proportional to the angle of the gaze direction is produced when the coil rotates in a high-power AC electromagnetic field. The scleral search coil system has the advantage of a real-time low latency analog electronics, low-noise, and high accuracy (<0.1°) [154]. Its bandwidth is sufficient to accurately characterize the kinematics of saccades [169]. The properties of the scleral search coil system allow a closed loop optogenetics experiment [124, 125] to be performed on a saccade while the movement is unfolding.

Capacitive transducers have a long history of sensing an interaction between humans and electronic devices. Capacitive sensors have been widely applied to various types of proximity sensing on monitoring a human's activities [10, 170]. Gesture recognition has been realized by capacitive proximity sensor array [112]. A car seat with a capacitive proximity sensor system has also been developed to monitor a driver to recognize their inattentiveness. Capacitive sensors can also be utilized to track the movements of the eyeball. The asymmetry in the geometrical shape of the eye near the scleral-corneal junction [171] changes the distance between the sensor and the eye upon rotation. The distance change affects the fringing electric field, which in turn changes the capacitance. The capacitance change due to the fringing electric field can be measured by either singled or differential modes. In another work, a plurality of capacitive sensors (array) detects the proximity of the eyeball during eye movement. It consists of a eyeglasses frame to support an array of capacitive sensors positioned in front of the eye. Control circuitry designed to receive real-time signals from the sensor array, with an electrode grounded to the subject's body.

5.2 OBJECTIVES

In this chapter, the challenges of implementing an eye tracking technique based on capacitive sensing for oculomotor research are addressed. We will validate the performance of a carbon nanotube paper composite (CPC) capacitive eyeglasses against the scleral search coil. The fabrication and characterization of CPC capacitive sensors has been described in Chapter 3. The high aspect ratio of length to diameter of carbon nanotubes (CNT) increases the surface charge density, sequentially enhancing the electric field. Such high aspect ratio structures increase the capacitance, thereby enhancing the overall sensitivity of the CPC sensor. The capacitive interaction between the CPC electrode and a spherical eyeball is analyzed by numerical study to understand how the shape and scale of the eyeball affect capacitive interaction. Non-human primate (NHP), implanted with a scleral search coil will be utilized to conduct an eyeball interaction study. The CPC eye tracker's response to smooth pursuit and saccadic movements will be investigated and validated against the scleral search coil.

5.3 NUMERICAL SIMULATION

A COMSOL electrostatic model was constructed to conduct the scaling analysis and analyzer the proximity sensitivity of a capacitive sensor to an eyeball. Fig. 36a shows the geometry of a spherical object mimicking an eyeball and a single, rectangular capacitive electrode. The capacitive sensor was placed at the bottom of a cubed domain (200 x 200 x 200 mm) with air permittivity. The potential of 5V was applied to the single electrode. For scaling analysis, six different eyeball radii were compared to study capacitive sensitivity to the proximity detection of a charged object. The rectangular electrode was represented by a monolithic rectangular slab with dimensions of 1 (width) x 5 (length) x 0.1 (height) mm. The sphere (representing an eyeball) had radii of 5, 10, 15, 20, 30, and 45mm. The distance between the sphere and electrode was 5 mm. The electrode was applied with a 5 V excitation, while the sphere was considered as ground. Since an electrostatic model was used, all conductors were assumed to be in complete electrical equilibrium, meaning the potential was constant over the electrodes. As such, the material dielectric constant and excitation frequency of the electrode was not of consideration. Capacitance was solved for via the Maxwell method with a single excitation electrode configuration. The Maxwell capacitance matrix solver described the relation between the charge of an i^{th} conductor to the voltages of all conductors in a system.

Computing the simulation with various sphere radii presented the fringing fields graphically depicted in Fig. 36b. With increasing radius, a shorter and more direct path was provided for the electrical field to fringe from the rectangular electrode to the sphere. The capacitance change (ΔC) due to the fringing field presented a non-linear relationship to increasing radii (Fig. 36c). The numerical simulation indicated ΔC of 8.78 fF between radius 5 to 15 mm and 2.08 fF between 15 to 45 mm. The plateau in capacitance after 15 mm occurred because the target

dimension was too large in comparison to the sensor dimension. Although the sphere radius increased, the capacitance was bound to the geometry of the rectangular electrode, which remained unchanged.

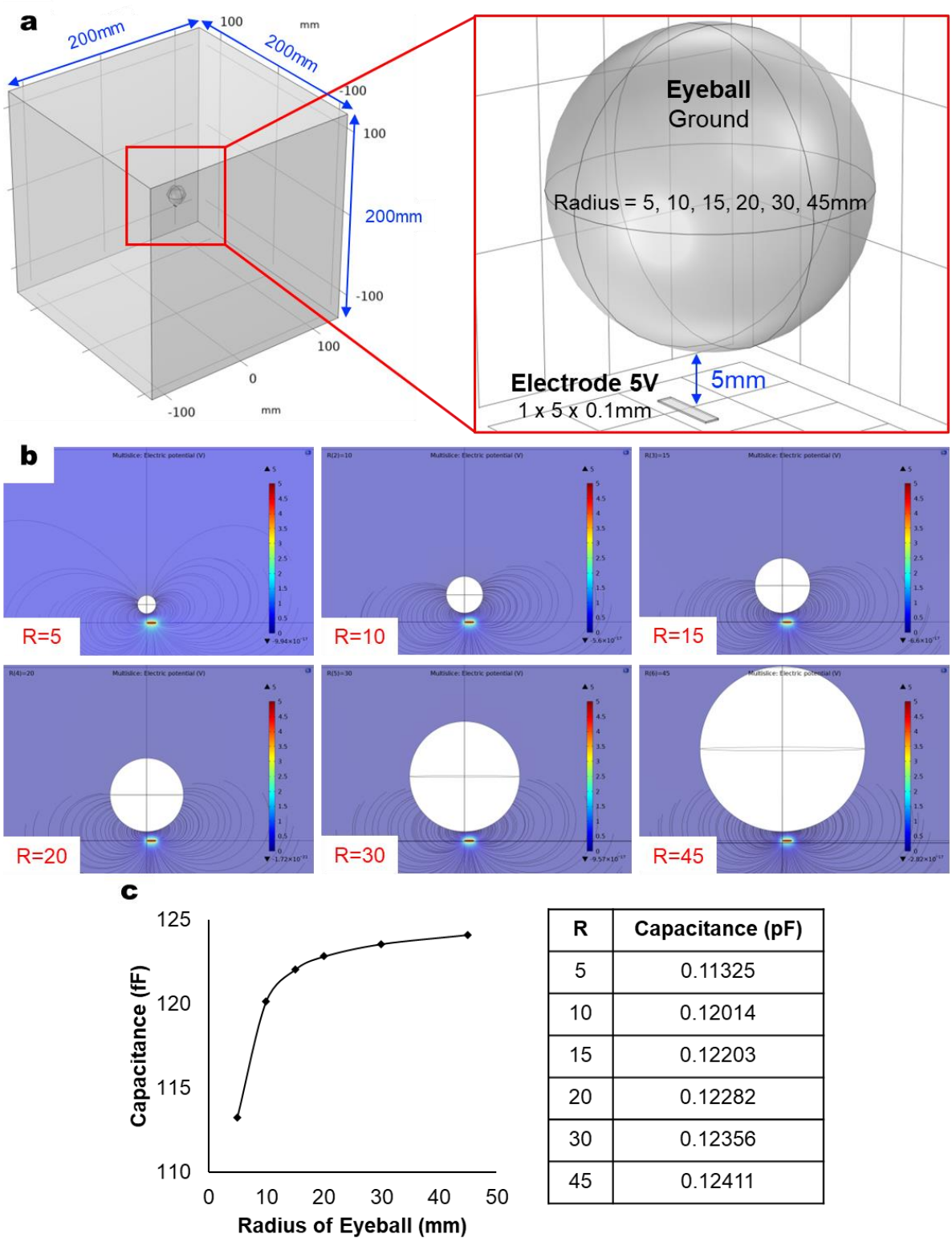

R	Capacitance (pF)
5	0.11325
10	0.12014
15	0.12203
20	0.12282
30	0.12356
45	0.12411

Fig. 36 a) COMSOL numerical model geometry. b) Graphical representation of changes in the fringing electric field with respect to change in radius. c) Numerical analysis of change in capacitance with increasing eyeball radius.

5.4 EXPERIMENTAL

5.4.1 *CPC sensor fabrication*

A capacitive sensor was made of carbon nanotube-paper composites using the previously reported methods [159, 160]. The fabricated CPC had a mean thickness of 88.4 ± 3.1 µm. For sensor fabrication, the initial material was cut into 5x20 mm^2 (Fig. 37). After patterning silver (MG Chemicals, 8330S-21G, USA) electrodes on both ends of the material, a 0.1 mm capillary pen was used to print a water line at the center of the material. With the water line weakening CPC fibers, tensional fracture was induced to separate the material. Through the wet-stretching process, a 5x10 mm^2 fibrous electrode was fabricated. A 50 µm-thick self-adhesive polyethylene terephthalate (PET) film was used for laminating the capacitive sensor, with a wire lead secured at the non-fracture end with silver epoxy.

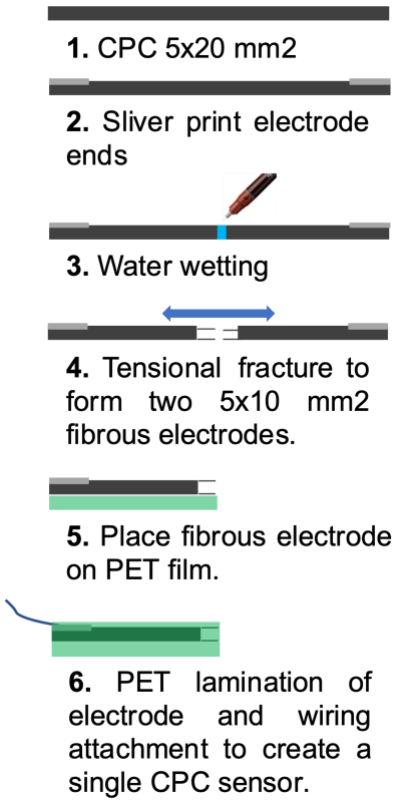

Fig. 37 CPC single electrode sensor fabrication process.

5.4.2 *Primate eye tracker prototype*

The primate eye tracker fixture (PETF) was custom designed based on cranial and facial measurements specific to the primate used in the study (see Fig. 38a). A metal rod connector was positioned atop the PETF, which fastened into a mounting ring on the primate head. The rob affixed the PETF in line with the primate's right eye. A conical mount extended from below the rod and in line with the primate's right cornea. Sensors were mounted around a trimmed tetrahedron slide plate with groves, that fit directly into the conical mount. The slide plates were designed with an interference fit to allow for adjustments towards the primate's eyeball. Sensors were adjusted to maintain a 10 mm gap to the primate's eye. CPC sensors were mounted on the external surface of slides with the fibers extending up to 5 mm from the slide plate edge. Fig. 38b shows the sensor position, where horizontal and vertical pairs are located equidistance from the center of the primate's cornea. To minimize the wire parasitic influences, sensor cables were trimmed and separated by pair designations while connected to the capacitance-to-digital converters (CDCs).

Two self-capacitance Analog Devices AD7747 CDCs were configured in differential modes to interpret horizontal and vertical capacitive changes. The AD7747 was a high-resolution, Σ-Δ capacitance-to-digital converter. The architecture featured inherent high resolution (24-bit no missing codes, up to 19.5-bit effective resolution), high linearity (±0.01%), and high accuracy (±10 fF). The AD7747 capacitance input range was ±8 pF (changing). The AD7747 was designed for single-ended or differential capacitive sensors systems. An I^2C protocol multiplexer (TCA9548A, Texas Instruments) was added in line to resolve the address conflict as well as schedule the measurements for each chip. An Atmel SAM D21 microcontroller interfaces with the CDCs and

multiplexer, to communicate capacitance data directly to a personal computer. Fig. 38c provides an electrical block diagram of the CDC and multiplexer integration to the microprocessor.

5.4.3 *Primate scleral search coil integration*

Two male rhesus macaques (Macaca mulatta) were used for this study. The technique to implant the scleral search coil has been previously reported by Soetedjo et al [172]. Briefly, a preformed 3-turn scleral eye coil (18-19 mm diameter) made of FEP (fluorinated ethylene propylene) insulated stranded stainless steel wire (0.0012" diameter, Alan Baird Industries) was placed surgically on the left eye of the animals under the conjunctiva. The eye coil was secured in place by tying it to both the lateral and medial rectus muscle insertions using absorbable suture. The two wire ends are twisted together, and then passed through a small hole drilled on the sphenoid bone. The twisted wires are then passed subcutaneously to the top of the skull, and soldered to a connector implanted on the frontal bone and secured using dental acrylic and titanium screws. Once recovered from the surgery, the animals were trained for both smooth pursuit and saccadic gaze tracking. The gaze target was a continuously lit laser spot that was aimed at orthogonal mirrors attached to galvanometers controlled by a computer. The laser was projected on the screen. A dollop of apple sauce was rewarded every second for continuous accurate tracking. The animal sit in a booth and its eye coil was placed in the center of two orthogonal AC magnetic fields with frequencies of 114 and 73 kHz for the horizontal and vertical fields, respectively. The amplified eye coil signal was then fed to a phase detector (CNC Engineering) that outputs voltages proportional to the angle of both horizontal and vertical gaze. The recorded analog signals of both horizontal and vertical eye and target positions were digitized at 1 kHz. Digitized data was output via a customized program developed in the laboratory. The program displays target positions, eye positions, and eye velocities.

5.4.4 *Gaze tracking experimental methodology*

Primate was secured in an acrylic cage, with a mount around its head to prevent all head movement. Fig. 38e provides a typical diagrammatic representation of a primate secured for experimentation with a feeder and tracking screen. Smooth pursuit and saccadic movements were examined in the horizontal and vertical eye movement directions. The range of ocular movement was bridged to $\pm 5^{o}$. Smooth pursuit and saccade movements had periods of 0.1 and 0.125 Hz, respectively. Capacitive signal from the PETF and scleral coil data were collected simultaneously during each trial. Capacitive data was collected at 21 Hz, with the scleral coil data at 1000 Hz. Data time stamps were correlated to synchronize capacitive and scleral coil datasets prior to processing.

Multiple trails were undertaken for three unique gaze movements: (1) horizontal smooth pursuit, (2) horizontal saccade, and (3) vertical smooth pursuit. A differential sensor pair recorded vertical eye movements and the other differential sensor pair recorded horizontal eye movements (see Fig. 38b).

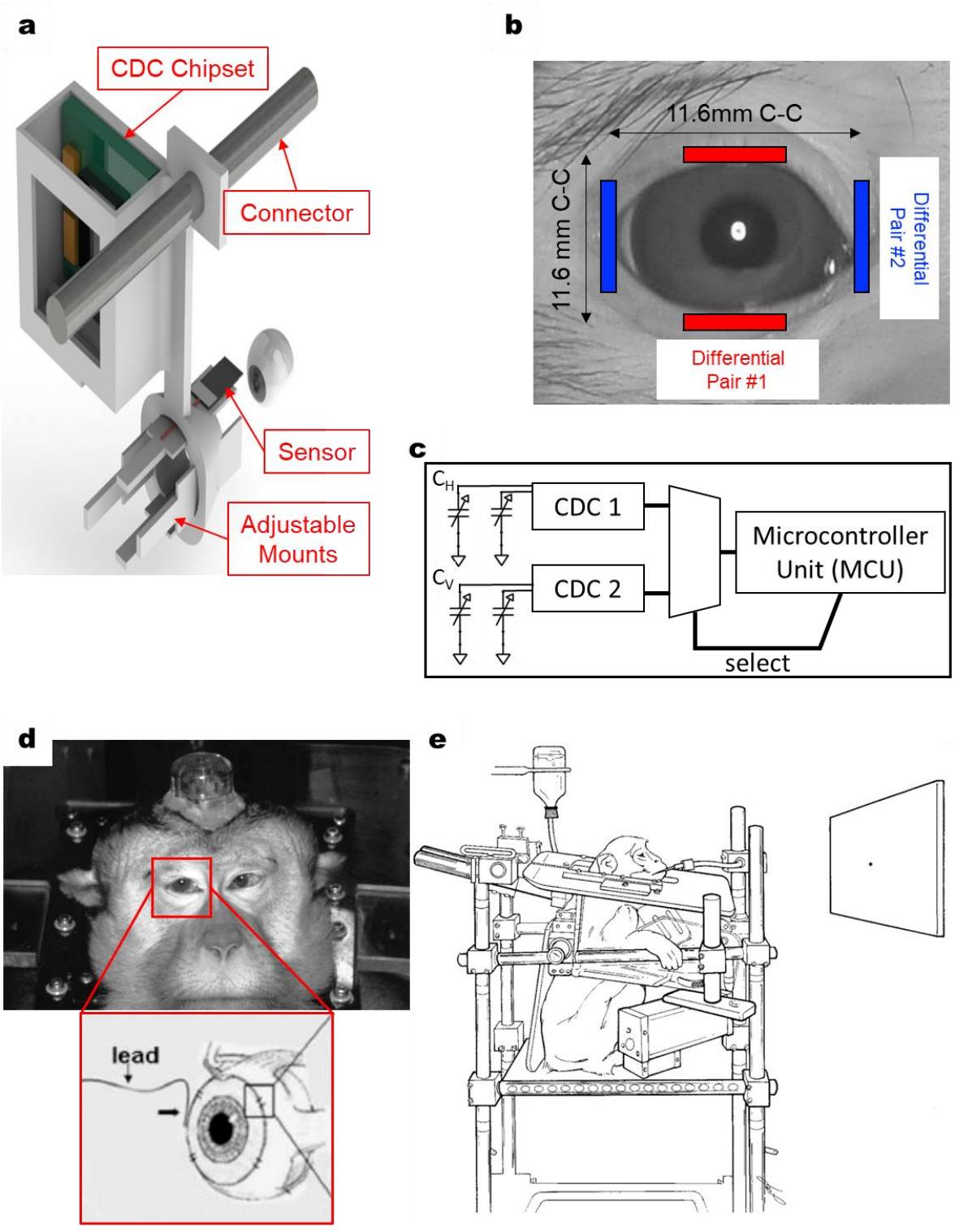

Fig. 38 a) Primate eye tracker fixture. b) Positioning of differential paired sensors around primate's eyeball. c) Electrical block diagram of capacitance to digital converter and microcontroller. d) Typical representation of a primate restraint structure during scleral coil gaze fixation study [173]. e) Typical representation of primate eye with scleral coil implant and head mount. Enlargement illustrates a closer representation of the scleral coil on the eye [174].

5.5 RESULTS

The scleral search was used to validate the performance of the capacitive eye tracker through monitoring smooth pursuit and saccade eye movement of a primate. All capacitance data were detrended and processed through a 16-point moving median algorithm. Data from the scleral coil were unfiltered and analysed without post-processing algorithms. The data were presented as nine cyclic segments from a single continuous smooth pursuit or saccade data set. Dividing the signal into segments allowed for investigating cyclic repeatability of the dataset at critical peaks. In Fig. 39a, horizontal smooth pursuit data are presented from capacitive differential sensor pair 2 and the scleral coil. The capacitive data shows a correlation coefficient of 0.95 to scleral coil data. Horizontal saccade (see Fig. 39b), like horizontal smooth pursuit, showed good periodic correlation between the capacitive and scleral coil data, with 0.95 correlation. Capacitive signal showed high peak noise during transitions from peak to peak. It was evident the capacitive eye tracker correlated eye movement periodically to the scleral search coil during horizontal gaze movements.

Vertical smooth pursuit (see Fig. 39c) also proved to have good periodic correlation to the scleral coil data, with a correlation coefficient of 0.91. Sensor adjustments were unidirectional, resulting in lack of adjustability vertically or horizontally from the eyeball. The eye tracker characterization analysis described in Chapter 3 and 4, proves how sensor position was critical to clarity of capacitive data. It was also speculated that the close proximity of the capacitive sensors to the eyeball and primates face could capture body potential near the eyeball. Further research will be needed to validate this hypothesis.

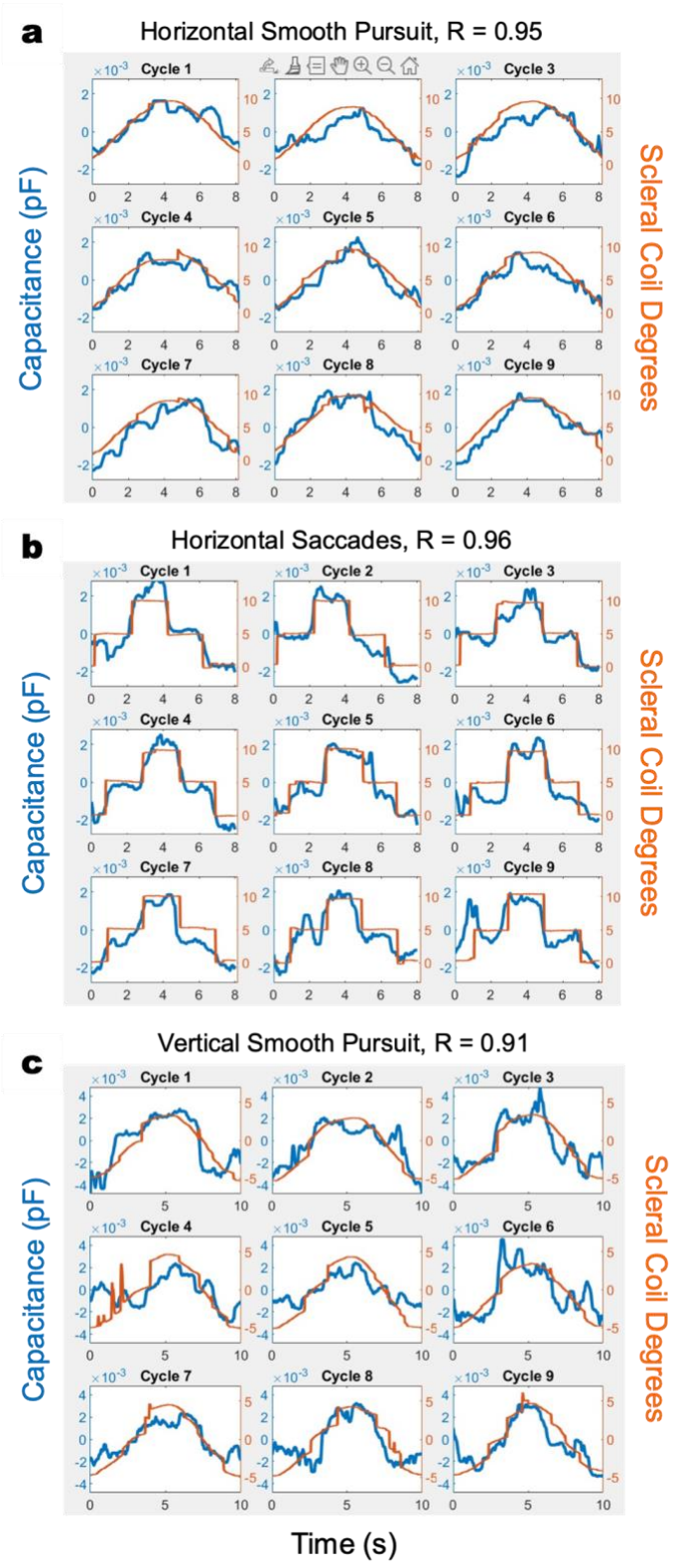

Fig. 39 Comparison of processed capacitance data and unfiltered scleral search coil data over a 60 sec time interval. a) Horizontal saccades, ±5º range, 0.125 Hz period. b) Horizontal smooth pursuit, ±5º range, 0.1 Hz period. c) Vertical smooth pursuit, ±5º range, 0.1 Hz period.

5.6 DISCUSSION

The capacitive eye tracker is a highly customizable and wearable device. Optimizing sensor geometry and signal processing software can bring forth high quality data in a non-invasive manner. The rhesus macaque (primate used for this study) eye was ~85% the size of a human eye. The sensitivity of the capacitive eye tracker was demonstrated through its ability to track the smaller eyeball of the primate. The variations in eyeball dimensions have been well documented with respect to age, sex diseases diagnosis, and vision disorders [175-177]. The numerical simulation displayed how varying only the eyeball size / shape, while maintaining all other variables in a system, could drastically influence the capacitance between the sensor electrode and eyeball. The correlation data from capacitive eye tracker to the scleral search coil showed the immense potential for the eye tracker for use in disease diagnosis and vision disorder monitoring.

5.7 CONCLUSION

A capacitive eye tracker was demonstrated to monitor eye movement of a primate. The scaling analysis using the numerical study showed that the capacitive signal could significantly decrease when the eyeball diameter was below 15 mm. In experiment, the capacitive eye tracker comprised of four CPC sensors in two pair differential configuration to track horizontal and vertical eye movements. The primate was implanted with a scleral search coil, the gold standard in eye tracking. Smooth pursuit and saccade eye movements were undertaken by the primate in horizontal and vertical gaze directions. Capacitive data was simultaneously collected alongside the output from the scleral coil to validate the eye tracker performance. Capacitive data displayed periodic correlation to the scleral coil with a maximum correlation coefficient of 0.96 during horizontal saccades. The capacitance was influenced by parasitic elements which presented as erratic spikes throughout the eye movement. Optimizing sensor location and proximity to the eyeball was a key aspect in reducing noise and parasitic capacitance. It was evident the capacitive eye tracker could correlate eye movement periodically to the scleral search coil during horizontal and vertical gaze movements. The eye tracker showed potential for disease diagnosis and vision disorder monitoring. Further research is required to investigate the cause of the parasitic capacitive elements and how they can be negated with more advanced signal processing techniques.

Chapter 6. CONCLUSIONS

6.1 SUMMARY OF CONCLUSIONS

A capacitive eye tracker was demonstrated to monitor eye movement. Based on our numerical analysis, a hybrid capacitive sensor made of fibrous and rectangular electrodes had the highest sensitivity due to the reduced initial capacitance and increased capacitance change in the presence of an eyeball. A single sensor in comparison to a differential sensor configuration showed enhanced detection performance. In the study using a face model, the human charge increased ΔC, but the face background reduced ΔC of eye movement. In the human subject test, the single capacitive measurement was optimal for vertical eye movement. For horizontal eye movement, differential capacitive methods were required for accurate measurement. The accuracies for vertical and horizontal movement were 1.1 and 0.8 degrees, respectively. The comparison of a capacitive eye tracker to a commercial eye tracker showed good correlation for horizontal and vertical eye movements. A phase diagram between vertical and horizontal signals was used to qualitatively assess eye movement. The presented capacitive eye tracker detected horizontal eye movement with the closed and open eyelids. The relationship between cornea and eyelid position was studied to understand their consequence on the capacitance signal. The cornea was found to dominate the capacitance signal, until the eyelid was fully closed.

The capacitive eye tracker was demonstrated to monitor the eye movement of a primate. A scaling analysis using a numerical study proved the capacitive signal could significantly decrease when the eyeball diameter was below 15 mm. The primate was implanted with a scleral search coil, the gold standard in eye tracking. Smooth pursuit and saccade eye movements were undertaken by the primate in horizontal and vertical gaze directions. The capacitive eye tracker comprised of four CPC sensors in two pairs of differential configuration to track horizontal and

vertical eye movements. Capacitive data were simultaneously collected alongside the scleral coil to validate the eye tracker performance. Capacitive data displayed periodic correlation to the scleral coil with a maximum correlation coefficient of 0.96 during horizontal saccades. The capacitance was influenced by parasitic elements which presented as erratic spikes throughout the eye movement. Optimizing sensor location and proximity to the eyeball was a key aspect in reducing noise and parasitic capacitance. It was evident the capacitive eye tracker could correlate eye movement periodically to the scleral search coil during horizontal and vertical gaze movements.

The presented wearable capacitive eye tracker shows potential for eye tracking in various fields, including neuroscience, cognitive science, eye function diagnosis, disease diagnosis, vision disorder monitoring, and entertainment.

6.2 FUTURE RESEARCH

With human subject testing and scleral search coil performance validation, further research is required to correlate capacitive data to more complex gaze paths. Eye tracker CPC sensor locations can be further optimized by realizing a more intuitive eye tracker frame that enables fine horizontal and vertical sensor adjustments, with respect to a subject's facial structure. Advanced signal processing including wavelet will facilitate better clarity of current capacitive eye tracker data. Machine learning will be algorithms to correlate the relationship between sensor signals to predict diagonal and circular gaze pathways. Superior active and passive shielding methods will be explored to negate parasitic capacitive influences and reduce noises, whereby providing a more sensitive signal output. The effect of EOG signals on CPC sensors will be further investigated to conclude the magnitude of their influence during eye movement.

Also, the learnings from the CPC eye tracker will be adopted to develop a capacitive sleep mask. Custom-integrated circuitry coupled with capacitive CPC sensors will enable high sampling rates capable of sleep staging and rapid eye movement (REM) sleep monitoring, and sleep disorder diagnosis.

REFERENCES

[1] J. Priestley, *The History and Present State of Electricity: With Original Experiments*. J. Dodsley, J. Johnson, B. Davenport, and T. Cadell, 1767.

[2] J. F. Keithley, *The Story of Electrical and Magnetic Measurements: From 500 BC to the 1940s*. Wiley, 1999.

[3] M. Cherington, P. R. Yarnell, and C. L. Cherington, "LIGHTNING, LEYDEN JAR, AND THE HISTORIC BEGINNINGS OF ELECTROPHYSIOLOGY," (in English), *Muscle Nerve,* Note vol. 17, no. 8, pp. 951-952, Aug 1994, doi: 10.1002/mus.880170818.

[4] A. Allerhand, "Who Invented the Earliest Capacitor Bank ("Battery" of Leyden Jars)? It's Complicated," (in English), *Proc. IEEE,* Editorial Material vol. 106, no. 3, pp. 496-503, Mar 2018, doi: 10.1109/jproc.2018.2795846.

[5] R. Cecchini and G. Pelosi, "Alessandro Volta and his battery," *IEEE Antennas and Propagation Magazine,* vol. 34, pp. 30-37, 1992.

[6] W. J. Sarjeant, J. Zirnheld, and F. W. MacDougall, "Capacitors," (in English), *IEEE Trans. Plasma Sci.,* Article vol. 26, no. 5, pp. 1368-1392, Oct 1998, doi: 10.1109/27.736020.

[7] M. Jayalakshmi and K. Balasubramanian, "Simple Capacitors to Supercapacitors - An Overview," (in English), *Int. J. Electrochem. Sci.,* Review vol. 3, no. 11, pp. 1196-1217, Nov 2008. [Online]. Available: <Go to ISI>://WOS:000260118800001.

[8] P. Sharma and T. S. Bhatti, "A review on electrochemical double-layer capacitors," (in English), *Energy Conv. Manag.,* Article vol. 51, no. 12, pp. 2901-2912, Dec 2010, doi: 10.1016/j.enconman.2010.06.031.

[9] K. Naoi, "'Nanohybrid Capacitor': The Next Generation Electrochemical Capacitors," (in English), *Fuel Cells,* Review vol. 10, no. 5, pp. 825-833, Oct 2010, doi: 10.1002/fuce.201000041.

[10] A. Braun, R. Wichert, A. Kuijper, and D. W. Fellner, "Capacitive proximity sensing in smart environments," (in English), *J. Ambient Intell. Smart Environ.,* Article vol. 7, no. 4, pp. 483-510, 2015, doi: 10.3233/ais-150324.

[11] K. Gann, "Theremin: Ether music and espionage," (in English), *Am. Music,* Book Review vol. 21, no. 4, pp. 519-521, Win 2003, doi: 10.2307/3250577.

[12] Y. Ye, C. Y. Zhang, C. L. He, X. Wang, J. J. Huang, and J. H. Deng, "A Review on Applications of Capacitive Displacement Sensing for Capacitive Proximity Sensor," (in English), *Ieee Access,* Review vol. 8, pp. 45325-45342, 2020, doi: 10.1109/access.2020.2977716.

[13] X. H. Hu and W. Q. Yang, "Planar capacitive sensors - designs and applications," (in English), *Sens. Rev.,* Article vol. 30, no. 1, pp. 24-39, 2010, doi: 10.1108/02602281011010772.

[14] P. T. Krein and R. D. Meadows, "THE ELECTROQUASISTATICS OF THE CAPACITIVE TOUCH PANEL," (in English), *IEEE Trans. Ind. Appl.,* Article; Proceedings Paper vol. 26, no. 3, pp. 529-534, May-Jun 1990, doi: 10.1109/28.55954.

[15] G. Barrett and R. Omote, "Projected-Capacitive Touch Technology," *Information Display,* vol. 26, pp. 16-21, 03/01 2010, doi: 10.1002/j.2637-496x.2010.tb00229.x.

[16] J. Yanase, K. Takatori, and H. Asada, "60.3L: Late-News Paper: Algorithm for Recognizing Pinch Gestures on Surface-Capacitive Touch Screens," *SID Symposium Digest of Technical Papers,* https://doi.org/10.1002/sdtp.10394 vol. 46, no. 1, pp. 899-902, 2015/06/01 2015, doi: https://doi.org/10.1002/sdtp.10394.

[17] H. Nam, K. H. Seol, J. Lee, H. Cho, and S. W. Jung, "Review of Capacitive Touchscreen Technologies: Overview, Research Trends, and Machine Learning Approaches," (in English), *Sensors,* Review vol. 21, no. 14, p. 26, Jul 2021, Art no. 4776, doi: 10.3390/s21144776.

[18] S. Jobs, "TOUCH SCREEN DEVICE, METHOD, AND GRAPHICAL USER INTERFACE FOR DETERMINING COMMANDS BY APPLYING HEURISTICS," US Patent US007479949B2, 01/20/2008, 2009.

[19] N. Jonassen, "Human body capacitance: static or dynamic concept? [ESD]," in *Electrical Overstress/ Electrostatic Discharge Symposium Proceedings. 1998 (Cat. No.98TH8347)*, 6-8 Oct. 1998 1998, pp. 111-117, doi: 10.1109/EOSESD.1998.737028.

[20] K. Chamberlin, W. PhD, C. Bsee, S. Bsee, and P. Bsee, "Analysis of the Charge Exchange Between the Human Body and Ground: Evaluation of "Earthing" From an Electrical Perspective," *Journal of Chiropractic Medicine,* vol. 13, 12/31 2014, doi: 10.1016/j.jcm.2014.10.001.

[21] W. Jayathilaka *et al.*, "Significance of Nanomaterials in Wearables: A Review on Wearable Actuators and Sensors," (in English), *Adv. Mater.,* Review vol. 31, no. 7, p. 21, Feb 2019, Art no. 1805921, doi: 10.1002/adma.201805921.

[22] P. Bindra and A. Hazra, "Capacitive gas and vapor sensors using nanomaterials," (in English), *J. Mater. Sci.-Mater. Electron.,* Review vol. 29, no. 8, pp. 6129-6148, Apr 2018, doi: 10.1007/s10854-018-8606-2.

[23] H. Z. Wang *et al.*, "Flexible capacitive pressure sensors for wearable electronics," (in English), *Journal of Materials Chemistry C,* Review vol. 10, no. 5, pp. 1594-1605, Feb 2022, doi: 10.1039/d1tc05304c.

[24] J. Lee *et al.*, "Conductive Fiber-Based Ultrasensitive Textile Pressure Sensor for Wearable Electronics," (in English), *Adv. Mater.,* Article vol. 27, no. 15, pp. 2433-2439, Apr 2015, doi: 10.1002/adma.201500009.

[25] V. Mitrakos, L. Macintyre, F. C. Denison, P. J. W. Hands, and M. P. Y. Desmulliez, "Design, Manufacture and Testing of Capacitive Pressure Sensors for Low-Pressure Measurement Ranges," (in English), *Micromachines,* Article vol. 8, no. 2, p. 10, Feb 2017, Art no. 41, doi: 10.3390/mi8020041.

[26] Q. Zhang *et al.*, "Flexible wide-range capacitive pressure sensor using micropore PE tape as template," (in English), *Smart Mater. Struct.,* Article vol. 28, no. 11, p. 8, Nov 2019, Art no. 115040, doi: 10.1088/1361-665X/ab4ac6.

[27] D. Kwon *et al.*, "Highly Sensitive, Flexible, and Wearable Pressure Sensor Based on a Giant Piezocapacitive Effect of Three-Dimensional Microporous Elastomeric Dielectric Layer," (in English), *ACS Appl. Mater. Interfaces,* Article vol. 8, no. 26, pp. 16922-16931, Jul 2016, doi: 10.1021/acsami.6b04225.

[28] D. H. Kim *et al.*, "Hollow polydimethylsiloxane (PDMS) foam with a 3D interconnected network for highly sensitive capacitive pressure sensors," (in English), *Micro Nano Syst. Lett.,* Article vol. 8, no. 1, p. 7, Dec 2020, Art no. 24, doi: 10.1186/s40486-020-00127-8.

[29] S. C. Chen, S. S. Xin, L. Yang, Y. J. Guo, W. Q. Zhang, and K. Sun, "Multi-sized planar capacitive pressure sensor with ultra-high sensitivity," (in English), *Nano Energy,* Article vol. 87, p. 8, Sep 2021, Art no. 106178, doi: 10.1016/j.nanoen.2021.106178.

[30] A. Albrecht *et al.*, "Screen-printed capacitive pressure sensors with high sensitivity and accuracy on flexible substrates," (in English), *Flex. Print. Electron.,* Article vol. 7, no. 3, p. 11, Sep 2022, Art no. 035005, doi: 10.1088/2058-8585/ac812d.

[31] D. J. Cohen, D. Mitra, K. Peterson, and M. M. Maharbiz, "A Highly Elastic, Capacitive Strain Gauge Based on Percolating Nanotube Networks," (in English), *Nano Lett.*, Article vol. 12, no. 4, pp. 1821-1825, Apr 2012, doi: 10.1021/nl204052z.

[32] V. Tsouti, V. Mitrakos, P. Broutas, and S. Chatzandroulis, "Modeling and Development of a Flexible Carbon Black-Based Capacitive Strain Sensor," (in English), *IEEE Sens. J.*, Article vol. 16, no. 9, pp. 3059-3067, May 2016, doi: 10.1109/jsen.2016.2524508.

[33] R. Nur, N. Matsuhisa, Z. Jiang, M. O. G. Nayeem, T. Yokota, and T. Someya, "A Highly Sensitive Capacitive-type Strain Sensor Using Wrinkled Ultrathin Gold Films," (in English), *Nano Lett.*, Article vol. 18, no. 9, pp. 5610-5617, Sep 2018, doi: 10.1021/acs.nanolett.8b02088.

[34] A. D. Qiu *et al.*, "Highly sensitive and flexible capacitive elastomeric sensors for compressive strain measurements," (in English), *Mater. Today Commun.*, Article vol. 26, p. 11, Mar 2021, Art no. 102023, doi: 10.1016/j.mtcomm.2021.102023.

[35] J. T. Lin *et al.*, "Development of capacitive pure bending strain sensor for wireless spinal fusion monitoring," (in English), *Sens. Actuator A-Phys.*, Article vol. 138, no. 2, pp. 276-287, Aug 2007, doi: 10.1016/j.sna.2007.04.069.

[36] X. He *et al.*, "Microstructured capacitive sensor with broad detection range and long-term stability for human activity detection," (in English), *npj Flex. Electron.*, Article vol. 5, no. 1, p. 9, Jul 2021, Art no. 17, doi: 10.1038/s41528-021-00114-y.

[37] Y. L. Zhu, X. Chen, K. M. Chu, X. Wang, Z. Q. Hu, and H. J. Su, "Carbon Black/PDMS Based Flexible Capacitive Tactile Sensor for Multi-Directional Force Sensing," (in English), *Sensors*, Article vol. 22, no. 2, p. 18, Jan 2022, Art no. 628, doi: 10.3390/s22020628.

[38] J. A. Dobrzynska and M. A. M. Gijs, "Flexible polyimide-based force sensor," (in English), *Sens. Actuator A-Phys.*, Article vol. 173, no. 1, pp. 127-135, Jan 2012, doi: 10.1016/j.sna.2011.11.006.

[39] T. Nagatomo and N. Miki, "Reduction of Parasitic Capacitance of A PDMS Capacitive Force Sensor," (in English), *Micromachines*, Article vol. 9, no. 11, p. 9, Nov 2018, Art no. 570, doi: 10.3390/mi9110570.

[40] J. L. Ye, T. T. Sun, D. Huang, Z. H. Li, and L. Lin, "Stand-alone differential capacitance force sensors with sub-nano-newton sensitivity," (in English), *J. Micromech. Microeng.*, Article vol. 27, no. 9, p. 10, Sep 2017, Art no. 095017, doi: 10.1088/1361-6439/aa81bc.

[41] J. Kim, J.-H. Cho, H.-M. Lee, and S.-M. Hong, "Capacitive Humidity Sensor Based on Carbon Black/Polyimide Composites," *Sensors*, vol. 21, no. 6, p. 1974, 2021. [Online]. Available: https://www.mdpi.com/1424-8220/21/6/1974.

[42] E. Zampetti *et al.*, "Design and optimization of an ultra thin flexible capacitive humidity sensor," *Sensors and Actuators B: Chemical*, vol. 143, no. 1, pp. 302-307, 2009/12/04/ 2009, doi: https://doi.org/10.1016/j.snb.2009.09.004.

[43] F. R. Hsiao and Y. C. Liao, "Printed Micro-Sensors for Simultaneous Temperature and Humidity Detection," *Ieee Sensors Journal*, vol. 18, no. 16, pp. 6788-6793, Aug 2018, doi: 10.1109/jsen.2018.2850372.

[44] J. J. Steele, M. T. Taschuk, and M. J. Brett, "Nanostructured metal oxide thin films for humidity sensors," *Ieee Sensors Journal*, vol. 8, no. 7-8, pp. 1422-1429, Jul-Aug 2008, doi: 10.1109/jsen.2008.920715.

[45] Z. G. Zhao, J. T. Zhang, J. H. Zhang, C. Li, Y. N. Li, and X. Wang, "Capacitance-type MWCNTs/SiO2 humidity sensor based on capillary condensation and percolation theory,"

Sensors and Actuators a-Physical, vol. 263, pp. 648-653, Aug 2017, doi: 10.1016/j.sna.2017.07.030.

[46] C. Gaspar, J. Olkkonen, S. Passoja, and M. Smolander, "Paper as Active Layer in Inkjet-Printed Capacitive Humidity Sensors," *Sensors,* vol. 17, no. 7, Jul 2017, Art no. 1464, doi: 10.3390/s17071464.

[47] N. Suryana *et al.*, "Optimization of Phase Shift-Based Capacitive Sensor for Water Content Detection in Biodiesel," *IEEE Sensors Journal,* vol. 22, no. 16, pp. 16131-16140, 2022, doi: 10.1109/JSEN.2022.3188039.

[48] P. K. Isgor, M. Marcali, M. Keser, and C. Elbuken, "Microfluidic droplet content detection using integrated capacitive sensors," *Sensors and Actuators B: Chemical,* vol. 210, pp. 669-675, 2015/04/01/ 2015, doi: https://doi.org/10.1016/j.snb.2015.01.018.

[49] C. S. A. Gong, H. K. Chiu, L. R. Huang, C. H. Lin, Z. D. Hsu, and P. H. Tu, "Low-Cost Comb-Electrode Capacitive Sensing Device for Liquid-Level Measurement," *IEEE Sensors Journal,* vol. 16, no. 9, pp. 2896-2897, 2016, doi: 10.1109/JSEN.2016.2524696.

[50] T. Islam, O. P. Maurya, and A. U. Khan, "Design and Fabrication of Fringing Field Capacitive Sensor for Non-Contact Liquid Level Measurement," *IEEE Sensors Journal,* vol. 21, no. 21, pp. 24812-24819, 2021, doi: 10.1109/JSEN.2021.3112848.

[51] S. R. A. Ruth, V. R. Feig, M. G. Kim, Y. Khan, J. K. Phong, and Z. N. Bao, "Flexible Fringe Effect Capacitive Sensors with Simultaneous High-Performance Contact and Non-Contact Sensing Capabilities," *Small Structures,* vol. 2, no. 2, Feb 2021, Art no. 2000079, doi: 10.1002/sstr.202000079.

[52] K. Chetpattananondh, T. Tapoanoi, P. Phukpattaranont, and N. Jindapetch, "A self-calibration water level measurement using an interdigital capacitive sensor," *Sensors and Actuators a-Physical,* vol. 209, pp. 175-182, Mar 2014, doi: 10.1016/j.sna.2014.01.040.

[53] Q. Yang *et al.*, "An inkjet-printed capacitive sensor for water level or quality monitoring: investigated theoretically and experimentally," *Journal of Materials Chemistry A,* vol. 5, no. 34, pp. 17841-17847, Sep 2017, doi: 10.1039/c7ta05094a.

[54] A. Dutta, S. K. Bera, S. Saha, H. Mandal, C. Dey, and S. C. Bera, "Study of a Noncontact Flow Transducer Using Semicylindrical Capacitive Sensor," *Ieee Transactions on Instrumentation and Measurement,* vol. 70, 2021, Art no. 9501910, doi: 10.1109/tim.2020.3024027.

[55] S. C. Bera and H. Mandal, "A Flow Measurement Technique Using a Noncontact Capacitance-Type Orifice Transducer for a Conducting Liquid," *Ieee Transactions on Instrumentation and Measurement,* vol. 61, no. 9, pp. 2553-2559, Sep 2012, doi: 10.1109/tim.2012.2192345.

[56] S. Jing *et al.*, "Capacitive-type liquid crystal temperature sensor," (in English), *Liq. Cryst.,* Article vol. 48, no. 8, pp. 1103-1110, Jun 2021, doi: 10.1080/02678292.2020.1846093.

[57] M. M. Othayq, N. Giganti, and M. Shavezipur, "Development of capacitive temperature sensors with high sensitivity using a multiuser polycrystalline silicon process," (in English), *Microelectron. Eng.,* Article vol. 226, p. 6, Apr 2020, Art no. 111287, doi: 10.1016/j.mee.2020.111287.

[58] U. Salmaz, T. Islam, and S. Sohail, "A Novel Linear Capacitive Temperature Sensor Using Polydimethylsiloxane," (in English), *IEEE Trans. Instrum. Meas.,* Article vol. 69, no. 10, pp. 7887-7894, Oct 2020, doi: 10.1109/tim.2020.2986120.

[59] H. Y. Ma, Q. A. Huang, M. Qin, and T. T. Lu, "A micromachined silicon capacitive temperature sensor for wide temperature range applications," (in English), *J. Micromech.*

Microeng., Article vol. 20, no. 5, p. 6, May 2010, Art no. 055036, doi: 10.1088/0960-1317/20/5/055036.

[60] Y. Wei, R. Torah, Y. Li, and J. Tudor, "Dispenser printed capacitive proximity sensor on fabric for applications in the creative industries," (in English), *Sens. Actuator A-Phys.*, Article vol. 247, pp. 239-246, Aug 2016, doi: 10.1016/j.sna.2016.06.005.

[61] M. Kim, W. Moon, E. Yoon, and K. R. Lee, "A new capacitive displacement sensor with high accuracy and long-range," (in English), *Sens. Actuator A-Phys.*, Article; Proceedings Paper vol. 130, pp. 135-141, Aug 2006, doi: 10.1016/j.sna.2005.12.012.

[62] N. Blaž, M. Kisić, L. Živanov, and M. Damnjanović, "Displacement sensor fabricated by 3D additive manufacturing," in *2017 40th International Spring Seminar on Electronics Technology (ISSE)*, 10-14 May 2017 2017, pp. 1-4, doi: 10.1109/ISSE.2017.8000998.

[63] J. L. Ye *et al.*, "Tunable seesaw-like 3D capacitive sensor for force and acceleration sensing," (in English), *npj Flex. Electron.*, Article vol. 5, no. 1, p. 9, Oct 2021, Art no. 28, doi: 10.1038/s41528-021-00125-9.

[64] W. M. Qu, C. Wenzel, and G. Gerlach, "Fabrication of a 3D differential-capacitive acceleration sensor by UV-LIGA," (in English), *Sens. Actuator A-Phys.*, Article vol. 77, no. 1, pp. 14-20, Sep 1999, doi: 10.1016/s0924-4247(98)00377-x.

[65] C. Burbaum, J. Mohr, P. Bley, and W. Ehrfeld, "FABRICATION OF CAPACITIVE ACCELERATION SENSORS BY THE LIGA TECHNIQUE," (in English), *Sens. Actuator A-Phys.*, Article; Proceedings Paper vol. 27, no. 1-3, pp. 559-563, May 1991, doi: 10.1016/0924-4247(91)87051-4.

[66] S. Kavitha, R. J. Daniel, and K. Sumangala, "Design and Analysis of MEMS Comb Drive Capacitive Accelerometer for SHM and Seismic Applications," (in English), *Measurement*, Article vol. 93, pp. 327-339, Nov 2016, doi: 10.1016/j.measurement.2016.07.029.

[67] D. J. Young, M. A. Zurcher, M. Semaan, C. A. Megerian, and W. H. Ko, "MEMS Capacitive Accelerometer-Based Middle Ear Microphone," (in English), *IEEE Trans. Biomed. Eng.*, Article vol. 59, no. 12, pp. 3283-3292, Dec 2012, doi: 10.1109/tbme.2012.2195782.

[68] K. Rao *et al.*, "A MEMS Micro-g Capacitive Accelerometer Based on Through-Silicon-Wafer-Etching Process," (in English), *Micromachines*, Article vol. 10, no. 6, p. 14, Jun 2019, Art no. 380, doi: 10.3390/mi10060380.

[69] T. K. Sethuramalingam and A. Vimalajuliet, "Design of MEMS based capacitive accelerometer," in *2010 International Conference on Mechanical and Electrical Technology*, 10-12 Sept. 2010 2010, pp. 565-568, doi: 10.1109/ICMET.2010.5598424.

[70] B. Luo, R. Mai, Y. Chen, Y. Zhang, and Z. He, "A voltage stress optimization method of capacitive power transfer charging system," in *2017 IEEE Applied Power Electronics Conference and Exposition (APEC)*, 26-30 March 2017 2017, pp. 1456-1461, doi: 10.1109/APEC.2017.7930890.

[71] X. Chen, Z. Zhang, S. Yu, and T.-G. Zsuzsan, *Fringing Effect Analysis of Parallel Plate Capacitors for Capacitive Power Transfer Application*. 2019.

[72] B. D. Hughes, "On the potential due to a circular parallel plate capacitor," *Journal of Physics A: Mathematical and General*, vol. 17, no. 6, p. 1385, 1984/04/21 1984, doi: 10.1088/0305-4470/17/6/033.

[73] V. Hutson, "The circular plate condenser at small separations," *Mathematical Proceedings of the Cambridge Philosophical Society,* vol. 59, no. 1, pp. 211-224, 1963, doi: 10.1017/S0305004100002152.
[74] R. P. Clayton, "The PerUnitLength Parameters for Multiconductor Lines," in *Analysis of Multiconductor Transmission Lines*: IEEE, 2008, pp. 160-239.
[75] Z. P. Ji *et al.*, "The Design and Characterization of a Flexible Tactile Sensing Array for Robot Skin," (in English), *Sensors,* Article vol. 16, no. 12, p. 11, Dec 2016, Art no. 2001, doi: 10.3390/s16122001.
[76] X. H. Hu *et al.*, "A flexible capacitive tactile sensor array with micro structure for robotic application," (in English), *Sci. China-Inf. Sci.,* Article vol. 57, no. 12, p. 6, Dec 2014, Art no. 120204, doi: 10.1007/s11432-014-5191-8.
[77] G. H. Liang, Y. C. Wang, D. Q. Mei, K. I. Xi, and Z. C. Chen, "Flexible Capacitive Tactile Sensor Array With Truncated Pyramids as Dielectric Layer for Three-Axis Force Measurement," (in English), *J. Microelectromech. Syst.,* Article vol. 24, no. 5, pp. 1510-1519, Oct 2015, doi: 10.1109/jmems.2015.2418095.
[78] L. M. Castano and A. B. Flatau, "Smart fabric sensors and e-textile technologies: a review," *Smart Mater. Struct.,* vol. 23, no. 5, p. 053001, 2014/04/01 2014, doi: 10.1088/0964-1726/23/5/053001.
[79] J. Meyer, B. Arnrich, J. Schumm, and G. Troster, "Design and Modeling of a Textile Pressure Sensor for Sitting Posture Classification," *IEEE Sens. J.,* vol. 10, no. 8, pp. 1391-1398, 2010, doi: 10.1109/JSEN.2009.2037330.
[80] S. Takamatsu, T. Kobayashi, N. Shibayama, K. Miyake, and T. Itoh, "Fabric pressure sensor array fabricated with die-coating and weaving techniques," *Sensors and Actuators A Physical,* vol. 184, pp. 57–63, 09/30 2012, doi: 10.1016/j.sna.2012.06.031.
[81] S. El-Molla *et al.*, "Integration of a Thin Film PDMS-Based Capacitive Sensor for Tactile Sensing in an Electronic Skin," *Journal of Sensors,* vol. 2016, pp. 1-7, 01/01 2016, doi: 10.1155/2016/1736169.
[82] S. R. Kim, J. H. Kim, and J. W. Park, "Wearable and Transparent Capacitive Strain Sensor with High Sensitivity Based on Patterned Ag Nanowire Networks," (in English), *ACS Appl. Mater. Interfaces,* Article vol. 9, no. 31, pp. 26407-26416, Aug 2017, doi: 10.1021/acsami.7b06474.
[83] K. Cammann, "Book Review: Sensors—A Comprehensive Survey. Series editors: W. Göpel, J. Hesse and J. N. Zemel. VCH Verlagsgesellschaft, Weinheim. Vol. 1: Fundamentals and General Aspects. Edited by T. Grandke and W. H. Ko. 1989. xxxiii, 641 pp., hardcover DM 350.00 (subscription price: DM 290.00).—ISBN 3-527-26767-0; Vol. 5: Magnetic Sensors. Edited by R. Boll and K. J. Overshott," *Angewandte Chemie International Edition in English,* https://doi.org/10.1002/anie.199101102 vol. 30, no. 1, pp. 110-111, 1991/01/01 1991, doi: https://doi.org/10.1002/anie.199101102.
[84] M. d. Vos, R. Torah, and J. Tudor, "A novel pneumatic dispenser fabrication technique for digitally printing electroluminescent lamps on fabric," in *2015 Symposium on Design, Test, Integration and Packaging of MEMS/MOEMS (DTIP)*, 27-30 April 2015 2015, pp. 1-4, doi: 10.1109/DTIP.2015.7160977.
[85] Z. Ahmed, R. Torah, and J. Tudor, "Optimisation of a novel direct-write dispenser printer technique for improving printed smart fabric device performance," in *2015 Symposium on Design, Test, Integration and Packaging of MEMS/MOEMS (DTIP)*, 27-30 April 2015 2015, pp. 1-5, doi: 10.1109/DTIP.2015.7160978.

[86] T. Li *et al.*, "Ultrasensitive Capacitive Sensor Composed of Nanostructured Electrodes for Human–Machine Interface," *Advanced Materials Technologies*, https://doi.org/10.1002/admt.202101704 vol. 7, no. 10, p. 2101704, 2022/10/01 2022, doi: https://doi.org/10.1002/admt.202101704.

[87] J. Fraden, "Jacob Fraden: Handbook of modern sensors: physics, designs, and applications," *Analytical and Bioanalytical Chemistry*, vol. 382, no. 1, pp. 8-9, 2005/05/01 2005, doi: 10.1007/s00216-004-3037-8.

[88] A. Cowen, B. Hardy, R. Mahadevan, and S. Wilcenski, *PolyMUMPs Design Handbook*, 13.0 ed. MEMSCAP Inc., 1992.

[89] M. Nath, S. Maity, and S. Sen, "Toward Understanding the Return Path Capacitance in Capacitive Human Body Communication," (in English), *IEEE Trans. Circuits Syst. II-Express Briefs*, Article vol. 67, no. 10, pp. 1879-1883, Oct 2020, doi: 10.1109/tcsii.2019.2953682.

[90] J. Zeng, L. B. Dong, W. X. Sha, L. Wei, and X. Guo, "Highly stretchable, compressible and arbitrarily deformable all-hydrogel soft supercapacitors," (in English), *Chem. Eng. J.*, Article vol. 383, p. 9, Mar 2020, Art no. 123098, doi: 10.1016/j.cej.2019.123098.

[91] Z. Y. Lei, Q. K. Wang, S. T. Sun, W. C. Zhu, and P. Y. Wu, "A Bioinspired Mineral Hydrogel as a Self-Healable, Mechanically Adaptable Ionic Skin for Highly Sensitive Pressure Sensing," (in English), *Adv. Mater.*, Article vol. 29, no. 22, p. 6, Jun 2017, Art no. 1700321, doi: 10.1002/adma.201700321.

[92] L. Dhakar, P. Pitchappa, F. E. H. Tay, and C. Lee, "An intelligent skin based self-powered finger motion sensor integrated with triboelectric nanogenerator," (in English), *Nano Energy*, Article vol. 19, pp. 532-540, Jan 2016, doi: 10.1016/j.nanoen.2015.04.020.

[93] M. Wilhelm, D. Krakowczyk, and S. Albayrak, "PeriSense: Ring-Based Multi-Finger Gesture Interaction Utilizing Capacitive Proximity Sensing," (in English), *Sensors*, Article vol. 20, no. 14, p. 23, Jul 2020, Art no. 3990, doi: 10.3390/s20143990.

[94] V. Sakthivelpathi *et al.*, "Capacitive eye tracker made of fractured carbon nanotube-paper composites for wearable applications," *Sensors and Actuators A: Physical*, vol. 344, p. 113739, 2022/09/01/ 2022, doi: https://doi.org/10.1016/j.sna.2022.113739.

[95] E. Luo, R. Fu, A. Chu, K. Vega, and C. H.-L. Kao, *Eslucent: an eyelid interface for detecting eye blinking*. 2020, pp. 58-62.

[96] A. Pantelopoulos and N. G. Bourbakis, "Prognosis-a wearable health-monitoring system for people at risk: methodology and modeling," (in eng), *IEEE Trans Inf Technol Biomed*, vol. 14, no. 3, pp. 613-21, May 2010, doi: 10.1109/titb.2010.2040085.

[97] P. C. Ng, S. S. Murray, S. Levy, and J. C. Venter, "An agenda for personalized medicine," (in eng), *Nature*, vol. 461, no. 7265, pp. 724-6, Oct 8 2009, doi: 10.1038/461724a.

[98] H. Huang *et al.*, "Graphene-Based Sensors for Human Health Monitoring," (in eng), *Front Chem*, vol. 7, p. 399, 2019, doi: 10.3389/fchem.2019.00399.

[99] P. K. Sekar *et al.*, "Simultaneous multiparameter whole blood hemostasis assessment using a carbon nanotube-paper composite capacitance sensor," (in English), *Biosensors & Bioelectronics*, Article vol. 197, p. 10, Feb 2022, Art no. 113786, doi: 10.1016/j.bios.2021.113786.

[100] M. Iwasaki *et al.*, "Capacitive-Type Pressure-Mapping Sensor for Measuring Bite Force," (in English), *Int. J. Environ. Res. Public Health*, Article vol. 19, no. 3, p. 9, Feb 2022, Art no. 1273, doi: 10.3390/ijerph19031273.

[101] S. W. Park, P. S. Das, and J. Y. Park, "Development of wearable and flexible insole type capacitive pressure sensor for continuous gait signal analysis," (in English), *Org. Electron.*, Article vol. 53, pp. 213-220, Feb 2018, doi: 10.1016/j.orgel.2017.11.033.
[102] S. K. Kundu, S. Kumagai, and M. Sasaki, "A Wearable Capacitive Sensor for Monitoring Human Respiratory Rate," (in English), *Jpn. J. Appl. Phys.*, Article vol. 52, no. 4, p. 7, Apr 2013, Art no. 04cl05, doi: 10.7567/jjap.52.04cl05.
[103] T. Hoffmann, B. Eilebrecht, and S. Leonhardt, "Respiratory Monitoring System on the Basis of Capacitive Textile Force Sensors," (in English), *IEEE Sens. J.*, Article vol. 11, no. 5, pp. 1112-1119, May 2011, doi: 10.1109/jsen.2010.2082524.
[104] S. D. Min, Y. Yun, and H. Shin, "Simplified Structural Textile Respiration Sensor Based on Capacitive Pressure Sensing Method," (in English), *IEEE Sens. J.*, Article vol. 14, no. 9, pp. 3245-3251, Sep 2014, doi: 10.1109/jsen.2014.2327991.
[105] Y. N. Zheng *et al.*, "A Wearable Capacitive Sensor Based on Ring/Disk-Shaped Electrode and Porous Dielectric for Noncontact Healthcare Monitoring," (in English), *Glob. Chall.*, Article vol. 4, no. 5, p. 10, May 2020, Art no. 1900079, doi: 10.1002/gch2.201900079.
[106] X. Fu *et al.*, "A high-resolution, ultrabroad-range and sensitive capacitive tactile sensor based on a CNT/PDMS composite for robotic hands," (in English), *Nanoscale*, Article vol. 13, no. 44, pp. 18780-18788, Nov 2021, doi: 10.1039/d1nr03265h.
[107] C. Scholl, A. Tobola, K. Ludwig, D. Zanca, and B. M. Eskofier, "A Smart Capacitive Sensor Skin with Embedded Data Quality Indication for Enhanced Safety in Human–Robot Interaction," *Sensors*, vol. 21, no. 21, doi: 10.3390/s21217210.
[108] N. Ni, L. Zhang, Y. Wang, L. X. Shi, and C. Zhang, "Transparent capacitive sensor for structural health monitoring applications," (in English), *Int. J. Appl. Electromagn. Mech.*, Article vol. 52, no. 3-4, pp. 1577-1584, 2016, doi: 10.3233/jae-162215.
[109] S. D. Nguyen, I. Paprotny, P. K. Wright, and R. M. White, "MEMS capacitive flow sensor for natural gas pipelines," (in English), *Sens. Actuator A-Phys.*, Article vol. 231, pp. 28-34, Jul 2015, doi: 10.1016/j.sna.2014.10.013.
[110] H. K. Mutha, H. J. Cho, M. Hashempour, B. L. Wardle, C. V. Thompson, and E. N. Wang, "Salt rejection in flow-between capacitive deionization devices," (in English), *Desalination*, Article vol. 437, pp. 154-163, Jul 2018, doi: 10.1016/j.desal.2018.03.008.
[111] A. Torkkeli, O. Rusanen, J. Saarilahti, H. Seppä, H. Sipola, and J. Hietanen, "Capacitive microphone with low-stress polysilicon membrane and high-stress polysilicon backplate," *Sensors and Actuators A: Physical*, vol. 85, no. 1, pp. 116-123, 2000/08/25/ 2000, doi: https://doi.org/10.1016/S0924-4247(00)00336-8.
[112] A. Nelson, G. Singh, R. Robucci, C. Patel, and N. Banerjee, "Adaptive and Personalized Gesture Recognition Using Textile Capacitive Sensor Arrays," *IEEE Transactions on Multi-Scale Computing Systems*, vol. 1, no. 2, pp. 62-75, 2015, doi: 10.1109/TMSCS.2015.2495100.
[113] J. M. Miao, R. M. Lin, L. Q. Chen, Q. B. Zou, S. Y. Lim, and S. H. Seah, "Design considerations in micromachined silicon microphones," (in English), *Microelectron. J.*, Article; Proceedings Paper vol. 33, no. 1-2, pp. 21-28, Jan-Feb 2002, doi: 10.1016/s0026-2692(01)00100-8.
[114] D. R. Thevenot, K. Toth, R. A. Durst, and G. S. Wilson, "Electrochemical biosensors: recommended definitions and classification," (in English), *BIOSENSORS & BIOELECTRONICS*, vol. 16, no. 1-2, pp. 121-131, JAN 2001, doi: 10.1016/S0956-5663(01)00115-4.

[115] H. C. Koydemir and A. Ozcan, "Wearable and Implantable Sensors for Biomedical Applications," in *ANNUAL REVIEW OF ANALYTICAL CHEMISTRY, VOL 11*, vol. 11, P. W. Bohn and J. E. Pemberton Eds., 2018, pp. 127-146.
[116] M. R. MacAskill and T. J. Anderson, "Eye movements in neurodegenerative diseases," (in English), *Current Opinion in Neurology,* Review vol. 29, no. 1, pp. 61-68, Feb 2016, doi: 10.1097/wco.0000000000000274.
[117] M. M. Bellah, S. Christensen, and S. M. Iqbal, "Nanostructures for Medical Diagnostics," (in English), *JOURNAL OF NANOMATERIALS*, vol. 2012, 2012, Art no. 486301, doi: 10.1155/2012/486301.
[118] A. Vaseashta and D. Dimova-Malinovska, "Nanostructured and nanoscale devices, sensors and detectors," (in English), *SCIENCE AND TECHNOLOGY OF ADVANCED MATERIALS*, vol. 6, no. 3-4, pp. 312-318, APR-MAY 2005, doi: 10.1016/j.stam.2005.02.018.
[119] J. Wang, "Carbon-nanotube based electrochemical biosensors: A review," (in English), *ELECTROANALYSIS,* vol. 17, no. 1, pp. 7-14, JAN 2005, doi: 10.1002/elan.200403113.
[120] R. J. Leigh and D. S. Zee, *The Neurology of Eye Movements*: Oxford University Press, 2015. [Online]. Available: https://doi.org/10.1093/med/9780199969289.001.0001.
[121] A. T. Duchowski, *Eye Tracking Methodology: Theory and Practice*. Springer International Publishing, 2017.
[122] R. G. Alexander, S. L. Macknik, and S. Martinez-Conde, "Microsaccade Characteristics in Neurological and Ophthalmic Disease," (in English), *Frontiers in Neurology,* Review vol. 9, Mar 2018, Art no. 144, doi: 10.3389/fneur.2018.00144.
[123] A. Galvan *et al.*, "Nonhuman Primate Optogenetics: Recent Advances and Future Directions," (in eng), *The Journal of neuroscience : the official journal of the Society for Neuroscience,* vol. 37, no. 45, pp. 10894-10903, Nov 8 2017, doi: 10.1523/jneurosci.1839-17.2017.
[124] L. Grosenick, J. H. Marshel, and K. Deisseroth, "Closed-loop and activity-guided optogenetic control," (in eng), *Neuron,* vol. 86, no. 1, pp. 106-39, Apr 08 2015, doi: 10.1016/j.neuron.2015.03.034.
[125] Y. El-Shamayleh, Y. Kojima, R. Soetedjo, and G. D. Horwitz, "Selective Optogenetic Control of Purkinje Cells in Monkey Cerebellum," (in eng), *Neuron,* vol. 95, no. 1, pp. 51-62.e4, Jul 5 2017, doi: 10.1016/j.neuron.2017.06.002.
[126] D. A. Robinson, "A METHOD OF MEASURING EYE MOVEMENT USING A SCLERAL SEARCH COIL IN A MAGNETIC FIELD," (in eng), *IEEE transactions on bio-medical engineering,* vol. 10, pp. 137-45, Oct 1963.
[127] S. J. Judge, B. J. Richmond, and F. C. Chu, "Implantation of magnetic search coils for measurement of eye position: an improved method," (in eng), *Vision research,* vol. 20, no. 6, pp. 535-8, 1980.
[128] C. Moller and F. P. Ribeiro, "Capacitive sensors for determining eye gaze direction," ed: Google Patents, 2018.
[129] D. W. Hansen and Q. Ji, "In the eye of the beholder: A survey of models for eyes and gaze," *IEEE transactions on pattern analysis and machine intelligence,* vol. 32, no. 3, pp. 478-500, 2010.
[130] I. Hooge, K. Holmqvist, and M. Nystrom, "The pupil is faster than the corneal reflection (CR): Are video based pupil-CR eye trackers suitable for studying detailed dynamics of

eye movements?," (in English), *Vision research,* vol. 128, pp. 6-18, NOV 2016, doi: 10.1016/j.visres.2016.09.002.
[131] D. Hansen and P. Majaranta, "Basics of Camera-Based Gaze Tracking," pp. 21-26, 01/01 2011, doi: 10.4018/978-1-61350-098-9.ch003.
[132] C. M. F. P. Ribeiro, "CAPACITIVE SENSORS FOR DETERMINING EYEGAZE DIRECTION," USA Patent Appl. 14/729,524, 12/08/2016, 2015.
[133] V. Acuna O, P. Aqueveque, and E. J. Pino, "Eye-tracking capabilities of low-cost EOG system," *Annual International Conference of the IEEE Engineering in Medicine and Biology Society. IEEE Engineering in Medicine and Biology Society. Annual International Conference,* vol. 2014, pp. 610-3, 2014 2014, doi: 10.1109/embc.2014.6943665.
[134] Y. X. Jia and C. W. Tyler, "Measurement of saccadic eye movements by electrooculography for simultaneous EEG recording," (in English), *BEHAVIOR RESEARCH METHODS,* vol. 51, no. 5, pp. 2139-2151, OCT 2019, doi: 10.3758/s13428-019-01280-8.
[135] S. D. E. D. Zee, "Vertigo and Imbalance: Clinical Neurophysiology of the Vestibular System," in *Handbook of Clinical Neurophysiology*, vol. 9, 2010, ch. 6, pp. 3-575.
[136] E. Whitmire *et al., EyeContact: scleral coil eye tracking for virtual reality*. 2016, pp. 184-191.
[137] K. K. Sadasivuni, A. Kafy, L. Zhai, H.-U. Ko, S. Mun, and J. Kim, "Transparent and Flexible Cellulose Nanocrystal/Reduced Graphene Oxide Film for Proximity Sensing," *Small,* https://doi.org/10.1002/smll.201402109 vol. 11, no. 8, pp. 994-1002, 2015/02/01 2015, doi: https://doi.org/10.1002/smll.201402109.
[138] R. P. Balandong, R. F. Ahmad, M. N. M. Saad, and A. S. Malik, "A Review on EEG-Based Automatic Sleepiness Detection Systems for Driver," (in English), *Ieee Access,* Review vol. 6, pp. 22908-22919, 2018, doi: 10.1109/access.2018.2811723.
[139] Q. Ran *et al.*, "Abnormal amplitude of low-frequency fluctuations associated with rapid-eye movement in chronic primary insomnia patients," (in English), *Oncotarget,* Article vol. 8, no. 49, pp. 84877-84888, Oct 2017, doi: 10.18632/oncotarget.17921.
[140] M. I. Posner, C. R. Snyder, and B. J. Davidson, "Attention and the detection of signals," *Journal of experimental psychology: General,* vol. 109, no. 2, p. 160, 1980.
[141] T. Van Gog and K. Scheiter, "Eye tracking as a tool to study and enhance multimedia learning," ed: Elsevier, 2010.
[142] T. Usui *et al.*, "Night blindness with depolarizing pattern of ON/OFF response in electroretinogram: A case report," (in English), *Documenta Ophthalmologica,* Article vol. 111, no. 1, pp. 15-21, Jul 2005, doi: 10.1007/s10633-005-3158-1.
[143] S. Montagnese, P. Amodio, and M. Y. Morgan, "Methods for diagnosing hepatic encephalopathy in patients with cirrhosis: A multidimensional approach," (in English), *Metabolic Brain Disease,* Article; Proceedings Paper vol. 19, no. 3-4, pp. 281-312, Dec 2004, doi: 10.1023/B:MEBR.0000043977.11113.2a.
[144] A. Paolozza, S. Treit, C. Beaulieu, and J. N. Reynolds, "Diffusion tensor imaging of white matter and correlates to eye movement control and psychometric testing in children with prenatal alcohol exposure," *Human brain mapping,* vol. 38, no. 1, pp. 444-456, 2017.
[145] M. P. Grant *et al.*, "Abnormal eye movements in Creutzfeldt-Jakob disease," (in eng), *Annals of neurology,* vol. 34, no. 2, pp. 192-7, Aug 1993, doi: 10.1002/ana.410340215.

[146] U. Rosenhall, E. Johansson, and C. Gillberg, "Oculomotor findings in autistic children," (in eng), *The Journal of laryngology and otology,* vol. 102, no. 5, pp. 435-9, May 1988, doi: 10.1017/s0022215100105286.
[147] G. M. Jones and J. D. DeJong, "Dynamic characteristics of saccadic eye movements in Parkinson's disease," (in eng), *Experimental neurology,* vol. 31, no. 1, pp. 17-31, Apr 1971, doi: 10.1016/0014-4886(71)90173-7.
[148] G. Avanzini, F. Girotti, T. Caraceni, and R. Spreafico, "Oculomotor disorders in Huntington's chorea," (in eng), *Journal of neurology, neurosurgery, and psychiatry,* vol. 42, no. 7, pp. 581-9, Jul 1979, doi: 10.1136/jnnp.42.7.581.
[149] A. F. Fuchs, C. R. Kaneko, and C. A. Scudder, "Brainstem control of saccadic eye movements," (in eng), *Annual review of neuroscience,* vol. 8, pp. 307-37, 1985, doi: 10.1146/annurev.ne.08.030185.001515.
[150] E. L. Keller, N. J. Gandhi, and J. M. Shieh, "Endpoint accuracy in saccades interrupted by stimulation in the omnipause region in monkey," (in eng), *Visual neuroscience,* vol. 13, no. 6, pp. 1059-67, Nov-Dec 1996.
[151] E. L. Keller, N. J. Gandhi, and S. Vijay Sekaran, "Activity in deep intermediate layer collicular neurons during interrupted saccades," (in eng), *Experimental brain research,* vol. 130, no. 2, pp. 227-37, Jan 2000.
[152] W. Becker, "The neurobiology of saccadic eye movements. Metrics," (in eng), *Reviews of oculomotor research,* vol. 3, pp. 13-67, 1989.
[153] A. F. Fuchs and D. A. Robinson, "A method for measuring horizontal and vertical eye movement chronically in the monkey," (in eng), *Journal of applied physiology,* vol. 21, no. 3, pp. 1068-70, May 1966.
[154] M. M. Houben, J. Goumans, and J. van der Steen, "Recording three-dimensional eye movements: scleral search coils versus video oculography," (in eng), *Investigative ophthalmology & visual science,* vol. 47, no. 1, pp. 179-87, Jan 2006, doi: 10.1167/iovs.05-0234.
[155] Y. Jia and C. W. Tyler, "Measurement of saccadic eye movements by electrooculography for simultaneous EEG recording," *Behavior Research Methods,* vol. 51, no. 5, pp. 2139-2151, Oct 2019, doi: 10.3758/s13428-019-01280-8.
[156] A. J. Golparvar and M. K. Yapici, "Toward graphene textiles in wearable eye tracking systems for human-machine interaction," (in English), *Beilstein Journal of Nanotechnology,* Article vol. 12, pp. 180-189, Feb 2021, doi: 10.3762/bjnano.12.14.
[157] S. Lee *et al.*, "Ultrathin Nanogenerators as Self-Powered/Active Skin Sensors for Tracking Eye Ball Motion," (in English), *Advanced Functional Materials,* Article vol. 24, no. 8, pp. 1163-1168, Feb 2014, doi: 10.1002/adfm.201301971.
[158] N. I. Kim *et al.*, "Highly-Sensitive Skin-Attachable Eye-Movement Sensor Using Flexible Nonhazardous Piezoelectric Thin Film," (in English), *Advanced Functional Materials,* Article vol. 31, no. 8, Feb 2021, Art no. 2008242, doi: 10.1002/adfm.202008242.
[159] A. B. Dichiara, A. Song, S. M. Goodman, D. He, and J. Bai, "Smart papers comprising carbon nanotubes and cellulose microfibers for multifunctional sensing applications," (in English), *Journal of Materials Chemistry A,* Article vol. 5, no. 38, pp. 20161-20169, Oct 2017, doi: 10.1039/c7ta04329e.
[160] J. Y. Zhang, S. M. Goodman, H. G. Wise, A. B. Dichiara, and J. H. Chung, "Electromechanical Coupling of Isotropic Fibrous Networks with Tailored Auxetic

Behavior Induced by Water-Printing under Tension," *Journal of Materials Chemistry C*, vol. DOI: 10.1039/D0TC05526C, 2021.
[161] A. E. Zavadskii, "X-ray diffraction method of determining the degree of crystallinity of cellulose materials of different anisotropy," (in English), *FIBRE CHEMISTRY*, vol. 36, no. 6, pp. 425-430, NOV-DEC 2004, doi: 10.1007/s10692-005-0031-7.
[162] S. M. Goodman *et al.*, "Scalable manufacturing of fibrous nanocomposites for multifunctional liquid sensing," (in English), *NANO TODAY*, vol. 40, OCT 2021, Art no. 101270, doi: 10.1016/j.nantod.2021.101270.
[163] S. Y. Bi, L. Hou, H. Zhao, L. Zhu, and Y. X. Lu, "Ultrasensitive and highly repeatable pen ink decorated cuprammonium rayon (cupra) fabrics for multifunctional sensors," (in English), *JOURNAL OF MATERIALS CHEMISTRY A*, vol. 6, no. 34, pp. 16556-16565, SEP 14 2018, doi: 10.1039/c8ta04809f.
[164] C. A. Scudder, C. S. Kaneko, and A. F. Fuchs, "The brainstem burst generator for saccadic eye movements: a modern synthesis," (in eng), *Experimental brain research*, vol. 142, no. 4, pp. 439-62, Feb 2002, doi: 10.1007/s00221-001-0912-9.
[165] J. J. Hopp and A. F. Fuchs, "The characteristics and neuronal substrate of saccadic eye movement plasticity," (in eng), *Progress in neurobiology*, vol. 72, no. 1, pp. 27-53, Jan 2004, doi: 10.1016/j.pneurobio.2003.12.002.
[166] R. Soetedjo, Y. Kojima, and A. F. Fuchs, "How cerebellar motor learning keeps saccades accurate," (in eng), *Journal of neurophysiology*, vol. 121, no. 6, pp. 2153-2162, Jun 1 2019, doi: 10.1152/jn.00781.2018.
[167] M. N. Shadlen and W. T. Newsome, "Neural basis of a perceptual decision in the parietal cortex (area LIP) of the rhesus monkey," (in eng), *Journal of neurophysiology*, vol. 86, no. 4, pp. 1916-36, Oct 2001, doi: 10.1152/jn.2001.86.4.1916.
[168] C. R. Camalier *et al.*, "Dynamics of saccade target selection: race model analysis of double step and search step saccade production in human and macaque," (in eng), *Vision research*, vol. 47, no. 16, pp. 2187-211, Jul 2007, doi: 10.1016/j.visres.2007.04.021.
[169] B. L. Zuber, J. L. Semmlow, and L. Stark, "Frequency characteristics of the saccadic eye movement," (in eng), *Biophysical journal*, vol. 8, no. 11, pp. 1288-98, Nov 1968, doi: 10.1016/s0006-3495(68)86556-7.
[170] K. K. Sadasivuni, A. Kafy, L. Zhai, H. U. Ko, S. Mun, and J. Kim, "Transparent and flexible cellulose nanocrystal/reduced graphene oxide film for proximity sensing," (in eng), *Small*, vol. 11, no. 8, pp. 994-1002, Feb 25 2015, doi: 10.1002/smll.201402109.
[171] A. Consejo, C. Llorens-Quintana, M. M. Bartuzel, D. R. Iskander, and J. J. Rozema, "Rotation asymmetry of the human sclera," (in eng), *Acta ophthalmologica*, vol. 97, no. 2, pp. e266-e270, Mar 2019, doi: 10.1111/aos.13901.
[172] R. Soetedjo, C. R. Kaneko, and A. F. Fuchs, "Evidence that the superior colliculus participates in the feedback control of saccadic eye movements," (in eng), *J Neurophysiol*, vol. 87, no. 2, pp. 679-95, Feb 2002, doi: 10.1152/jn.00886.2000.
[173] P. Foeller and L. Tychsen, "Eye movement training and recording in alert macaque monkeys: 1. Operant visual conditioning; 2. Magnetic search coil and head restraint surgical implantation; 3. Calibration and recording," (in eng), *Strabismus*, vol. 10, no. 1, pp. 5-22, Mar 2002, doi: 10.1076/stra.10.1.5.8154.
[174] Y. Tang *et al.*, "Eye Position Compensation Improves Estimates of Response Magnitude and Receptive Field Geometry in Alert Monkeys," *Journal of Neurophysiology*, vol. 97, no. 5, pp. 3439-3448, 2007/05/01 2007, doi: 10.1152/jn.00881.2006.

[175] B. J. Carr and W. K. Stell, "The Science Behind Myopia," in *Webvision: The Organization of the Retina and Visual System*, H. Kolb, E. Fernandez, and R. Nelson Eds. Salt Lake City (UT): University of Utah Health Sciences Center Copyright: © 2022 Webvision . 1995.
[176] I. Bekerman, P. Gottlieb, and M. Vaiman, "Variations in eyeball diameters of the healthy adults," (in eng), *J Ophthalmol*, vol. 2014, p. 503645, 2014, doi: 10.1155/2014/503645.
[177] A. Roy, M. Kar, D. Mandal, R. S. Ray, and C. Kar, "Variation of Axial Ocular Dimensions with Age, Sex, Height, BMI-and Their Relation to Refractive Status," (in eng), *J Clin Diagn Res*, vol. 9, no. 1, pp. Ac01-4, Jan 2015, doi: 10.7860/jcdr/2015/10555.5445.

VITA

Vigneshwar Sakthivelpathi is an Indian-born, naturalized Australian. In 2009, he garnered his B.Eng. with Honors in Mechanical Engineering from Curtin University of Technology, Western Australia. Upon graduation, he pursued a career in the energy industry for six years as a Project Engineer. His industry experience led to an eagerness to innovate, which initiated his journey toward further education. In fall of 2017, he commenced his doctoral research under the guidance of Professor Jaehyun Chung, where he focused his work on nanotechnology and nanomanufacturing techniques that aid in developing human-machine interface devices.